STARS

Electronic Theses and Dissertations, 2004-2019

2004

Detection And Evaluation Of Exisiting Pavement System With Brick Base

Karishma Desai

University of Central Florida

Part of the Civil Engineering Commons

Find similar works at: https://stars.library.ucf.edu/etd

University of Central Florida Libraries http://library.ucf.edu

University of Central Florida

STARS
Showcase of Text, Archives, Research & Scholarship

DETECTION AND EVALUATION OF EXISITING PAVEMENT SYSTEM WITH BRICK BASE USING GROUND PENETRATING RADAR

by

KARISHMA ROHIT DESAI
B.S.C.E. University of Central Florida, 2002

A thesis submitted in partial fulfillment of the requirements
for the degree of Master of Science
in the Department of Civil and Environmental Engineering
in the College of Engineering and Computer Science
at the University of Central Florida
Orlando, Florida

Fall Term
2004

ABSTRACT

At the turn of the century, the City of Orlando initiated the "Neighborhood Horizon Program." This program involved local citizens to help improve their community resources by engaging in a process of planning where the problems associated with the communities were identified. Many residents favored to bring back the brick roads that were overlaid with asphalt concrete to provided better transportation in the mid 1900s. With majority of the neighborhood streets already bricked, removing asphalt ensured safety, served as a technique for slowing traffic, and added to the historical integrity.

Since there were no official documentations available that stated the definite existence of bricks beneath the asphalt surface course, it would have been rather impossible to core hundreds of locations to ensure the whereabouts of these anomalies. Thus, without time delays and excessive coring costs, a nondestructive instrumentation of Ground Penetrating Radar (GPR) was employed in the detection of bricks. This geophysical survey system distinguishes materials based on their different electrical properties that depend upon temperature, density, moisture content and impurities by providing a continuous profile of the subsurface conditions. The Ground Penetrating Radar operates on the principle of the electromagnetic wave (EMW) theory.

The main objectives of this study was to investigate the existing pavement by using Ground Penetrating Radar (GPR) in detecting the brick base and to analyze the performance of pavement system for fatigue and rutting. The results of this study will assist the City of Orlando in removing asphalt layer, rebuilding of brick roads, and facilitate in better zoning and planning of the city.

The construction of controlled test area provided with a good sense of brick detection, which helped in precise locations bricks for sections of Summerlin Avenue, Church Street and Cherokee Drive. The project demonstrated a good sense of detecting the subsurface anomalies, such as bricks. The validation of the profile readings was near to a 100%.

To my Parents

With all my Love

ACKNOWLEDGEMENTS

TABLE OF CONTENTS

LIST OF FIGURES

LIST OF TABLES

CHAPTER 1

INTRODUCTION

Cars began to appear in the City of Orlando approximately a century ago. In order to accommodate the populating traffic, the City began to build brick roads for several areas, including residential areas. As Orlando grew, the traffic progressively grew with rising demands. Over time, these roads developed potholes, depressions and uneven surfaces, which caused tremendous traffic hazards. As a result, many traditional brick roads in the City of Orlando were overlaid with asphalt concrete to provide a smoother ride for the drivers.

At the turn of the century, the mayor, Glenda Hood, of the City of Orlando initiated the "Neighborhood Horizon program," where residents were engaged in the process of planning for the new millennium. The program provided the residents with workshops where they were able to identify and prioritize issues and conditions that affected the appearance, safety, livability and desirability of their neighborhood. Among many changes like providing park/community centers, decorative street lamps, containerized garbage etc., the local citizens favored removing the asphalt from the few remaining paved streets in downtown Orlando. With most neighborhood streets already bricked under the existing pavements, removing asphalt ensured safety, served as a technique for slowing traffic, and most of all, added to the historical integrity. There have been no official documents that provided with any record of the existence of bricks at any exact location on a lane of a certain road, or where the bricks may have been removed due to the extension of roads, any repairs or installation of the subsurface utilities.

Thus, the investigation of existing pavement system became very important. Subsurface exploration commonly comprises of several steps that includes collection of preliminary information, reconnaissance, and site investigation (Das, 2004). The investigation of the subsurface bricks commonly consists of traditional coring methods such as drilling boreholes. The process of drilling boreholes and examining core samples is considered an expensive, and time consuming process. The numbers of boreholes that needs to be drilled may usually be limited by its high cost demand. In most cases, traditional coring methods may not provide a complete assessment of the subsurface features. Even so, one quick, efficient and inexpensive method of subsurface investigation is a technique that has developed in the last centaury, a technique of Ground Penetrating Radar (GPR) survey.

GPR distinguishes materials based on their different electrical properties that depend upon temperature, density, moisture content and impurities (Tannous, 1987), by providing a continuous profile of the subsurface conditions. The calibration of the depth scale GPR profile is directly related to the time of travel and the propagation velocity of the radar signal. These velocities are a function of the dielectric constant and conductivity of the materials that are being investigated. The Ground Penetrating Radar operates on the principle of the electromagnetic wave (EMW) theory. EMW propagation in conducting media has been implemented worldwide, and in the recent years, several major universities and businesses have developed this theory into several applications.

The City of Orlando officials provided no official documentations with information regarding re-pavement of the asphalt on city streets due to negative effects of brick base. Additionally, selection of a base and subbase materials in designing a pavement system is

extremely critical. Excessive deterioration of pavements such as potholes, depressions, rutting, fatigue cracking, as well as numerous traffic accidents due to heavy loadings and traffic volume may arise.

The scope of this study was based on the following:

1. Selecting of sites with brick base pavement sections by the City of Orlando,

2. Making transit GPR survey along the selected traverses,

3. Comparing of profiles of with and without the brick base from the test pit built at UCF campus,

4. Detouring of local traffic using traffic signs and traffic crew provided by the City of Orlando,

5. Investigating, from the result of GPR profile, samples of the ground truth by removing the pavement surface courses for Summerlin Avenue and Cherokee Drive,

6. Comparing GPR profiles with and without the brick base,

7. Analyzing the life expectancy of existing pavement without brick base according to the best knowledge of material characteristics, and analyzing the existing pavement system with brick base using KENPAVE computer program,

8. Determining tensile strain at the bottom of the asphalt layer for fatigue remaining life and compressive strain at the top of subgrade layer for rutting criterion from the brick base pavement system using KENPAVE computer program.

In order to accurately understand the brick base exhibited on the GPR profiles, a brick base test pit was constructed at UCF's Circular Accelerated Test Track (CATT). Several types of bricks were acquired, and laid perpendicular to the existing lime-rock base. The bricks were

overlaid by hot mixed asphalt, supplied by the Orlando Paving Company, with an approximate thickness of 3 − 4 inches. The purpose of the test pit was to calibrate the GPR outputs at shallow depths, and to better interpret radar profiles.

With the assistance of the City of Orlando and Ardaman & Associates, Inc., three City streets were chosen for the investigation in this study. The streets of interest were located in Downtown Orlando, sections of South Summerlin Avenue and Church Street, and Cherokee Drive. The location and whereabouts of the streets mentioned are presented in the Figures A-2 and A-3 in Appendix A of this report.

The objective of this research was to investigate the existing pavement by employing the Ground Penetrating Radar (GPR) System in detecting the brick base beneath the pavement system in order to remove asphalt layer and performed restoration of brick roads. The analysis of the life expectancy of the existing pavement system with and without brick base is also performed.

In general, the existing pavement system of all selected sites consisted of an approximate 2 to 6-inchs of asphalt layer. The heavy-duty construction bricks were installed as the base layer with an approximate thickness of 3 inches. Underneath the brick base, subbase layer was constructed with A-3 AASHTO classified sandy soils, typically found in Florida.

The result of this study would provide the City with locations of brick base along Orlando streets. Using these results, the City of Orlando would efficiently restore brick roads by removing the asphalt course. This study would also provide the City a better idea for future planning and zoning of Orlando streets. Lastly, the life expectancy analysis will offer the city

4

with structural integrity of the existing pavement system, which in turn, will help with future pavement rehabilitation programs.

CHAPTER 2

LITERATURE REVIEW

In the last three decades, nondestructive testing (NDT) technology applied to the evaluation of pavement systems has substantially advanced. Over 260 papers, patents, and standards on NDT and pavements have been recorded (Olhoeft, 2000). Among the NDTs, ground penetrating radar (GPR) has been a very promising system as it has not only helped in investigations of endless buried and non-buried man-made structures, but it has helped in solving specific problems like material curing, aging, moisture determination, subgrade compaction, hydrology, voids, leakages, and even victim locations. GPR has been used in evaluating of concrete and asphalt pavements have flourished with commendable results without time delays.

First asphalt roadway was constructed in 1870 in Newark, New Jersey. By 1990, there were 2.2 million miles of paved roadway reported in the United States (Haung, 1993). Over the years, pavement engineers have faced several challenges in the design and analysis of the roadways even after the development of several performance and deterioration models. The first full scale pavement design field test was conducted in Maryland by AASHTO. Now, the trend is more towards the mechanistic-empirical pavement design methods, which uses finite element analysis technique coupled with pavement performance observation. Predicting the future conditions of pavement systems with or without maintenance and rehabilitation (M&R) actions are an important element of Pavement Management System (PMS).

GPR and its Applications to Pavements

Since the early 1900s, studies have been conducted with the use of propagation of electromagnetic waves (Sweeney, 1986), and has been proven as a promising method in many investigations (Hunaidi & Giamou, 1998). Radar signals had been developed in determining remote terrestrial metal since the 1904s. First description of its use in locating buried objects appeared in Germany in 1910 by two German patents, Leimbach and Lowy (Daniels, 1996). First application of pulsated technique in determining buried structures appeared in 1926, and in the 1929, GPR was first used to determine the depth of glacier (Olhoeft, 1996). Since then, the technique had been applied in the measure of fresh water, salt deposits, desert sand and rock formations. In the 1970s, applications of GPR signals were applied on lunar investigation and landings. Ever since the 1970s, the range of applications have developed and expanded. The radar technique has now been implemented on buildings and structural nondestructive testing, roads and tunnels assessment for quality and performance, location of voids and containers, pipes, cables, mineshafts, and over seismic locations (Daniels, 1996).

Radar wave technology has been implemented around the world with capable results. Several universities and companies have adopted the method as it has confirmed to be nondestructive, noninvasive, and inexpensive. With the developing technologies, progress has been made on the electromagnetic equipment in terms of advance applications, techniques, and data-processing. Researchers along with several practitioners have united to develop surface-penetrating radar that not only is used in detecting subsurface anomalies, but it is now being used for a wide range of problems from archaeology to geology, glaciology, environmental, engineering, mining, military, and many others.

Nonetheless, surface-penetrating radar have been flown at height of approximately 1312 feet (400 meters) in synthetic-aperture radar (SAR) mode that have imaged buried metallic mines (Daniels, 1996). Recent studies have shown that the use of ground penetrating radar has been simulated and designed for exploration in Mars, as there has been evidence of the planet undergoing several geological changes due to the changes in its surface waters (Leuschen et al., 2001). Research with great success in the detection of leaks in buried plastic water distribution pipes and buried tanks and pipes had been reported by Hunaidi and Giamou (1998), and Zeng and McMechan (1997), respectively. Olhoeft (1996) has reported the use of ground penetrating radar in imaging mode to project and map the subsurface events of the ground water table (GWT). Hauser (2001) has studied and published several research papers with the use of GPR. His studies have compiled of assessing animal burrows that damage earthen levees, evaluation of roadway collapse in Northern Ohio along with 3-D imaging of Neodani Fault, in Central Japan, including several more that have not been listed herein.

Extreme importance is given to hydrological and geotechnical applications in a detailed structural investigation, especially for shallow subsurface investigations. For a detailed interpretation of a structure, high-resolution imaging is important for the monitoring of the structural integrity of the infrastructure, roadways, bridges, or any form of structure being investigated. For a case of geotechnical application, the characteristics of shallow subsurface anomalies, such as soils, bedrock, etc., are to be determined (Cardimona, 2002). To this day, specific research on brick base pavements has not been reported anywhere. Although several researchers have reported their studies on brick walls for location of rebars and voids (STATS Geophysical, 2003), and old brick-lined sewer beneath pavements (Lewis et al., 2002). Hauser

and Howell (2001) reported the detection of void found under a pavement system consisting of a layer of asphalt overlaying brick pavement, which overlaid 6-inches of concrete.

GPR has been used for many shallow subsurface investigations. For instance, the United States Army has utilized GPR to detect sub-surface landmines (Lacko, 2003). Several police agencies have searched buried human remains by the employing GPR (Powell, 2004). GPR has emerges as an effective tool in investigation of near surface objects such as pipes, cables, archaeological structures, hidden tunnels, contaminated areas, leakages, etc. (Das et al. 2003).

Choice of antenna for GPR is perhaps an extremely critical component. Olhoeft (1996), Daniels (1996), Hunaidi & Giamou (1998), Chen et al. (2001), Cardimona (2002), and Lacko et al. (2003) have shown great concern towards the choice of antennas that are utilized for a shallow surface study. The concern arises mainly because the transmitting antennas operate in megahertz range that propagates into the earth tends to have wavelengths of approximately 3 ft or less. Nonetheless, the resolutions (horizontal and vertical) of the waves are dependent on the wavelengths, which insinuates that the smaller the wavelength, the better the resolutions, which also means that the frequency is higher (Cardimona, 2002). Furthermore, it has been reported that for shallow applications, 1000-6000 MHz frequency range antennas provide data with possible substitution between depth resolution and penetration of the radar waves (Chen et al., 2001). For example, for a 900 MHz antenna, the maximum penetration depth is approximately 3 feet or less in typical soils, but the reflections generated by the antenna can resolve features to a few inches. Table 1 presents the frequency of the antenna as a function of depth.

Table 1

Antenna Frequency as a Function of Depth

Approximate Depth (m)	Approximate Depth (ft)	Frequency (MHz)
0.3-0.5	1.0-1.6	1500
0.5-1	1.6-3.3	1000
1.0-2.0	3.3-6.6	500
2.0+	6.6+	200
7.0	23.0	100

Source: Ground Penetrating Radar (2003)

GPR is still a developing technology used for several applications that have never been investigated before.

Pavement System— Design and Analysis

Pavements are complicated physical structures that respond in a complex manner to influence many variables such as pavement materials, loads applied on the pavements, aging of pavement system, and environmental conditions (Ullidtz, 1999 a). Pavements have a relatively short service lives and may deteriorate rapidly because of loads or environment conditions. Researchers have estimated that in United States, large portions of existing pavements require some kind of reconstruction or rehabilitation (Mikhail & Mamlouk, 1997).

Distress is an important factor in pavement design. There are several types of distresses such as alligator or fatigue cracking, block cracking, longitudinal and transverse cracking,

depression and rutting, patch and utility cut, lane/shoulder drop-off or heave, swell, bleeding, paveling and weathering, slippage cracking, and many more (Haung, 1993). The two most important distress mechanisms in flexible pavement systems are permanent deformation or rutting and fatigue or alligator cracking (Weissman, 1999).

Fatigue or Alligator cracking is caused by a series of interconnecting cracks caused by fatigue failure of asphalt surface, or under repeated traffic loading. It comprises of two successive stages of crack initiation and crack propagation (Uzan, 1997). The cracking of the asphalt is initiated at the bottom of the asphalt course or where the tensile stress or stain is highest under a wheel load and the crack propagate to the surface as one or more longitudinal parallel cracks as shown in Figure 1 (a). Due to the repeated traffic, cracks start to connect forming many shape angled and sided pieces that portrays the skin of an alligator, hence the name. This is seen in Figure 1 (b). Alligator cracks are considered a major structural distress (Haung, 1993).

(a)   (b)

Figure 1. Fatigue Cracking (Pavement Distress, 2003)

Rutting or permanent deformation in pavement systems occur when pavement surface areas have elevations slightly less than the elevation due to wheel path compared to the surrounding pavement. Much of rutting occurs due to rainfall as the wheel paths fills up with water, which may cause hydroplaning of vehicles. Depressions may also be caused by improper construction, or foundation settlement. Rutting may also be caused by plastic movement asphalt mix in hot weathers. Rutting can lead to major structural failures (Haung, 1993). Figure 9 depicts depression or rutting caused by vehicular paths.

<center>(a)   (b)</center>

<center>**Figure 2**. Rutting (Kestler, 2000)</center>

The computer program used to evaluate fatigue life and permanent deformation are called Kenlayer, subprogram of KENPAVE. Kenlayer is programmed for the application for flexible pavements. The program is based on elastic multilayer system under a circular loaded area (Haung, 1993).

<center>Burmister's Layered System Theory</center>

Burmister developed the layered pavement system theory in 1943. Flexible pavements are layered systems with better materials, such as hot mixed asphalt (HMA), on the top and can not be represented by a homogenous mass (Haung, 1993). The following assumptions are made while using the layered system:

1. All layers in a pavement system are homogenous isotropic, linearly elastic with modulus of elasticity and Poison ratio,

<center>13</center>

2. The materials are weightless and infinite,

3. All layers have finite thickness with a infinite thickness of the bottom layer,

4. Uniform pressure is applied on the surface of the layered system over a circular area with a radius,

5. Lastly, continuity conditions are satisfied at the layer interfaces. This is indicated by the same vertical stresses, shear stresses, vertical displacement, and radial displacement, and for frictionless interface, the continuity of shear stresses and radial displacement is replaced by zero shear stress at each side of the interface (Haung, 1993).

Behavior of a flexible pavement under a circular wheel load is characterized by considering it as a homogenous half-space (Haung, 1993). A half-space is an infinitely large area and with an infinite depth where the loads are applied on the top plane. Thus, the theory on concentrated loads being applied on an elastic half-space is called Boussinesq's theory developed in 1885.

Traffic Loading on Pavement System

Pavement systems are subjected to a wide range of vehicular loads. The consideration of the number of load repetitions from mixed traffic and the evaluation of its damage from different axle loads is a tedious process. Furthermore, if traffic data is not readily available, then the Asphalt Institute recommends Table 2: summary of the classification of traffic for a range of trucks in a design period.

Table 2

Classification of Traffic

Traffic Class	Types of Streets and Highways	Range of Trucks in Design Period	ESAL
I	Parking Lots Driveways Light Traffic Residential Streets and Farm Roads	< 7,000	5,000
II	Residential Streets Rural Residential and Farm Roads	7,000 to 15,000	10,000
III	Urban Minor Collector Streets Rural Minor Collector Roads	70,000 to 150,000	100,000
IV	Urban Minor Arterial and Light Industrial Streets Rural Major Collector and Minor Arterial Highways	700,000 to 1,500,000	1,000,000
V	Urban Freeways and Expressways	2,000,000 to 4,500,000	3,000,000
VI	Urban Interstate Highways	7,000,000 to 15,000,000	10,000,000

Source: Haung (1993)

For the design of pavement systems, a simplified and widely accepted procedure relies on converting each load group into an equivalent 18-kip (80 kN) single axle load as proposed by AASHTO (Haung, 1993). An equivalent axle load factor defines the damage per pass to a pavement by the axle in question relative to the damage per pass of a standard axle load, which is usually the 18-kip (80 kN) single axle load. The major failure criteria of flexible pavements are

fatigue cracking and permanent deformation or rutting. The equations of fatigue failure and rutting or deformation proposed by the Asphalt Institute and other agencies are as follows:

$$N_f = f_1 * (\varepsilon_t)^{-f_2} (E_1)^{-f_3} \tag{1}$$

$$N_d = f_4 * (\varepsilon_c)^{-f_5} \tag{2}$$

Where, N_f = Number of allowable load repetitions to prevent fatigue

ε_t = Tensile strain at the bottom of the asphalt layer, or

$$\varepsilon_t = \frac{\varepsilon_x + \varepsilon_y}{2} - \sqrt{\left(\frac{\varepsilon_x - \varepsilon_y}{2}\right)^2 + \gamma_{xy}^2} \tag{3}$$

where

$$\gamma_{xy} = \frac{2(1+\upsilon)}{E} \tau_{xy} \tag{4}$$

E_1 = Elastic modulus of asphalt concrete

f_1, f_2, f_3 = constants determined from laboratory fatigue tests

N_d = Number of allowable load repetitions to limit permanent deformation

ε_c = Compressive strain on top of the subgrade

f_4, f_5 = Constants determined from road test or road performance

Table 3 provides a list of the constants (f) recommended by the Asphalt Institute.

Table 3

Constants determined by the Asphalt Institute

Constant	Asphalt Institute Value
f_1	0.0796
f_2	3.291
f_3	0.854
f_4	1.365×10^{-9}
f_5	4.477

Source: Huang (1993)

Fatigue cracking of a flexible pavement system is mainly based on the horizontal tensile strain at the bottom of the hot mixed asphalt (HMA) and it relates to the allowable number of load repetitions to the tensile strain based on pilot scale testing, or actual traffic data collected (Haung, 1993). Given traffic data for the downtown area, the computation of the remaining pavement life either fatigue or rutting can be computed by KENPAVE computer program.

CHAPTER 3

THEORITICAL BACKGROUND OF GROUND PENETRATING RADAR

Ground penetrating radar (GPR) is an integrated geophysical technique used to detect subsurface conditions. The Ground Penetrating Radar operates on the principle of the electromagnetic wave (EMW) theory. Two primary electrical properties determine the behavior of the current in a medium: electrical resistivity and dielectric constant. Electrical resistivity is a measure of the difficulty encountered in establishing a long-term current flow in a material, and is inversely proportional to the conductivity of the material. Dielectric constant is a substance that is a poor conductor of electricity, but an efficient supporter of electrostatic fields, hence, it is an easy measure with which short-term currents may be excited when voltage is applied to material.

The EMW travel through the material at velocities those are proportional to the electrical characteristics of the earth materials. The electromagnetic properties of materials depend on their structural nature and the water content. Thus, changes in the material properties cause changes in the EMW speed, and in the partial reflection of material's energy. The frequency antenna is towed along the surface of the earth while the pulsation is radiated into the earth, and a continuous stream of reflected signals of the subsurface interface is produced in a two-dimensional digital graphic profile.

The equations and principles governing the proliferation of EMW are well documented. If the speed of the spread through a stratum is known, the travel times of the echoing pulses can be converted to depths to various interfaces. Since material properties of earth vary

considerably under natural conditions, the depths of penetration of the radar signals become function of these properties. Thus, many variables influence the radar signal, which makes it difficult to obtain the penetration depth. The electrical properties of the rocks, soils and water vary greatly. For this reason, the non-homogeneity in earth materials that are being probed reduces the radar strength into reflections of several layered interfaces. Consequently, geography, geology, atmospheric conditions, sizes and shapes of the target will also affect the detection ability of GPR system.

<u>SIR-20 GPR</u>

The equipment employed in this study is the Subsurface Interface Radar (SIR-20) System manufactured by Geophysical Survey Systems, Inc. (GSSI). The SIR-20 equipment shown in Figures 5 and 6 consists of a control unit, a "Toughbook" laptop, transmitting and receiving antenna of 900 MHz, and a 200 feet long cable. The antenna can be pulled along the surface of the strata by hand or it can be towed behind a vehicle for long distances, and a 12-volt DC battery may provide the power for this system.

The operation of GPR is described as sliding radar that emits a short pulse of electromagnetic energy into the ground and measures the pulsated reflection. The reflected pulses are equated with distance to obtain depth to desired targets and interfaces. The EMW generated in the antenna in the duration of a cycle, travel through the subsurface medium, until the signal strikes another medium with a varying dielectric constant, at this time fraction of the signal remains continuous towards the subsequent interface and other fraction reflects back.

19

Figure 3. SIRveyor SIR-20
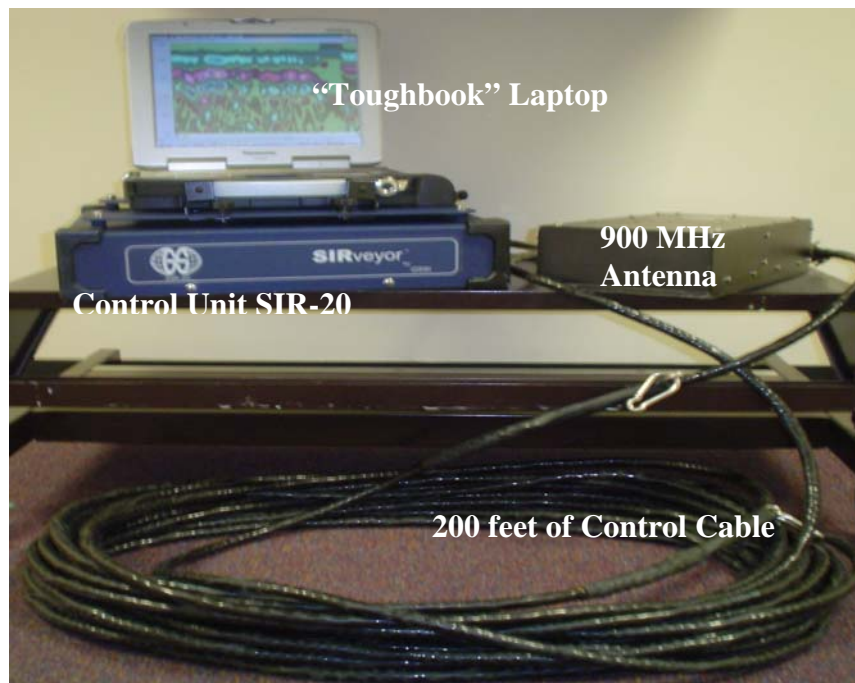
Figure 4. Equipment Layout with 900 MHz antenna

For the duration of the each cycle, a fast acting control unit creates a time-limited signal, which is sent directly to the antenna. The transmitted pulsations travel through the subsurface until it reaches the soil interface. Depending on the electrical characteristics of the interface, a section of the transmitted pulsation reflects back to the surface, and is then received by the system antenna as depicted in Figure 2.3. The strength of the reflected wave, which travels at the speed of light, is indicated by the intensity of the receiving signal. Thus, the reflected field strength between two materials is described by the reflection coefficient r as given by Equation (5):

$$r = \frac{E_r}{E_o} = \frac{1 - \sqrt{\dfrac{\varepsilon_2}{\varepsilon_1}}}{1 + \sqrt{\dfrac{\varepsilon_2}{\varepsilon_1}}} \tag{5}$$

Where ε_1 and ε_2 = dielectric constants for two different materials

E_r = angle of reflection

E_o = angle of incidence
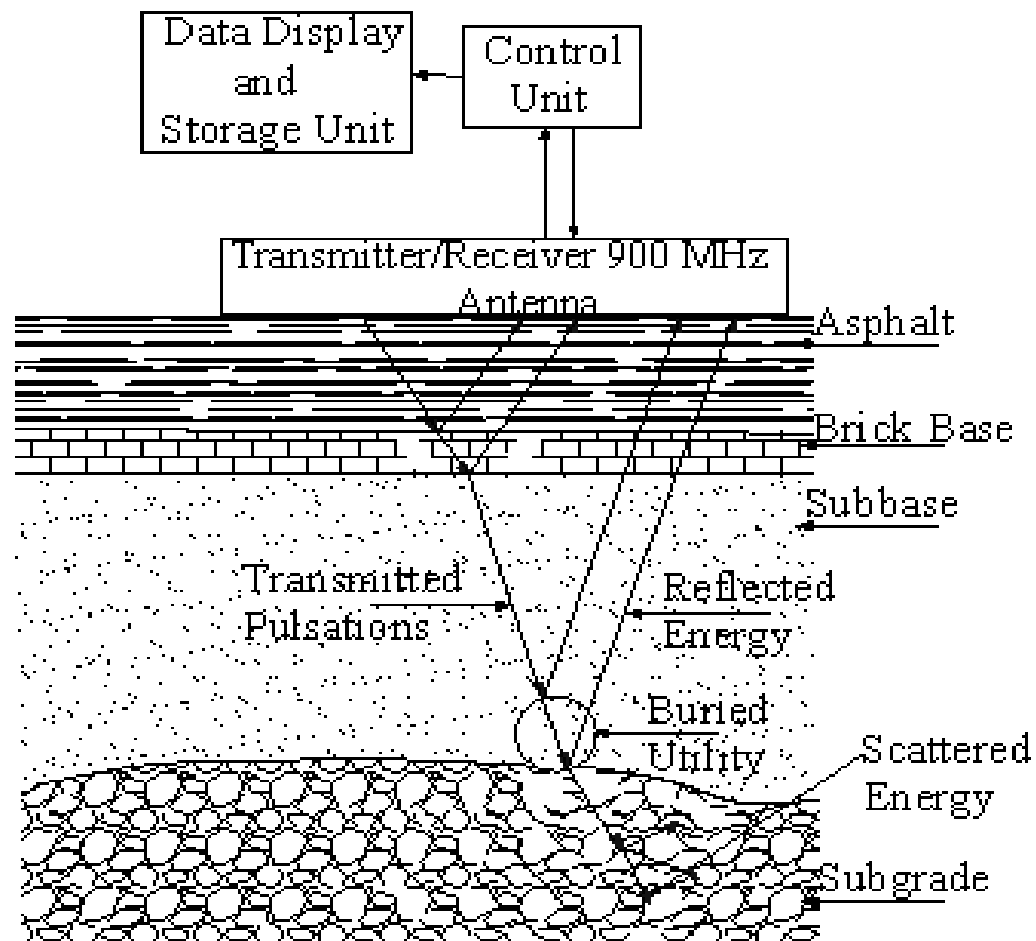
Figure 5. Reflection of Radar Signals

Furthermore, if the values of dielectric constants of two materials vary tremendously, then the reflection coefficient is approximated to be one while most of the incident energy continuous through the interface and ultimately projects a strong signal. Conversely, if the dielectric constant of the materials is same for both materials, the reflection coefficient is approximately to be zero. This means there is no reflection of signal. For this instance, most of the incident energy is transmitted through the interface, and vaguely appears on the GPR profile. The received signals are then amplified using a time-domain sampling technique to construct a waveform of similar shape of the actual signal received, but with a rather long time base. The vertical and horizontal scales indicate the time delay from the received signals and the position of the antenna, respectively (Chen et al., 2001). The traces of the processed waveforms are displayed by oscilloscope on the control unit (Sweeney, 1986). The subsurface features appear in reflected bands of several colorations, and delay in time determines the depth of the interfaces.

Next, the waveform is sent to the data storage that has the capability of acquiring data at very high rates, up to 1 megabyte per 10 seconds, resulting in very large GPR data sets (GSSI 2003). The data is displayed on-site in multiple colorations that depend directly on the amplitude of the returning signals, and amplitude depends on the conductivity of the material, which is discussed in latter section of this chapter. A typical GPR multi-colored profile is shown in Figure 6. Once the antenna is pulled across the ground surface, the "Toughbook" laptop digital recorder records and stores the multiple colored sequential pulsations for future processes and playback as necessary. The operator can modify the maximum time delays and adjust the gain for optimum display of reflected signals. Gain adjustment is needed when radar signal
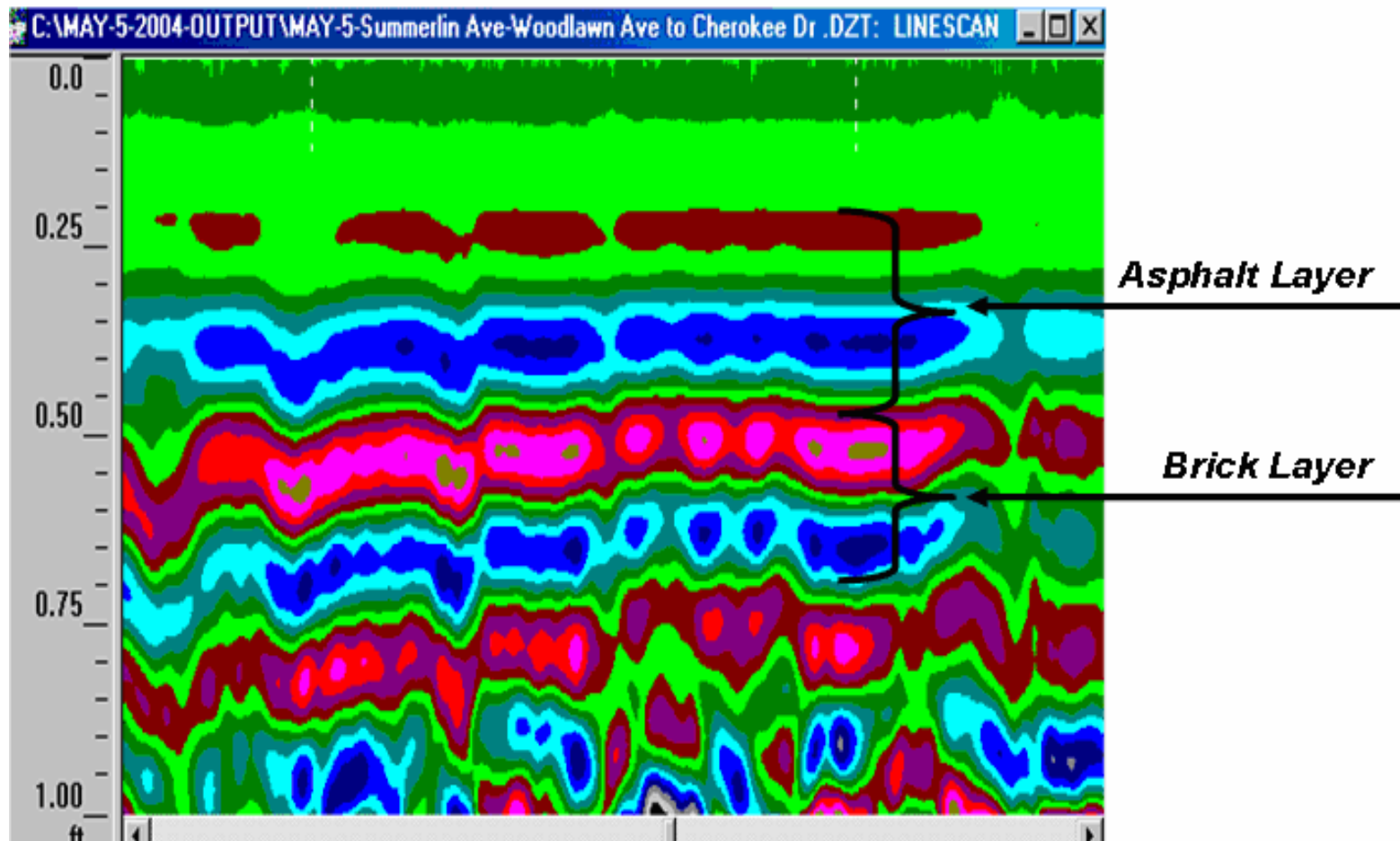
Figure 6. Typical GPR Profile of Asphalt Overlaying Brick base on Summerlin Avenue

amplitude is reduced when filtration of unneeded signals caused by moving traffic, cell phones, cables, etc. is executed (GSSI 2003). Lastly, to ensure quality control and quality assurance, adjusting the system to obtain optimum data is the most fundamental element of the survey causing minimal error.

<p align="center">Interpretation of GPR Outputs</p>

Interpretation of GPR outputs can be difficult at times due to the fact that the profiles are different for soil horizons, rock/air, soil/air, soil/rock interfaces, synthetic objects such as pipes and bricks, or any interface that creates a contrast in complex dielectric properties. Refer to resultant graphic output in Figure 7, which is an example of the reflected GPR signals. The vertical scale, as seen, is the elapse time converted to depth in feet. The horizontal scale is dependent upon the speed at which the antenna is being pulled by hand or by vehicle. The horizontal scale, as seen in Figure 7, is a white dashed line at 10 feet interval. By inspection, if these lines does not appear to be evenly distributed, as seen in Figure 7 is simply because the tow speed of the radar antenna was not maintained to a consistent speed (walking or car speed), and bumping of antenna on an uneven asphalt surface. The simplest way of interpreting GPR profile is by considering three basic components (Tannous, 1987) of the received signals:

1.   Transmitted pulsations,

2.   Surface reflections and

3.   Interface reflections.

Referring again to Figures 6 and 7, in both figures the top most layer of a solid and continuous band is the transmitted pulsations that travel through the receiver and serve as time reference in the units of nanoseconds (ns). The surface reflection for both figures is the asphalt

<p align="center">25</p>
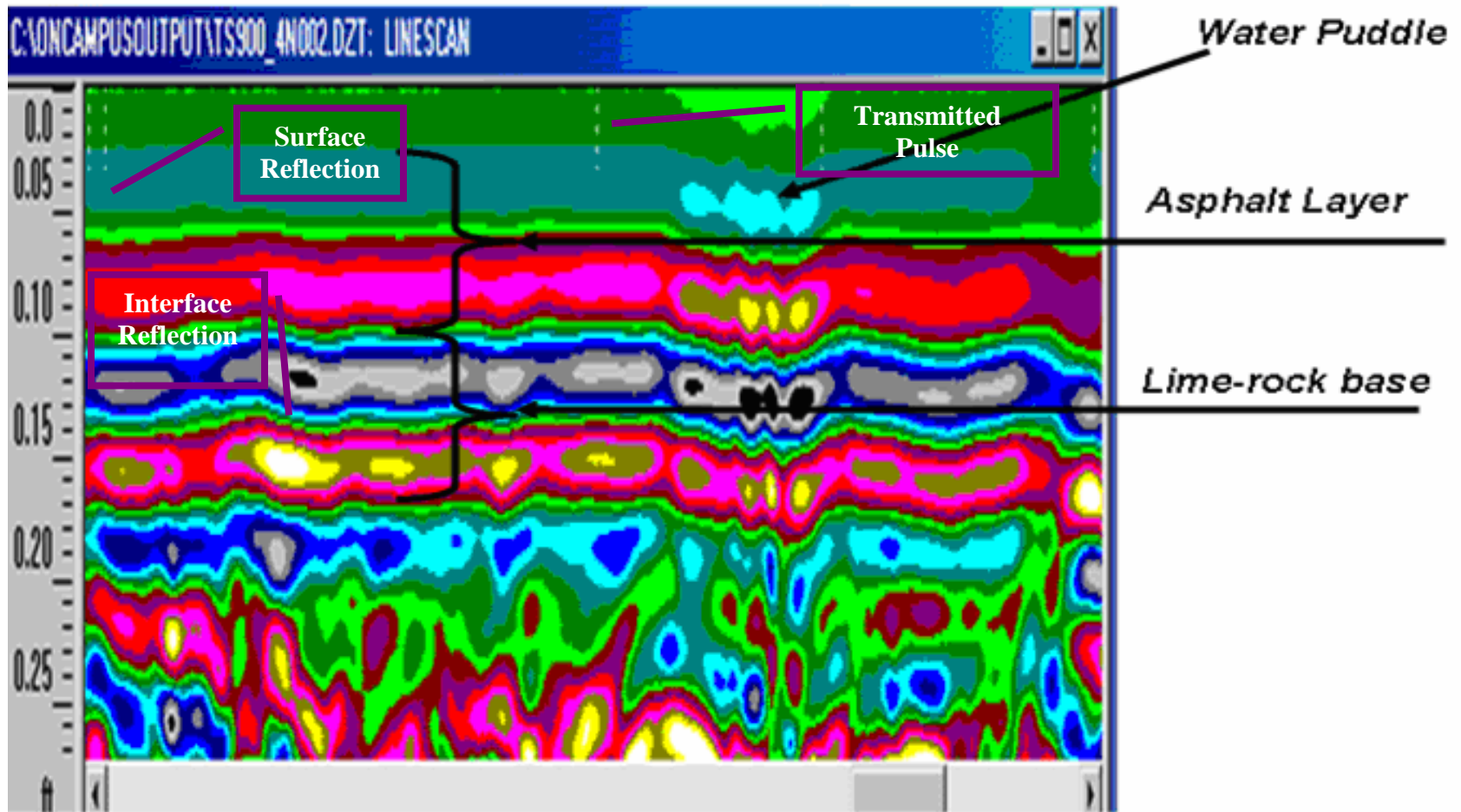
Figure 7. GPR Profile from Lime Rock Base Pavement at Test Pit—CATT

layer, which are the second and third bands in both figures. The fourth and the fifth fatal bands reflect of the bricklayers, which is the interface reflections. One of the major differences between the asphalt and bricklayers is that the state of the profile being discontinuous or broken bands from the bricks that are individually distinguishable. Sometimes, it becomes difficult to distinguish between the interface layers as is easily noticed in both reference Figures 6 and 7. The multiple bands are caused by oscillation of the pulse reflections between two interfaces, such as the asphalt and bricks or asphalt and limerock base. The oscillation effect is to limit the ability of the system to distinguish between two closely spaced interfaces that lie within two feet of each other. Thus, the reflection signals for both interfaces are superimposed on each other (Tannous, 1987). The interface subsequent to the brick base represents soil or the subbase layer that is discontinuous, indicating a break in the layer.

The radiated impulses penetrate into the ground and form a conical beam cross-section if it is over a circular shape anomaly (Daniels, 1996). The beam forms a front to back angle of approximately 90 degrees and a side-to-side angle of 60 degrees. Once the signals are transmitted through the ground, the pulsation strikes the interface at a 90-degree angle. In case of a horizontal layer, if the object is parallel to the path of the antenna, the radar will only detect the object when the antenna is directly on top of it. For the case of round objects such as pipes, a section of the curved surface is perpendicular to the path of the antenna, and the reflection is collected before and after the antenna crosses over the pipe or the curved surface. Thus, a hyperbolic reflection profile is exhibited. Figure 8 depicts the radar transmission phenomenon over a pipe with reflected hyperbolic reflected profile.
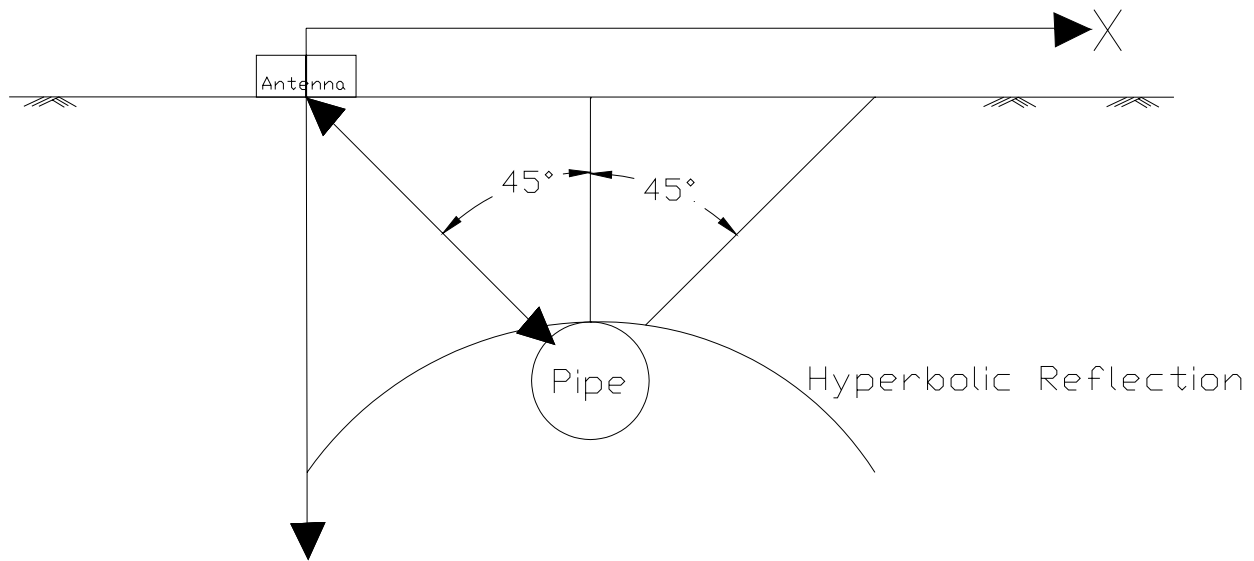
Figure 8. Hyperbolic reflection from a circular structure in (X, Z) Plane (Daniels, 1996 and Tannous, 1987)

First, the pipe reflection is received as the antenna approaches 45-degree angle with in a vertical line passing through the center of the pipe. Streams of reflections are continuously received by the antenna until the antenna travels a twice the distance from its initial point. The apex of hyperbola representing the true depth of the pipe is formed (Sweeney, 1986 & Tannous, 1987).

<u>Electrical Properties of Earth Materials</u>

Researchers have shown experimentally that the attenuation of the electromagnetic radiation rises with frequency. This merely means that at a given frequency, wetter materials exhibit higher losses in attenuating radiation than dry materials. It is extremely important to understand the characteristics of materials as they have an effect on the attenuation and velocity of propagation (Daniels, 1996). The propagation velocity of the GPR signal is governed by the

permittivity of the material, which depends on the water content of the material. The penetration depth of the radar is inversely dependent on the conductivity of the earthen materials (Sweeney, 1986).

Two physical models have been presented by Daniels (1996) to predict the propagation of EMW in dielectric materials, which are divided into two principals: EMW theory and geometrical optics. As discussed previously, the EMW theory is employed when the materials being radiated are considered electrical insulators. On the other hand, the optical theory is more predominant to dry materials. Thus, materials that contain excessive moisture will behave as conducting dielectrics only if the water contains ions, nevertheless, natural waters contain ionic conduction to some extent and act as aqueous electrolytes (Daniels, 1996). Since water demonstrates strong influences on the electrical properties, the conductivity and the dielectric constant of a moistened material is increased by greater percentage. This may also depend on the amount of total suspended and dissolved solids present in the water, and the composition and porosity of the material (Sweeney 1986). Typical values of dielectric constants and conductivity of common material are presented in Table 4. The soil contaminated with low pH solvent, for instance acidic storm water, will practically block the radar signal.

The variability in geological conditions and in material properties causes great difficulties in predicting the propagation behavior. Any change in material properties causes propagating energy to scatter; thus, scattering becomes a function of contrast in material properties at a boundary, the spatial scale of the contrast, the angle of the propagating wave to the boundary, polarization of wave, and propagating wave's wavelength. In other words, the scattered energy

behaves as a reradiated energy from a different antenna at the interface (Olhoeft, 2003). Scattered Energy may be seen in Figure 5 previously.

It is also difficult to replicate the characteristics of a material in laboratory settings compared to in-situ conditions. Manufactured materials such as PVC, cement, concrete, etc., show difficultly in predicting propagation behavior as they exhibit both properties, electrically insulating and conducting, and their characteristics are controlled by their atomic, molecular and granular structure (Daniels, 1996).

Table 4

Dielectric Constants and Conductivity for Common Materials

Material Type	Dielectric Constant (unitless)	Conductivity (mhos/m)
Air	1	0
Asphalt	3 – 6	$10^{-3} – 10^{-1}$
Average Soil	16	$10^{-4} – 10^{-2}$
Clay (dry)	3	$10^{-2} – 10^{-1}$
Clay (saturated)	8 – 15	$10^{-1} – 1$
Concrete	6 – 8	$10^{-3} – 10^{-1}$
Granite	5 – 8	$10^{-8} – 10^{-2}$
Limestone (dry)	7 – 9	$10^{-9} – 10^{-1}$
Permafrost	1 – 8	$10^{-5} – 10^{-2}$
Sand, dry	4 – 10 (W >11%)	$10^{-7} – 10^{-3}$
Sand, saturated (fresh water)	30	$10^{-4} – 10^{-2}$
Saturated Silty Sand to Sandy Clay	10 – 14	$10^{-3} – 10^{-2}$
Water (fresh)	81	$10^{-4} – 3 \times 10^{-2}$
Water (sea)	81	4

Source: GSSI (2002)
　　　　Daniels (1996)
　　　　Sweeney (1986)
　　　　Tannous (1987)

Calibration of Depth

When the transmitted waves strikes an interface between two layers of the media, part of the waves reflect back while the remaining waves continue to transmit to the next interface; if not, the signal dies out after a certain time span. While the antenna is traversing the ground, continuous stream of reflected signals are processed and displayed by a continuous profile that features soil stratum, revealed zones, cavities, and other subsurface anomalies, such as utilities, that may are not necessarily be at the same penetrating depth. The calibration of a depth scale of the GPR profile is important as it is directly related to the time of travel and the propagation velocity of the radar signal. These are also a function of the dielectric constant and conductivity of the materials that are being investigated. Thus, the two-way travel times of the radar signal must be transformed into depth, given the propagation velocity. Assuming the earth material is homogenous, the dielectric constant may be easily obtained through which the velocity of the radar pulsation may be calculated by the following Equations (6) or (7):

$$v = \frac{c}{\sqrt{\varepsilon_r}} \tag{6}$$

or

$$v = \frac{1}{\sqrt{\varepsilon_r}} \tag{7}$$

where v = average propagation velocity of the signal [nsec/feet]

c = velocity of light [$\cong 1$ feet/nsec]

ε_r = dielectric constant of the material [unitless].

Since the velocity of light is approximately one foot per nanosecond, term c in Equation (6) may be replaced by one as given in Equation (7). The depths of several interfaces may be approximated as shown in Equations (8) or (9) if the dielectric constant of the material is known:

$$D = \frac{ct}{2\sqrt{\varepsilon_r}} \tag{8}$$

or

$$D = \frac{vt}{2} \tag{9}$$

where D = depth of the interface [feet]

$\quad\quad t$ = two-way travel time (twt) [nsec].

It is easier to determine the depth of a known object, such as locating bricks for this study, rather than an unknown object buried in the ground. Likewise, if the depth of an object is known, and the two-way travel time is measured, then velocity can be calculated by rearranging Equation (9):

$$v = \frac{2D}{t} \tag{10}$$

Likewise, the dielectric constant can be calculated by rearranging Equation (7). According to the literature and Geophysical Surveys Systems, Inc., the velocities and dielectric constants of some common earth materials are listed in Table5:

Table 5

Dielectric Constants and Propagation Velocities for Common Materials

Material Type	Dielectric Constant (unit less)	Velocity (mm/ns)
Air	1	300
Asphalt	3 – 6	134 – 173
Average Soil	16	75
Clay (dry)	3	173
Clay (saturated)	8 – 15	86 – 110
Concrete	6 – 8	55 – 112
Granite	5 – 8	106 – 120
Limestone (dry)	7 – 9	100 – 113
PVC	3	173
Sand, dry	4 – 10 (W >11%)	120 – 170
Sand, saturated (fresh water)	30	55 – 60
Saturated Silty Sand to Sandy Clay	10 – 14	95 – 173
Water (fresh)	81	33
Water (sea)	81	33

Source: GSSI (2002)
        Daniels (1996)
        Sweeney (1986)
        Tannous (1987)

<u>Penetration Depth of Radar Signal</u>

The effectiveness of the radar survey is limited by the penetrating distance into the earth as the EMW are attenuated with distance due to the geometric spreading of the signal as it travels from the antenna. The EMW are also attenuated due to the energy absorbed as the signal travels through a medium. Nonetheless, the penetration depth of the signal also depends on the conductivity of the material, which is governed by water content and salinity (Sweeney 1986). Conductivity is a function of frequency, density, and temperature of the EMW. The Equation (11) defines the relationship between conductivity and attenuation:

$$A = 12.863x10^{-8} f \sqrt{\varepsilon} \sqrt{\sqrt{1 + \frac{\sigma^2}{(2\pi f)^2 \varepsilon^2}} - 1} \qquad (11)$$

where A = attenuation [db/m]

   f = frequency of the antenna [Hz]

   $c = \varepsilon_o \varepsilon_r = 8.85x10^{-12} \varepsilon_r$

   σ = conductivity (mhos/m).

It can be noticed in Equation (11) that the conductivity of the propagating material governs the depth of the penetration of the radar pulsation. Thus, an increase in conductivity will increase in signal attenuation. For instance, sand, gravel and limestone are materials with low conductivity, which allows the radar signal to penetrate over hundred feet (Sweeney, 1986). Alternatively, if the conductivity of the soil increases drastically, and if soils contain large amounts of moisture, for which, the attenuation of the radar signal is rapid. Table 6 summarizes typical materials and associating conductivity and attenuation. From Equation (11), it is also

apprehended that low frequency of antenna attributes to low attenuation. Therefore, low frequency antennas are used to achieve higher depths while higher frequency antennas are uses for greater resolution. In this study, a 900 MHz antenna was employed for lower penetration depth.

Table 6

Conductivity and Attenuation for Common Materials

Material Type	Conductivity (mhos/m)	Attenuation (dB/m)
Air	0	0
Asphalt	$10^{-3} - 10^{-1}$	2 – 20
Clay	$10^{-2} - 1$	10 – 100
Concrete	$10^{-3} - 10^{-1}$	2 – 25
Granite	$10^{-8} - 10^{-2}$	0.5 – 5
Limestone (dry)	$10^{-9} - 10^{-1}$	0.5 – 25
Permafrost	$10^{-5} - 10^{-2}$	0.1 – 5
Sand, dry	$10^{-7} - 10^{-3}$	0.01 – 1
Sand, saturated (fresh water)	$10^{-4} - 10^{-2}$	0.003 – 0.3
Sandstone	$10^{-9} - 10^{-5}$	2 – 20
Water (fresh)	$10^{-4} - 3 \times 10^{-2}$	0.1
Water (sea)	4	1000

Source: GSSI (2002)
       Daniels (1996)
       Sweeney (1986)
       Tannous (1987)

CHAPTER 4

FIELD EXPLORATION

Zeng and McMechan (1997) stated that the qualifications of the GPR targets have had its limitations through research because of the lack of controlled experiments. It is rather difficult to perform borings at numerous locations or wait until the City of Orlando removed the asphalt from the proposed street to validate the GPR profile readings. For a better understanding and interpretation of data produced by GPR profiles, the research team built a brick base test area at UCF's Circular Accelerated Test Track (CATT). The construction of test pit and lines of survey are presented in this report.

Field investigations in Downtown Orlando were conducted according to the priority (from major city route to minor) and schedule of brick removal. Thus, the order was Summerlin Avenue first, Cherokee Drive next and Church Street being the last.   Locations of the investigation sites are shown in Appendix A.   GPR was used to survey these city streets for the location of bricks suspected to be buried beneath the existing asphalt. The survey area and survey traverses are presented in detail in this chapter.

Construction of Test Pit

First, several types of bricks were acquired for the construction of test pit. Among these included three types of bricks: drainage bricks, garden bricks, and heavy-duty construction clay bricks. The reason for using a variety of bricks was mainly that information on the existing bricks was not provided by the City of Orlando. In addition, this was done to ensure proper detection and explanation of brick for the Orlando streets. An area perpendicular to the existing

lime-rock base test track and adjacent to the test track gate was chosen for the construction of the test pit. This gave an easy excess for the future paving process.

The test pit area was constructed approximately 10 feet by 3 feet. From the edge of the existing lime-rock based pavement, the heavy weight clay bricks were laid for an estimated of 4 feet in length. These bricks were used for the construction of buildings. Following the heavy weight clay bricks, commercial drainage bricks, provided by Rinker Materials Corporation, were laid for another four feet. Drainage bricks with three oval holes were used for an easy flow of storm water. Drainage bricks are photographed as seen in Figure 9 (a). The last 2 feet of bricks laid were the lightweight garden purchased locally at Lowe's Home Improvement store. Figures 9 (a) – (j) illustrate the sequence of the test pit construction.
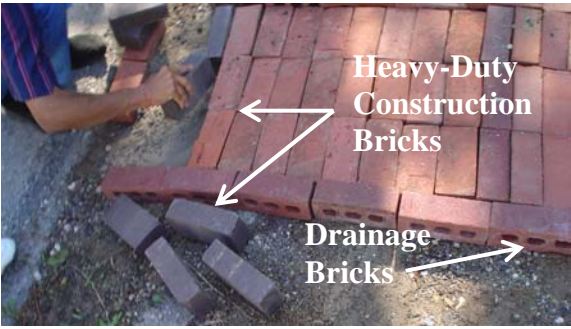
(a)
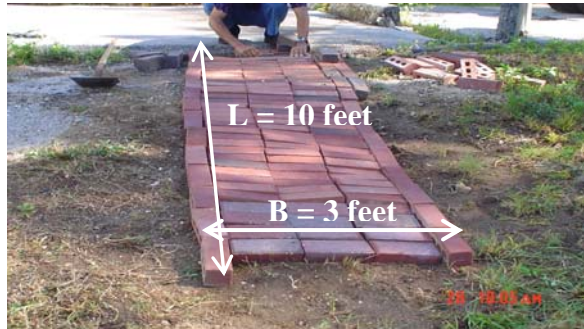
(b)
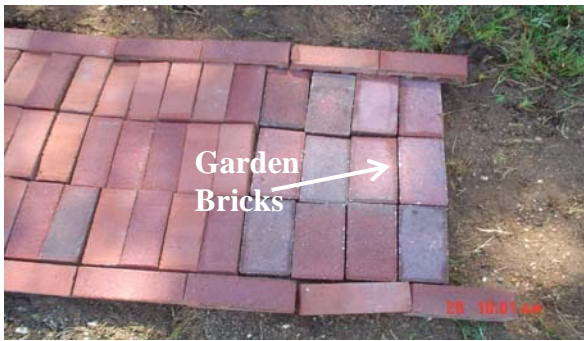
(c)

(d)

(e)

(f)

(g)

(h)

(i)

(j)

Figure 9. Construction of Test Pit

The asphalt was shoveled and hand poured, and roller compacted by the Orlando Paving company on April 28, 2004. The initial leveling of it was done by the hand as seen in Figures 9 (i) and (j). For asphalt compaction, the paving company employed a lightweight asphalt Wacker brand vibratory double drum roller (Model RD 11) with a water sprinkling system. This system is able to compact up to 4 inches of asphalt. The thickness of the asphalt lying on the bricks was approximately 3.5 inches.

GPR Survey of Test Pit

The field GPR survey of the test pit consisted of several GPR traverses on the brick base asphalt as well as the existing limerock based asphalt pavement and the bridge deck. The location of the test pit is presented in the Appendix A. The test pit GPR profiles are presented and discussed in Results of Study in Chapter 5. The distance between each mark on the GPR profile was spaced with 10 feet, typically. The 900 MHz antenna was hand-pulled in all traverses at a walking speed. The maximum depth of 1 foot of GPR penetration was calibrated based on a range of 6 to 13 dielectric constant and saved as a control program. A few vertical dashed lines on the GPR profiles reflect the changes in ground surface anomalies, such as bricks, concrete, grass, manholes, etc. The double-dashed or triple-dashed vertical lines show the beginning and end of each traverse.

In detection of asphalt concrete using GPR, researchers have used a dielectric constant of 13, and the recommended dielectric constant of asphalt by GSSI Inc. was six. Therefore, GPR profiles with dielectric constants of 6 through 13 were also collected, which are also discussed thoroughly in Chapter 5. Seven traverses were preformed with dielectric constants of 6 through 13. Furthermore, three additional profiles were obtained by pulling 900 MHz antenna at slow and faster walking pace, and one with a 15 ns two way travel time or simply 2 feet of calibrated depth. GPR survey on test pit is shown in Figures 10 (a) – (c). A typical GPR profile of brick base at test pit is shown in Figure 11.

(a)

(b)

(c)

Figure 10. GPR Survey of Test Pit
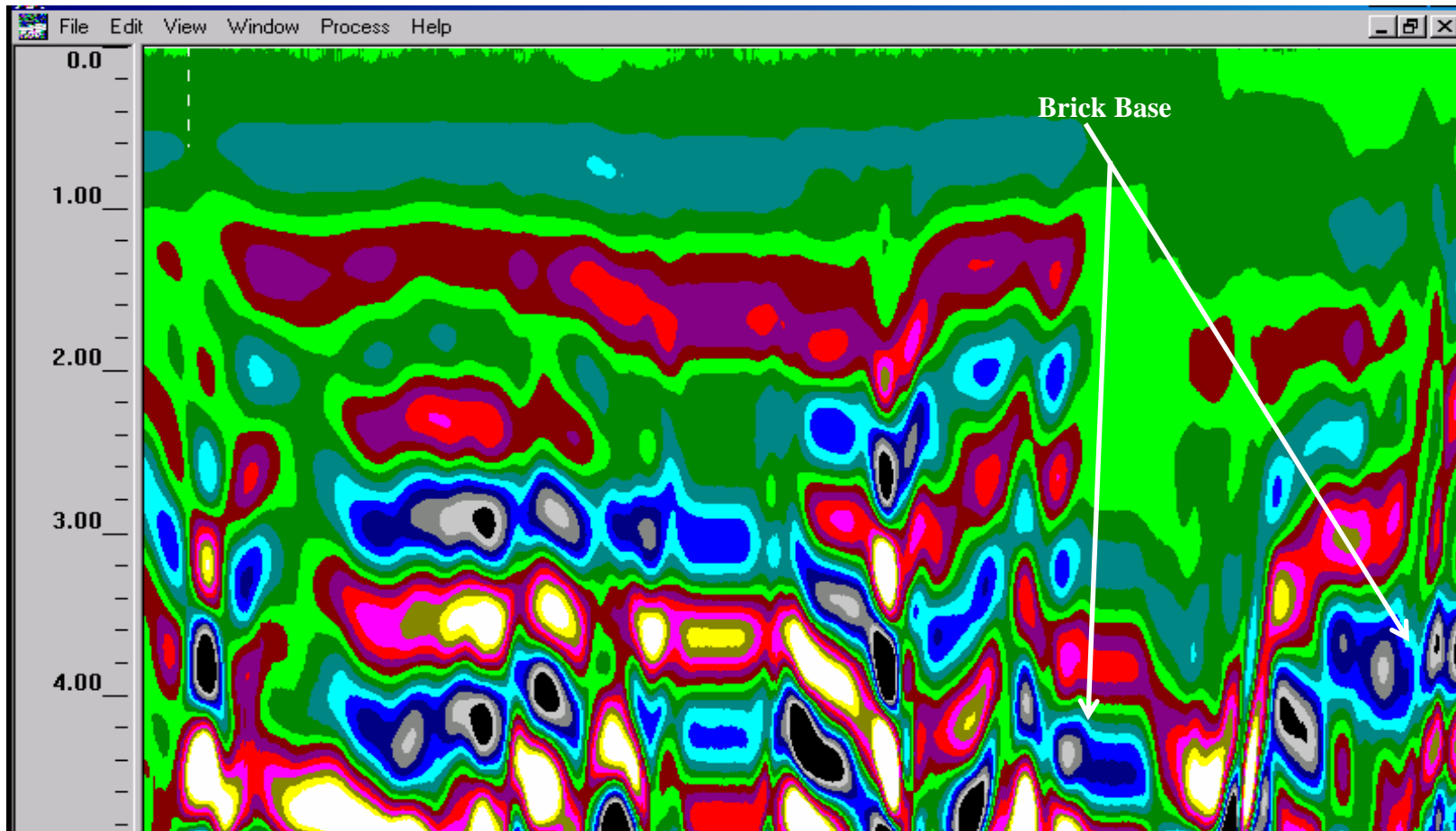
Figure 11. GPR Profile of Brick Base at Test Pit

44

Site Description of Downtown Orlando

Mr. Richard Howard, City Engineer of Orlando selected three city streets located in Downtown Orlando for the GPR survey. These streets are Summerlin Avenue, Cherokee Drive, and Church Street. The first line of GPR survey was conducted on May 5, 2004. The survey began from the new section of asphalt at the intersection of Cherokee Drive and South Summerlin Avenue to the new section of asphalt at the intersection of Woodlawn Boulevard and South Summerlin Avenue, on South Summerlin Avenue. The approximate distance was measured to be 380 feet with 810 feet of perimeter and acreage of 0.22. The traverses of GPR survey on Summerlin Avenue is presented in Figure 12.

The second street of survey for potential brick base was Cherokee Drive on May 7, 2004. The survey began (at the curb) at the intersection of South Summerlin Avenue and Cherokee Drive on Cherokee Drive until the stop sign that merged the traffic, on Delaney Avenue as shown in Figure 13. The total area surveyed was approximately equals to 1.51 acres with a length of 2200 feet and a perimeter of 4,505 feet. Additional, GPR survey was conducted again on May 28, 2004 for a better interpretation of GPR profiles and flawless location of buried bricks.

A map of Church Street proposed for GPR survey is shown in Appendix A. The GPR survey took place from Church Street approximately at South Terry Avenue to South Westmoreland Drive on Church Street starting at the center turning lane, and then westbound and eastbound Church Street. Additional traverses were surveyed three feet from the edge of pavement on Church Street for westbound and eastbound lanes. Figure 14 shows a detailed

view of lines of survey. A total of 1.54 acres, 3,966 feet perimeter, and approximately 2,230 feet in length were covered in the survey.

GPR Survey Layout

The field exploration survey consisted of eight GPR traverse on Church Street on May 7, two GPR traverses on Cherokee Drive on May 5 and 3 GPR traverses on May 28, and 3 on South Summerlin Avenue on May 5. The locations and directions of streets are shown in Appendix B. The paint was sprayed every 10 feet spacing on the streets for calibration of distances on the GPR profiles. Again, for all GPR survey, the penetration depth was calibrated to be a maximum of 1 foot. During the survey, the 900 MHz antenna was hand-pulled for all traverses at a walking speed. The vertical dashed lines on the GPR profiles reflect the 10 feet distance marked on the streets. The double-dashed or tripled-dashed vertical lines show the beginning and end of each traverse.

SUMMERLIN AVENUE

New Asphalt

Woodlawn Boulevard

South Summerlin Avenue

NOT-TO-SCALE

2

Cherokee Drive

South Summerlin Avenue

1

3

New Asphalt

Survey of Traverses

Start point

End point
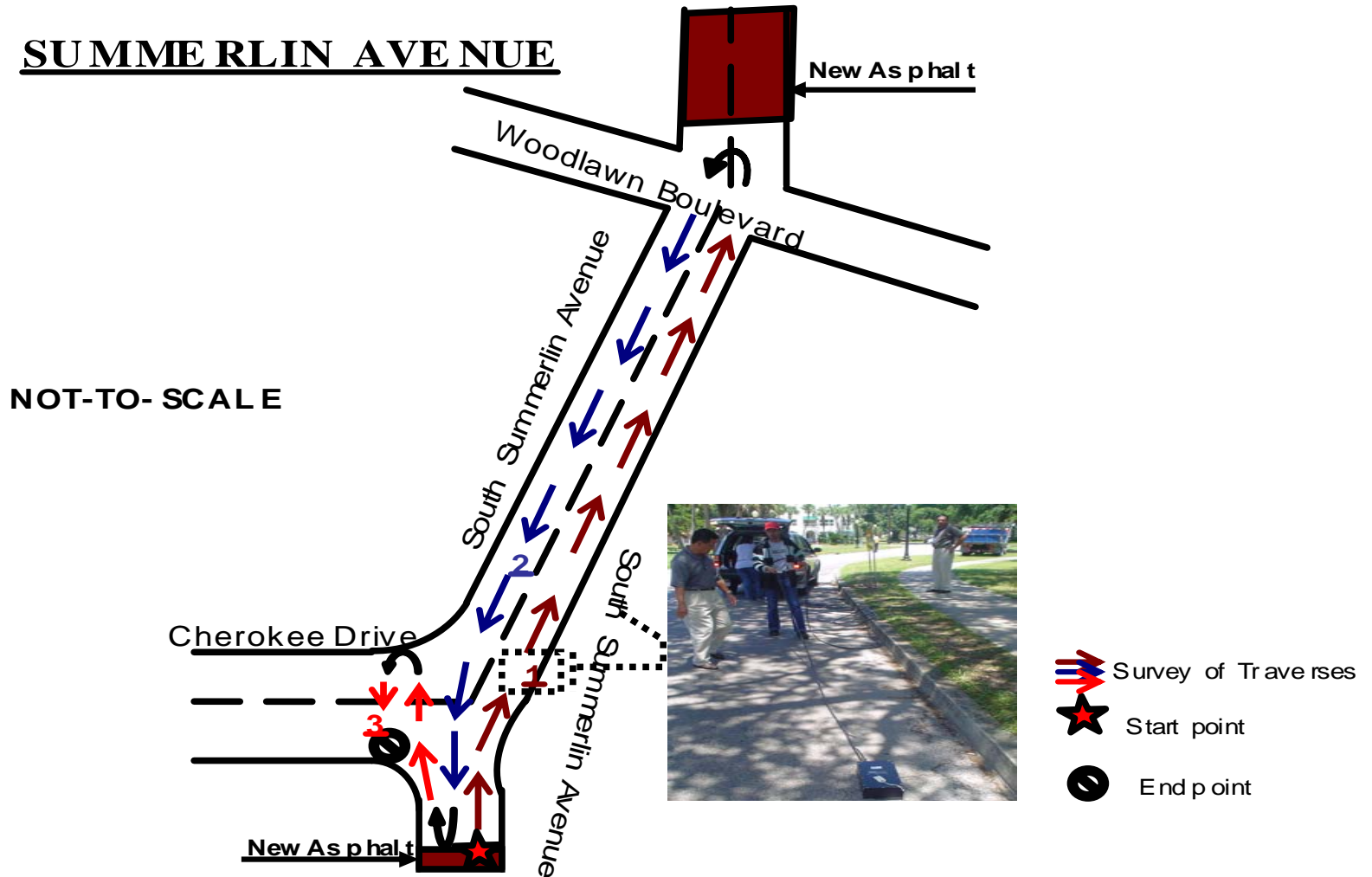
Figure 12. Traverses of GPR Survey along Summerlin Avenue

Figure 13. Traverses of GPR Survey along Cherokee Drive

CHURCH STREET

South Westmoreland Drive

S Paramore Avenue

South Terry Avenue

3

1

Church Street

2

4

3 ft

5

Survey
Traverses

Start point

End point

NOT-TO-SCALE
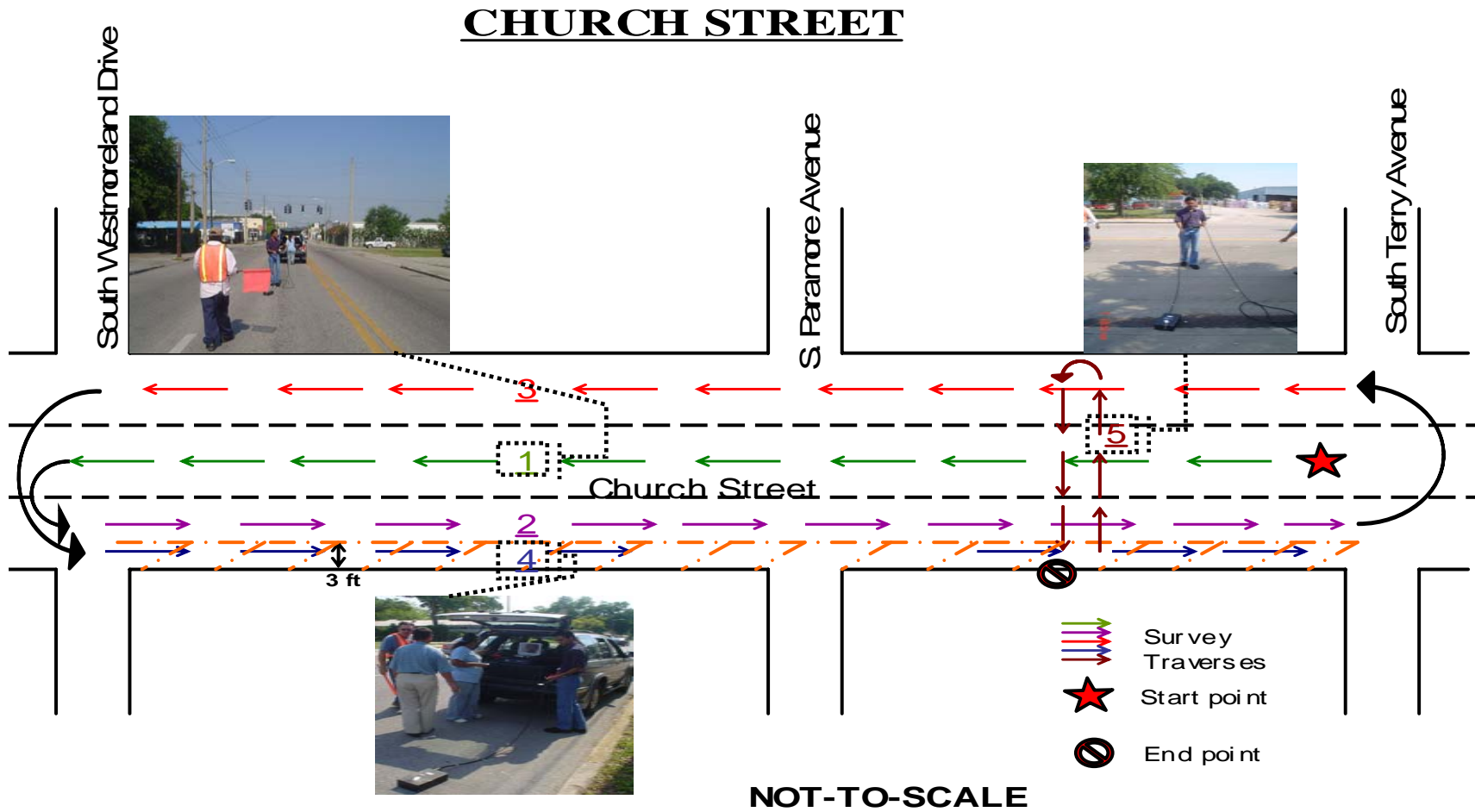
Figure 14. Traverses of GPR Survey along Church Street

Meteorological Conditions for Downtown Orlando

The site of interest lies in a subtropical region characterized by warm, humid summers and mild, dry winters. Generally, some rainfall occurs during most months of the year; nonetheless, excessive percent of rainfall occurs between June and October. Most of the summer rainfall is in the form of afternoon thundershowers and the occasional winter showers are generally associated with cold fronts. Due to the heavy storm runoff, some base materials at certain sections might be washed away, which may cause the detection of brick from GPR profile a somewhat difficult to interpret.

The penetration capabilities of GPR signals depend highly on the frequency of the antenna and the electrical properties of the earth materials, which are depended of atmospheric conditions. Materials with high conductivity such as clayey soils may drastically reduce the penetration depth. An increase of moisture content and looseness of soils will greatly increase both, the conductivity and dielectric constants, and thus, decreases the propagation of penetration of the signal. Therefore, GPR penetration will be limited in loose saturated sand. GPR penetration also decreases as chemical intrusion or mineralization increase in the soil-water system.

Cored Pavement Components

At the time of GPR survey on the City streets, boring test were not performed nor was any asphalt removed to validate GPR profiles. The process of removing asphalt was not difficulty, but rather, time consuming. The following steps were taken by the city to bring back the brick roads:

50

1. First, the asphalt was removed by heating at very high temperatures and plowing the asphalt using a Volvo manufactured scraping truck.

2. Then, the bricks were removed by fully restoring its initial integrity,

3. The streets where then leveled, if necessary, by reusing the existing subgrade material,

4. Lastly, the bricks were restored on the City streets.

The sequence of restoration process of brick roads were based on the priority of service, major to minor routes.

South Summerlin Avenue as given the first priority as it served as a major route through the downtown area. The process of brick removal began on May 18, 2004 on this street. Photographs of asphalt remover for Summerlin Avenue are shown in Figures 15 (a) – (d). Following Summerlin Avenue, restoration of bricks resumed on Cherokee Drive starting mid July, and Church Street, for which was unannounced to the research team at the University of Central Florida.

| (a) | (b) |

<div align="center">(c)</div>

<div align="center">(d)</div>

Figure 15. Removal of Asphalt on Summerlin Avenue

Lake Eola Heights was one of the many neighborhoods involved in the "Neighborhood Horizon program" that included a section of North Summerlin Avenue. Figure 16, adapted from the city of Orlando, illustrate some of the issues and ideas identified for improvements by the residents of Lake Eola Heights. The Orlando official did not provide a similar plan for the streets surveyed mentioned in this report.
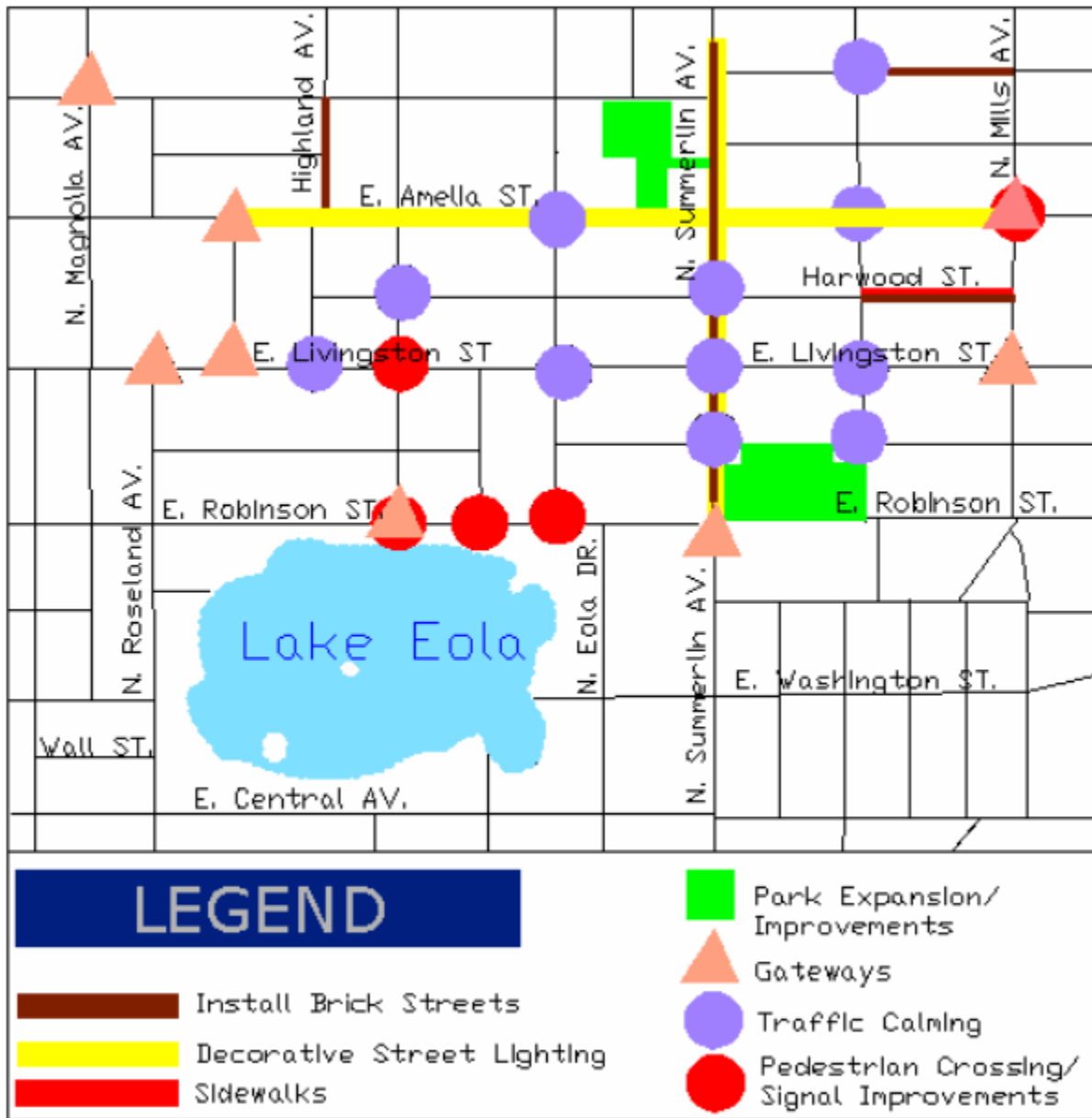
Figure 16. Neighborhood Horizon Program for Lake Eola Heights (adapted from Lake Eola Heights, 2002)

CHAPTER 5

RESULTS OF STUDY

The field investigations were conducted at the test track and through the selected city streets of Orlando. All GPR parameters were kept consistent for all profiles; use of 900 MHz antenna traveling with a consistent walking speed. Using factory settings, the dielectric constant for all readings was reserved as 6, and the transmit frequency was 50 KHz. The two-way-travel-time was set to be 5 ns, not a program setting. The findings of the survey include identification of brick base and non brick base areas, and subsurface anomalies. Due to the gigantic size of the radar profiles, some selected sections of the profiles are appended. The interpretation of the distinguishing bricks and other subsurface conditions are reported to the best of the abilities.

Test Track GPR Profiles

The several traverses were performed at the test-pit and over the existing circular accelerated test-track. Figure 17 and 18 are GPR profiles from test-track also presented in Appendix A. The top most layer of a solid and continuous band is the transmitted pulsations that traveled through the receiver and served as time reference in the units of nanoseconds (ns). The first solid band in Figure 17 is air, or the distance between the transmitting device that is mounted at the center, inside the antenna and asphalt surface. This is followed by two reflected bands that appear for the same interface. The first layer is the surface of the asphalt layer, while the second layer is the bottom of asphalt. The fourth and the fifth fatal bands reflect the lime rock layer. The fifth band clearly depicts the lime rock coloration of yellow. The sensitivity of the antenna was clearly demonstrated in this figure as a small puddle of water on the asphalt

54

layer is detected. Water is a highly conductive material as compared to asphalt. It may also be seen in Figure 17 that high conductive materials produce strong and dark amplitude reflections of the water puddle on the profile.

Figure 18 is partial profile of the second area of survey, where the asphalt is overlying the brick base asphalt constructed predominantly for the project. This was the basis of the superlative interpretation of the detection of clay bricks underneath the asphalt. Similar to Figure 17, the first band of dark green is air, the second and the third bands represent are the surface and bottom layers of the asphalt. The fourth and the fifth fatal bands reflect of the brick layers. One of the major differences between the asphalt and brick layers is that the state of the profile being discontinuous or broken bands from the bricks that are individually distinguishable.

The multiple bands are caused by oscillation of the pulse reflections between two interfaces, such as the asphalt and bricks or asphalt and limerock base. The oscillation effect is to limit the ability of the system to distinguish between two closely spaced interfaces that lie within two feet of each other. Thus, the reflection signals for both interfaces are superimposed on each other. The interface subsequent to the brick base represents soil or the subbase layer that is discontinuous, indicating a break in the layer.
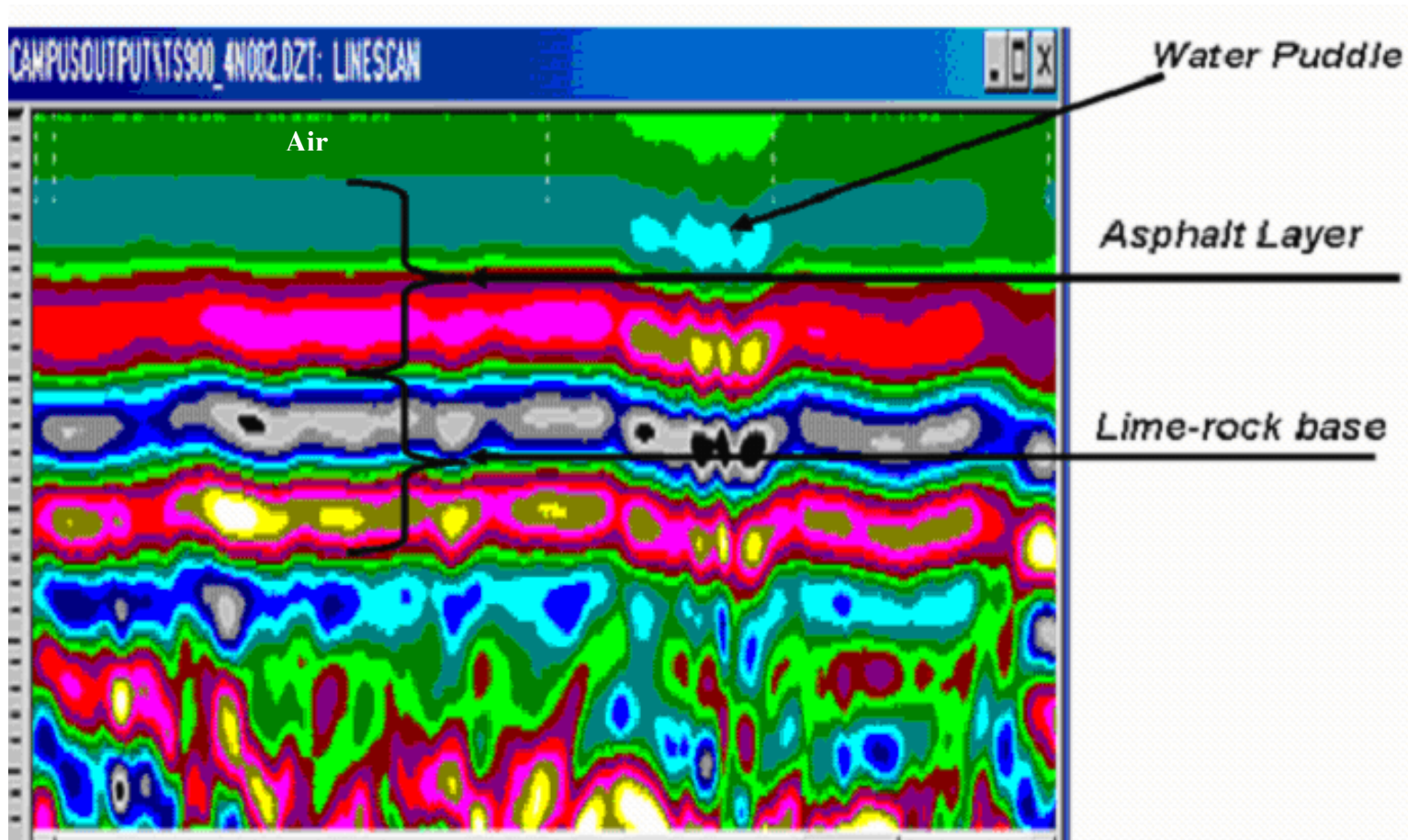
Figure 17. GPR Profile from Lime Rock Base Pavement at Test Pit
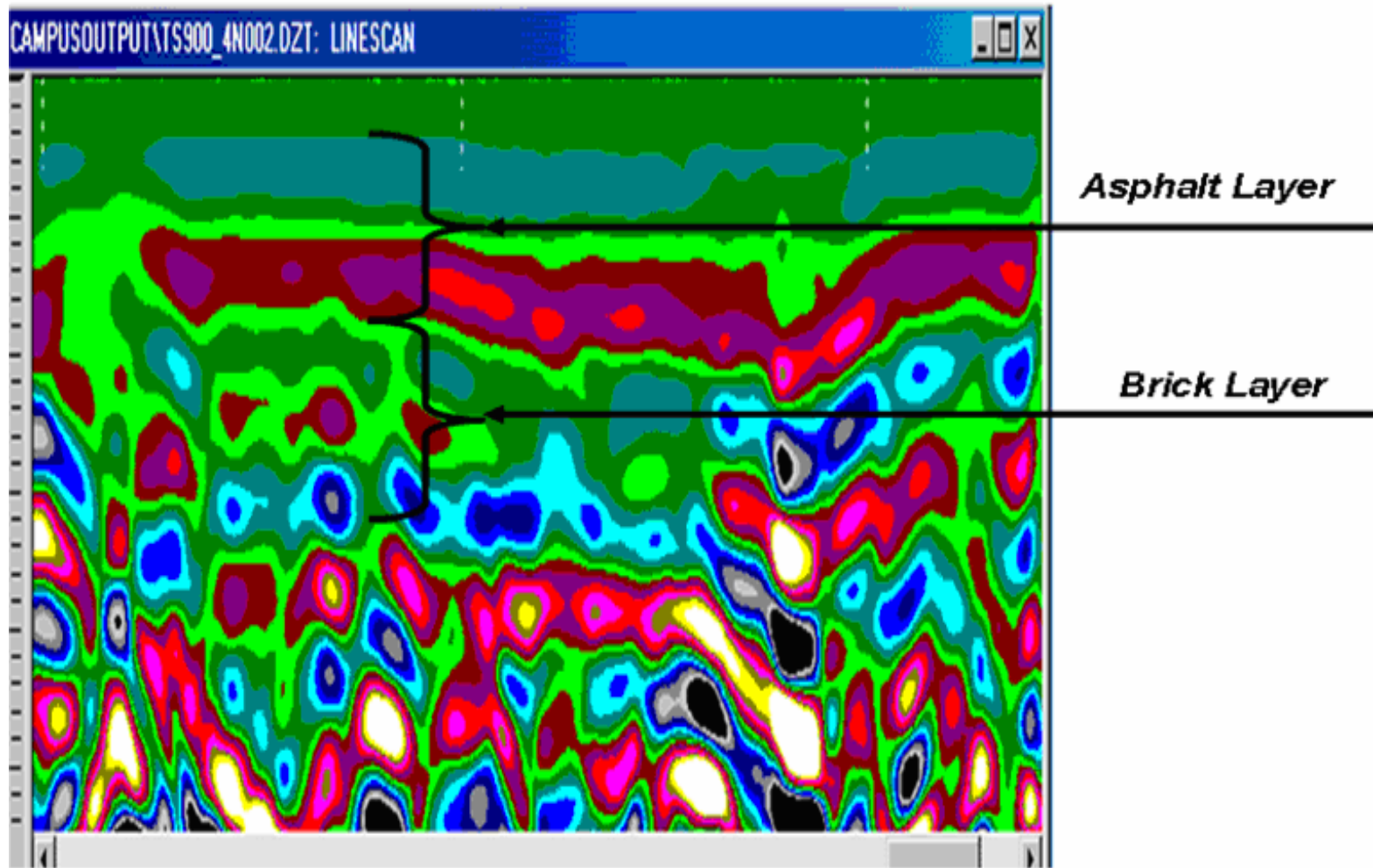
Figure 18. Pavement Profile with Brick Base—Circular Accelerated Test Track

57

Variation of Dielectric Constants and GPR Profiles

From the literature, it was revealed that many researchers adopted a dielectric constant of 13 to evaluate asphalt concrete. However, GSSI recommended the use of dielectric constant of 6 for asphalt concrete. In order to have a better interpretation of the true profiles, seven more traverses were preformed using dielectric constants of 6 through 13 as seen in Figures 19-26. Furthermore, three additional profiles where collected with pulling of 900 MHz antenna at slow and faster walking pace (Figures 27 and 28), and one with a 15 ns two way travel time for 2 feet of penetration depth (Figure 29).

By closely observing the first seven profiles, it is easily seen that GSSI recommended dielectric constant of 6 was indeed the best choice. It is also observed that as the dielectric constant increased, the capability of the radar system to capture and produce distinguishable image of buried anomalies was dissipated. By carefully comparing all seven profiles, it was concluded to use the dielectric constant of 6. Pace of walking as pulling the antenna also had significant effect on the GPR profiles, as is seen in Figures 27 and 28. The faster or normal walking speed produces a profile with individualized bricks, which is not observed in the slower speed. In this case, the brick signals are elongated giving no indication of individuality. It was also observed that a range of 5-7 ns or 1.02 to 1.45 feet of penetration depth gave a better sense of location bricks in GPR profiles.
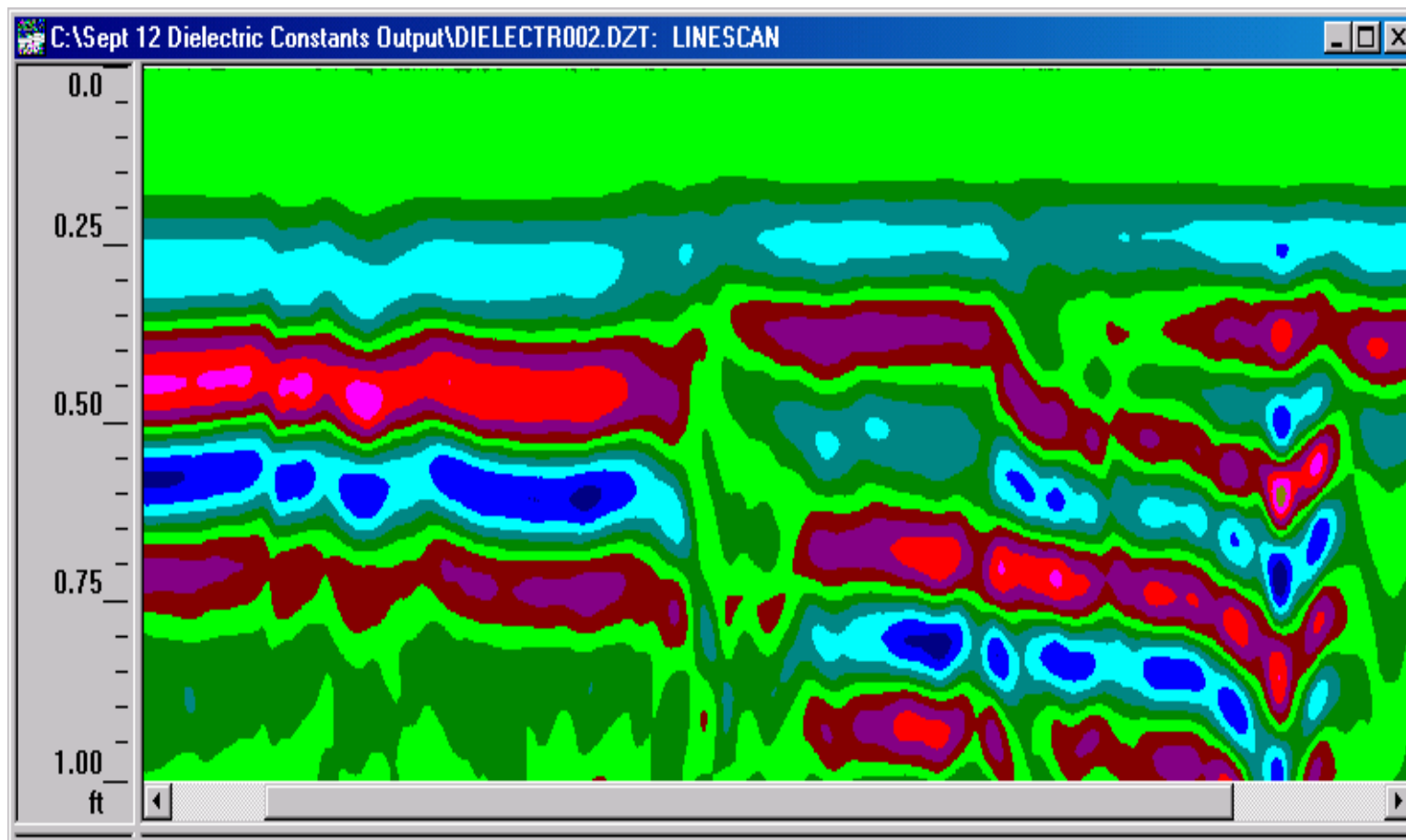
Figure19. GPR Profile of Test Pit using 900 MHz antenna with Dielectric Constant of 6
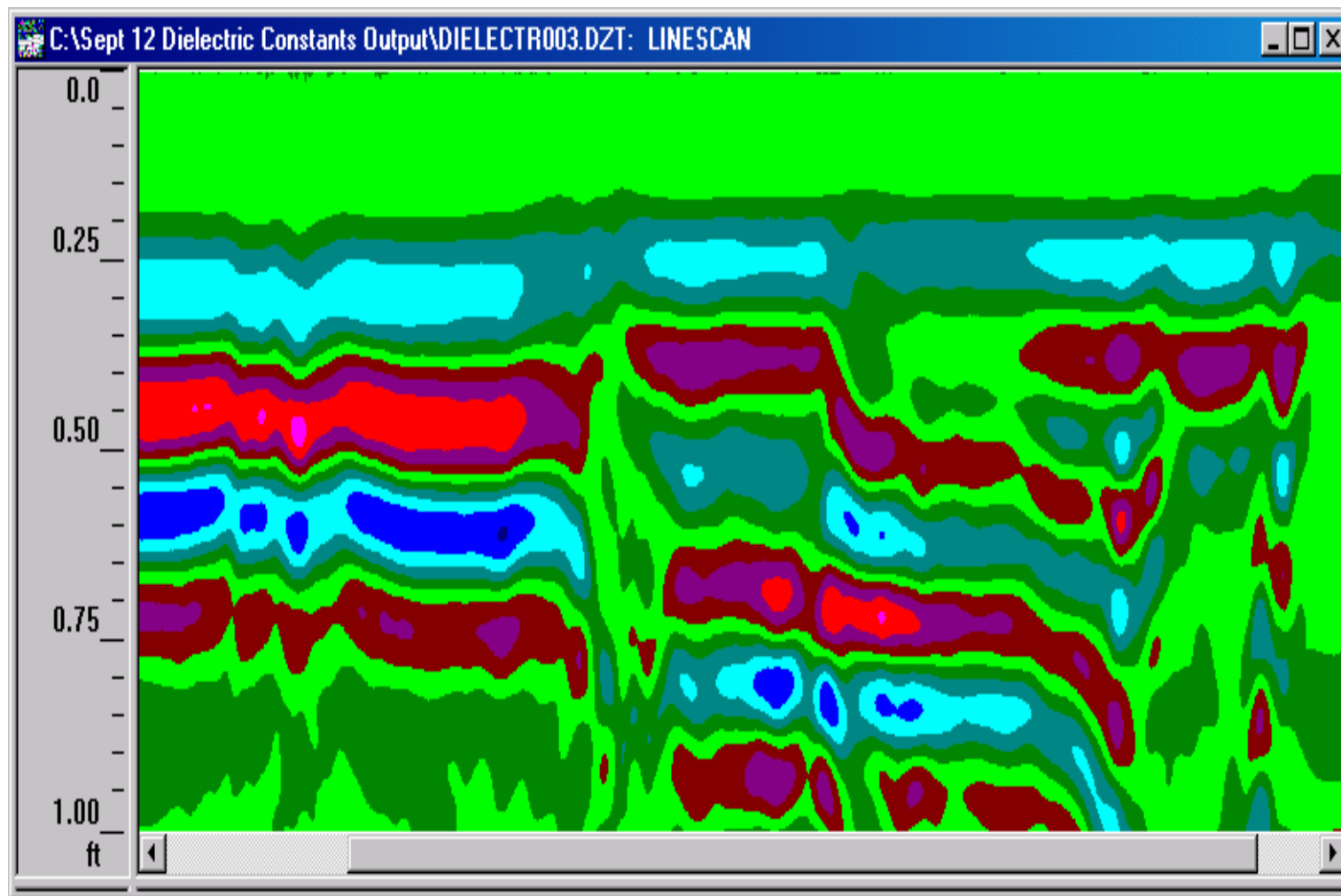
Figure 20. GPR Profile of Test Pit using 900 MHz antenna with Dielectric Constant of 7
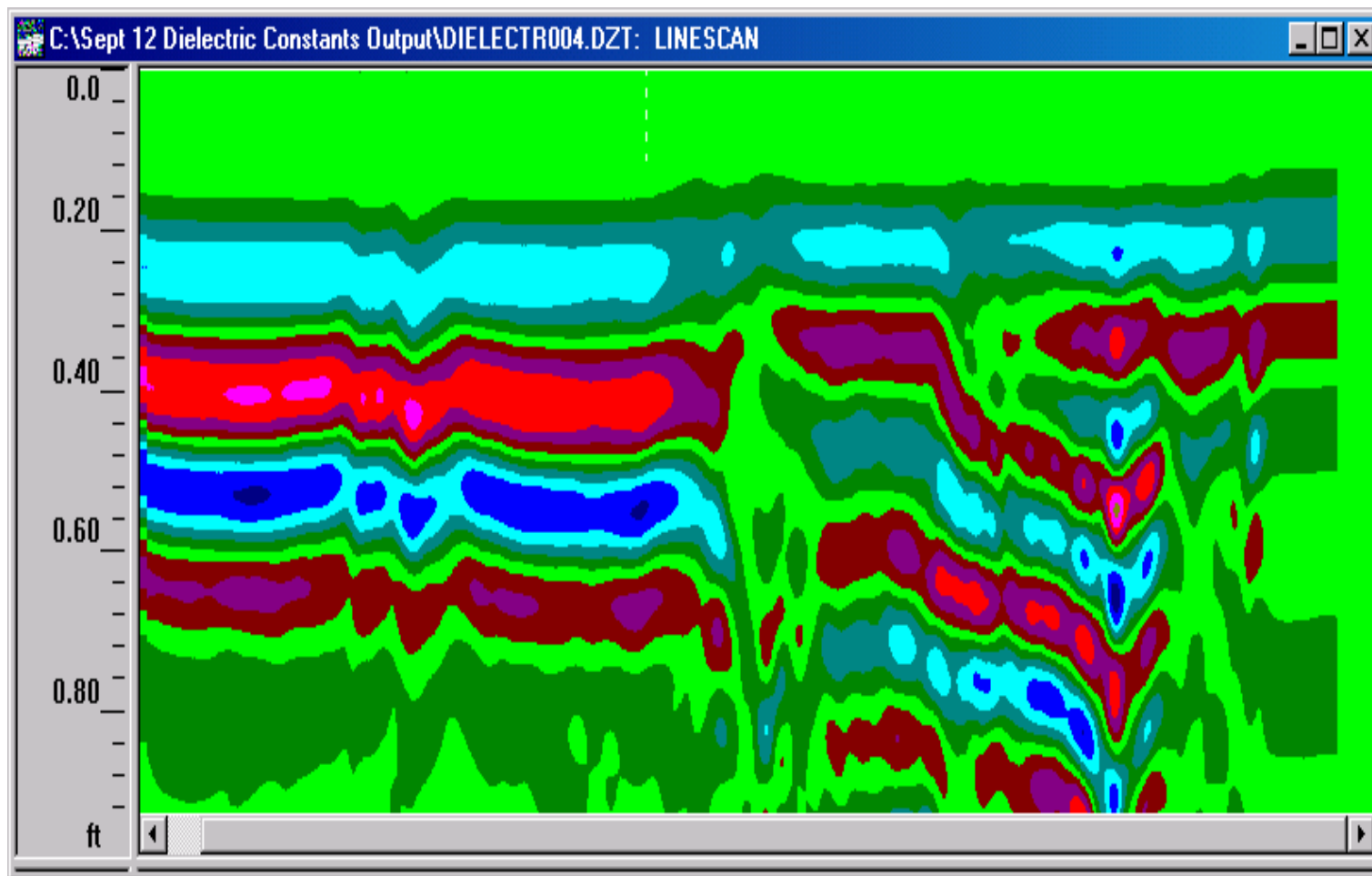
Figure 21. GPR Profile of Test Pit using 900 MHz antenna with Dielectric Constant of 8
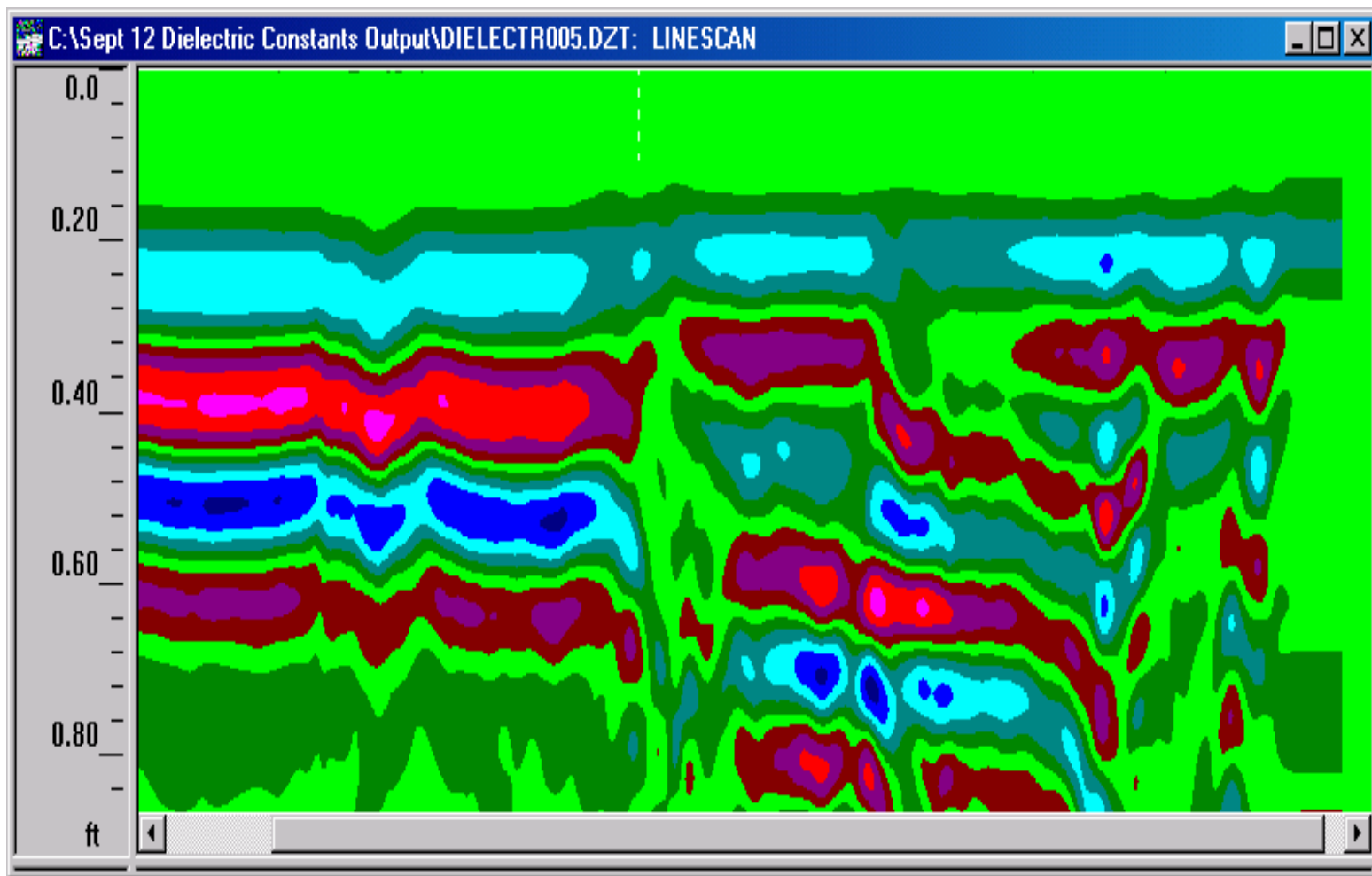
Figure 22. GPR Profile of Test Pit using 900 MHz antenna with Dielectric Constant of 9

62
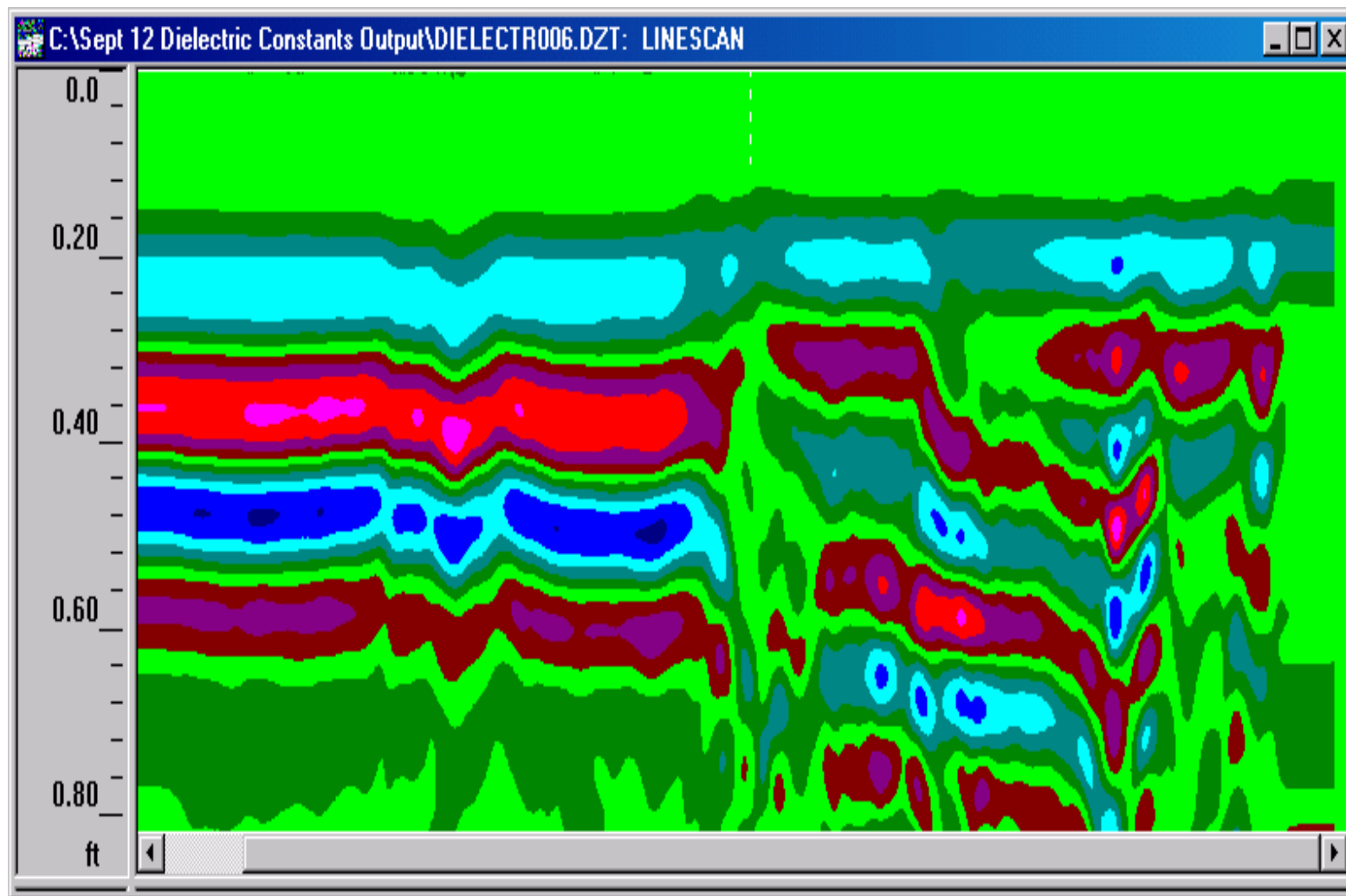
Figure 23. GPR Profile of Test Pit using 900 MHz antenna with Dielectric Constant of 10

63
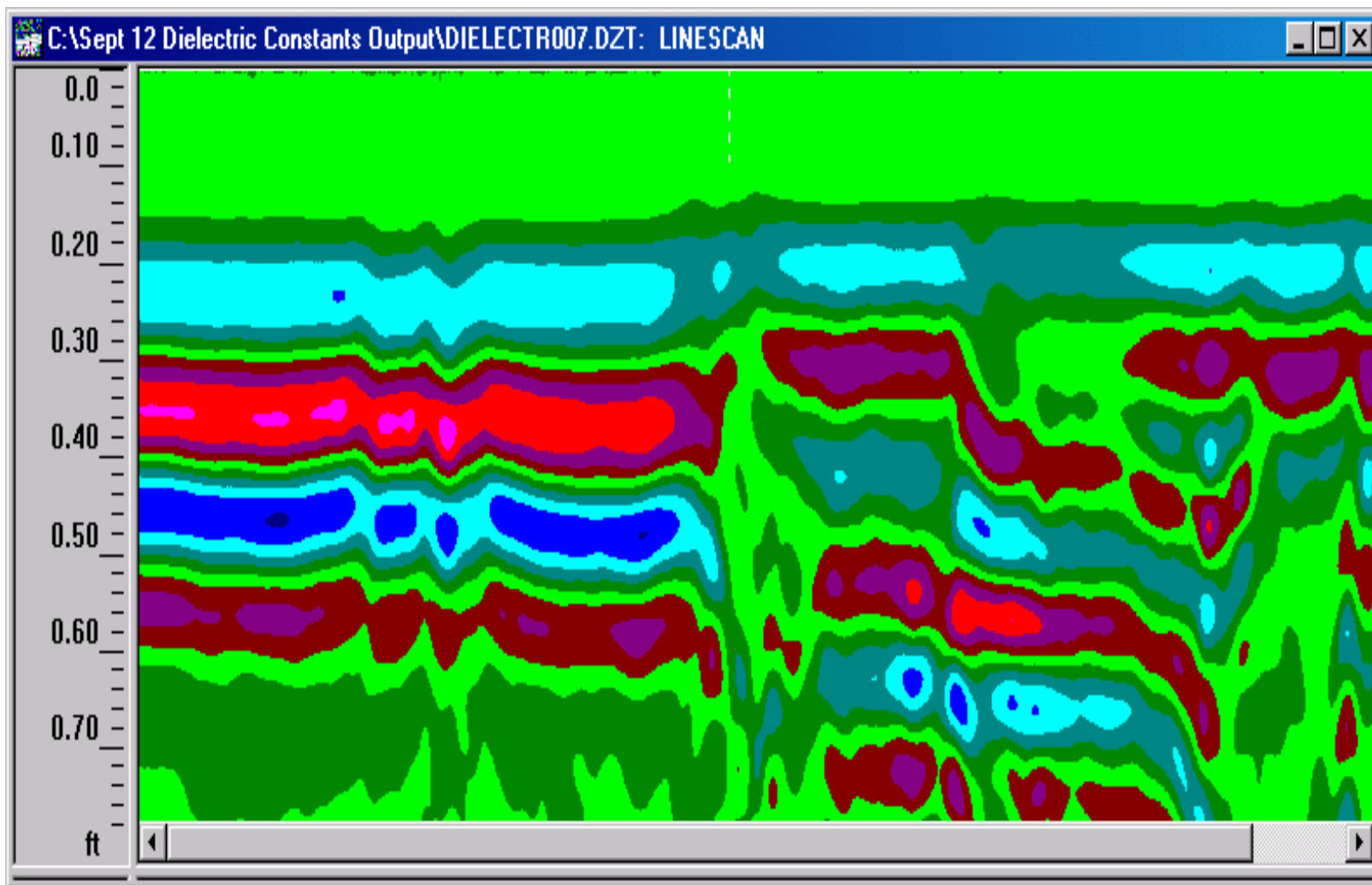
Figure 24. GPR Profile of Test Pit using 900 MHz antenna with Dielectric Constant of 11

64
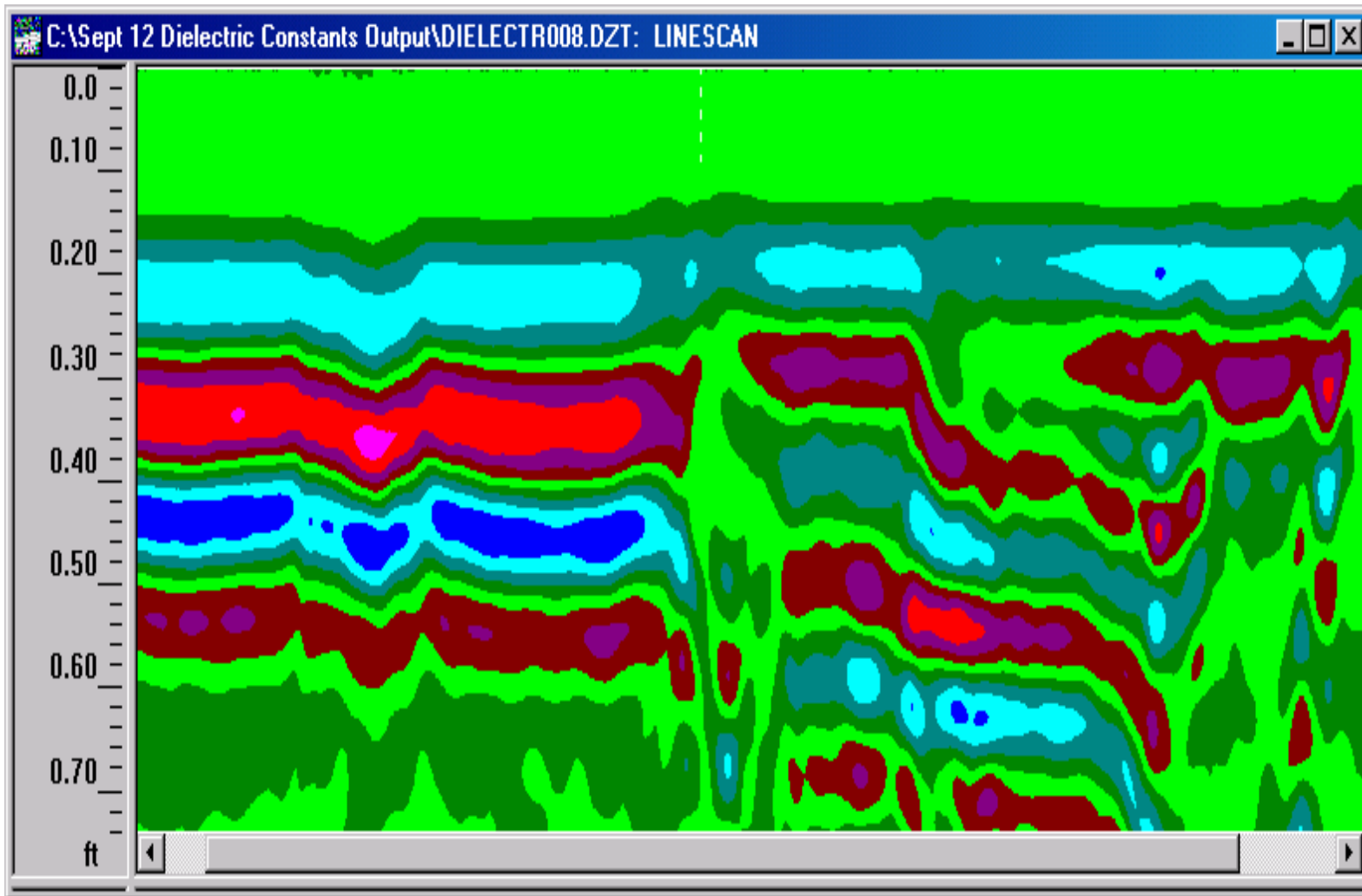
Figure 25. GPR Profile of Test Pit using 900 MHz antenna with Dielectric Constant of 12

65
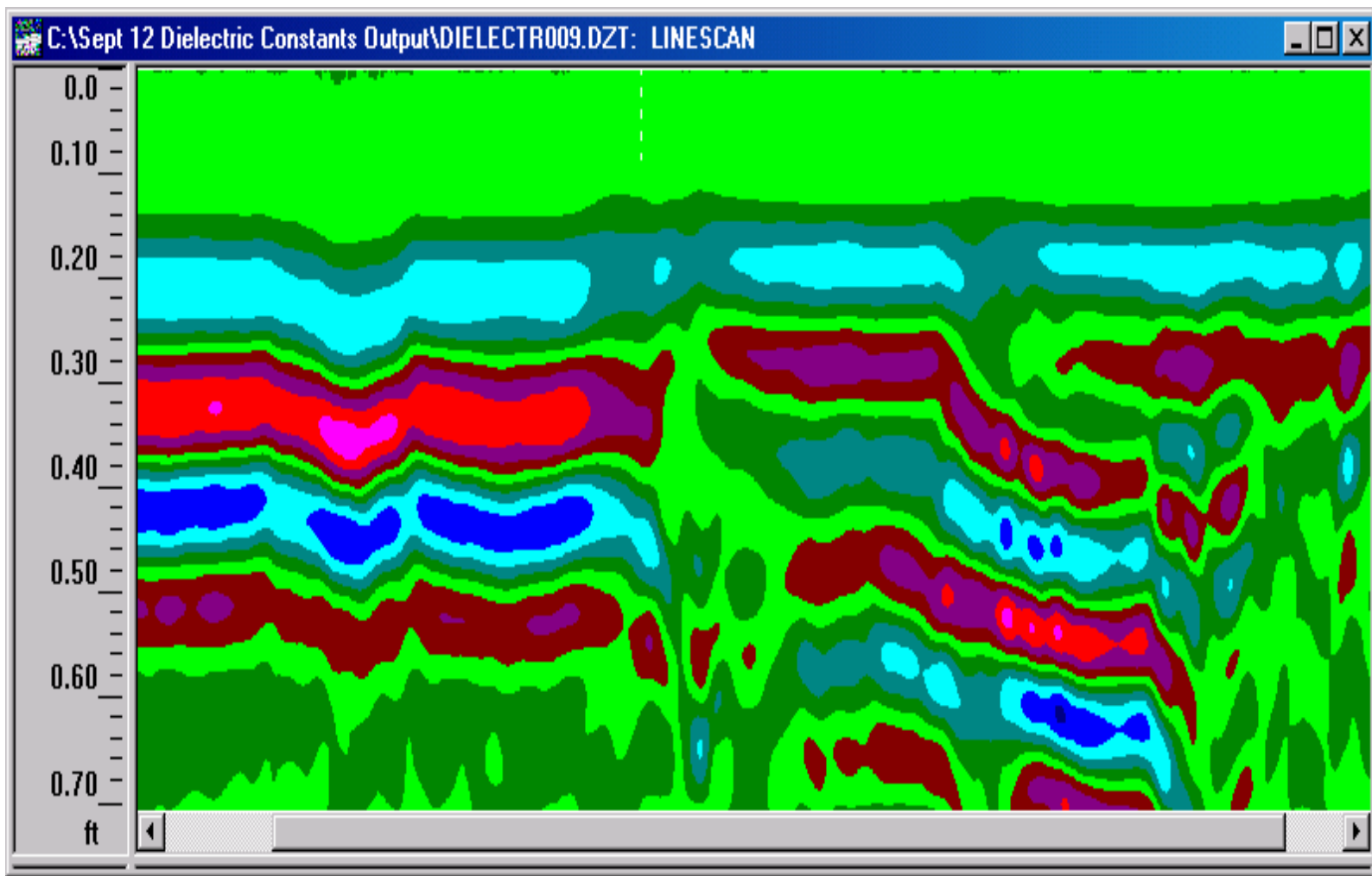
Figure 26. GPR Profile of Test Pit using 900 MHz antenna with Dielectric Constant of 13

66
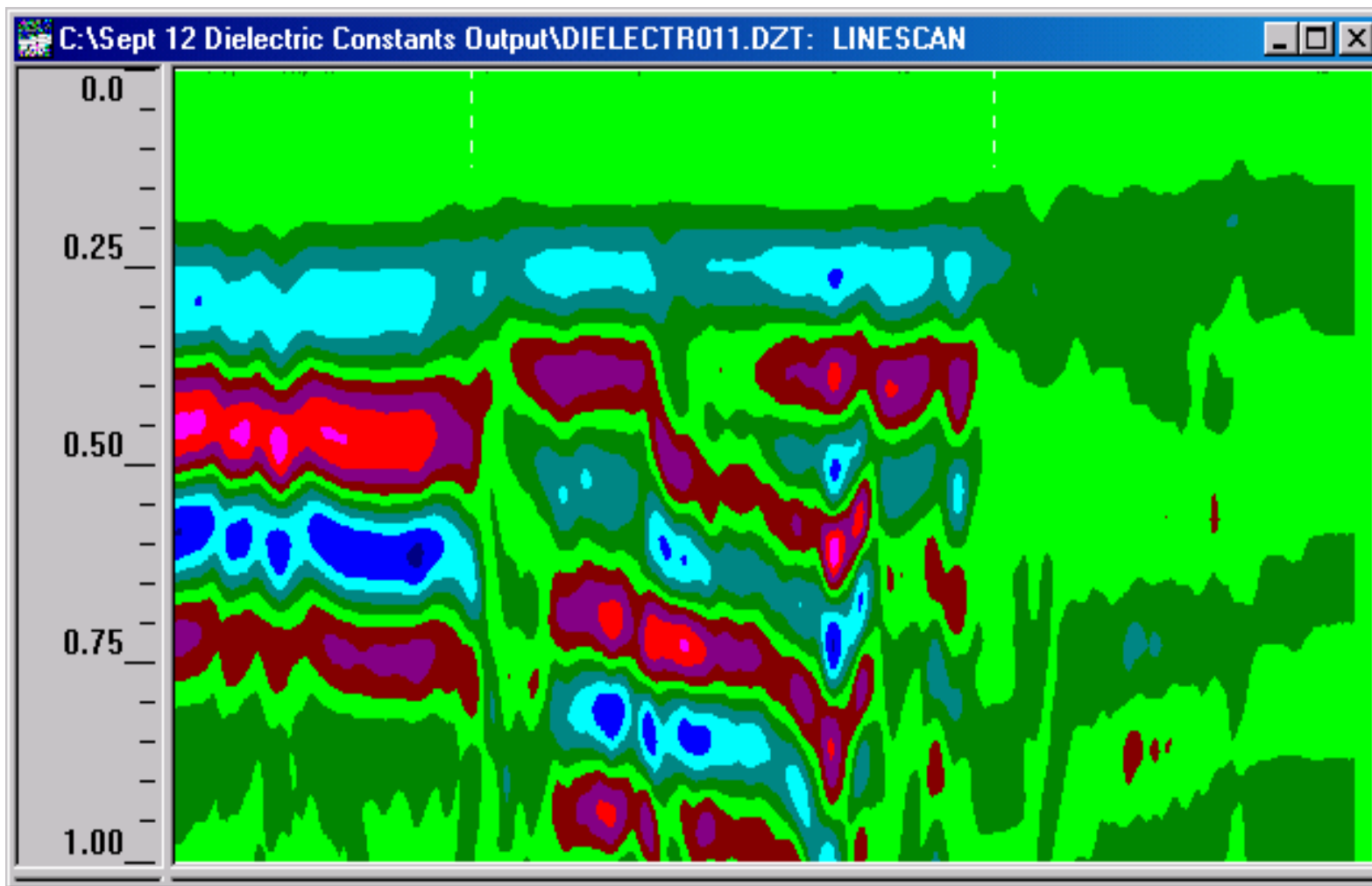
Figure 27. Profile of Test Pit using 900 MHz antenna with Dielectric Constant of 6 at fast walking speed

(a)

68
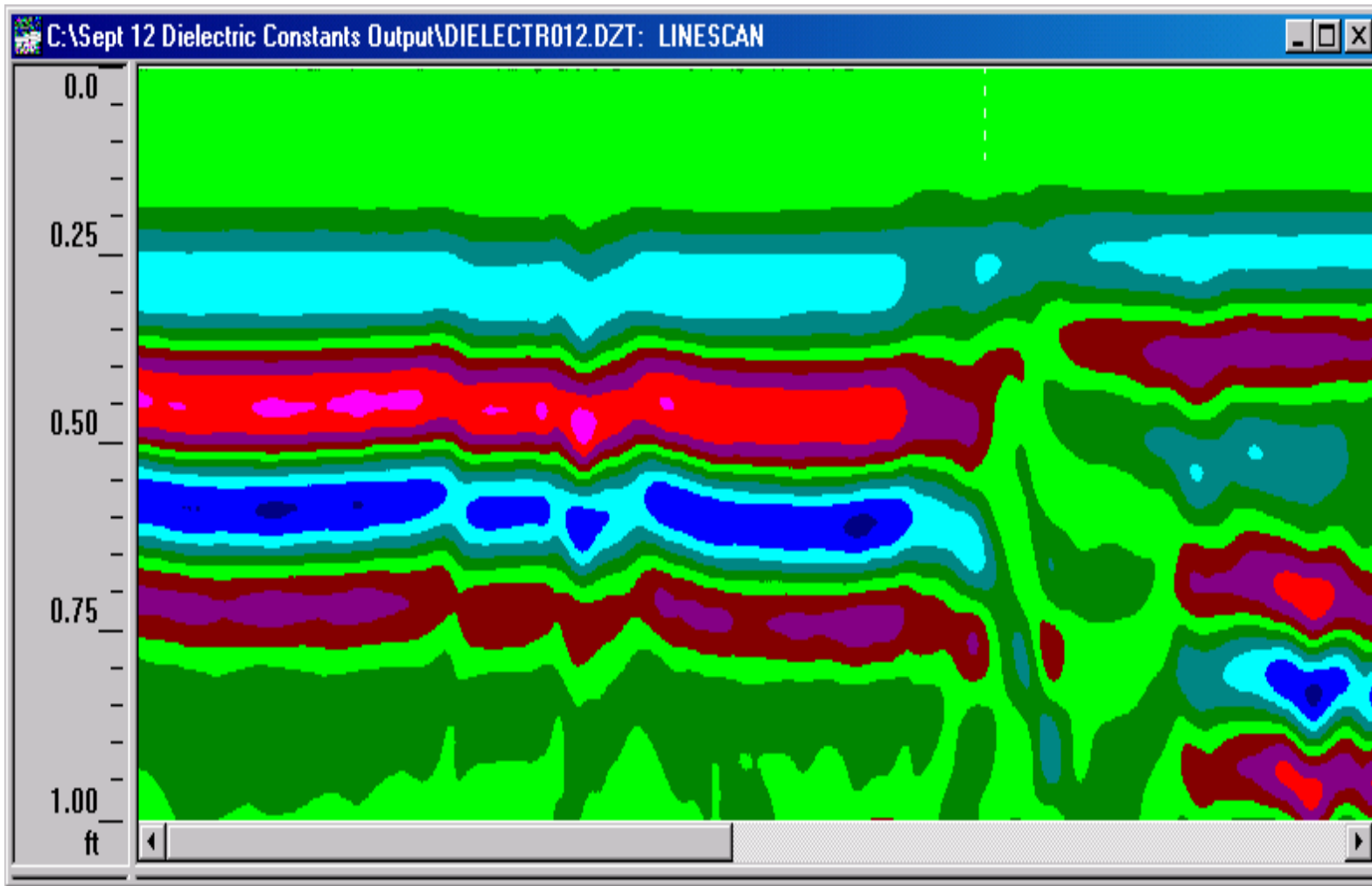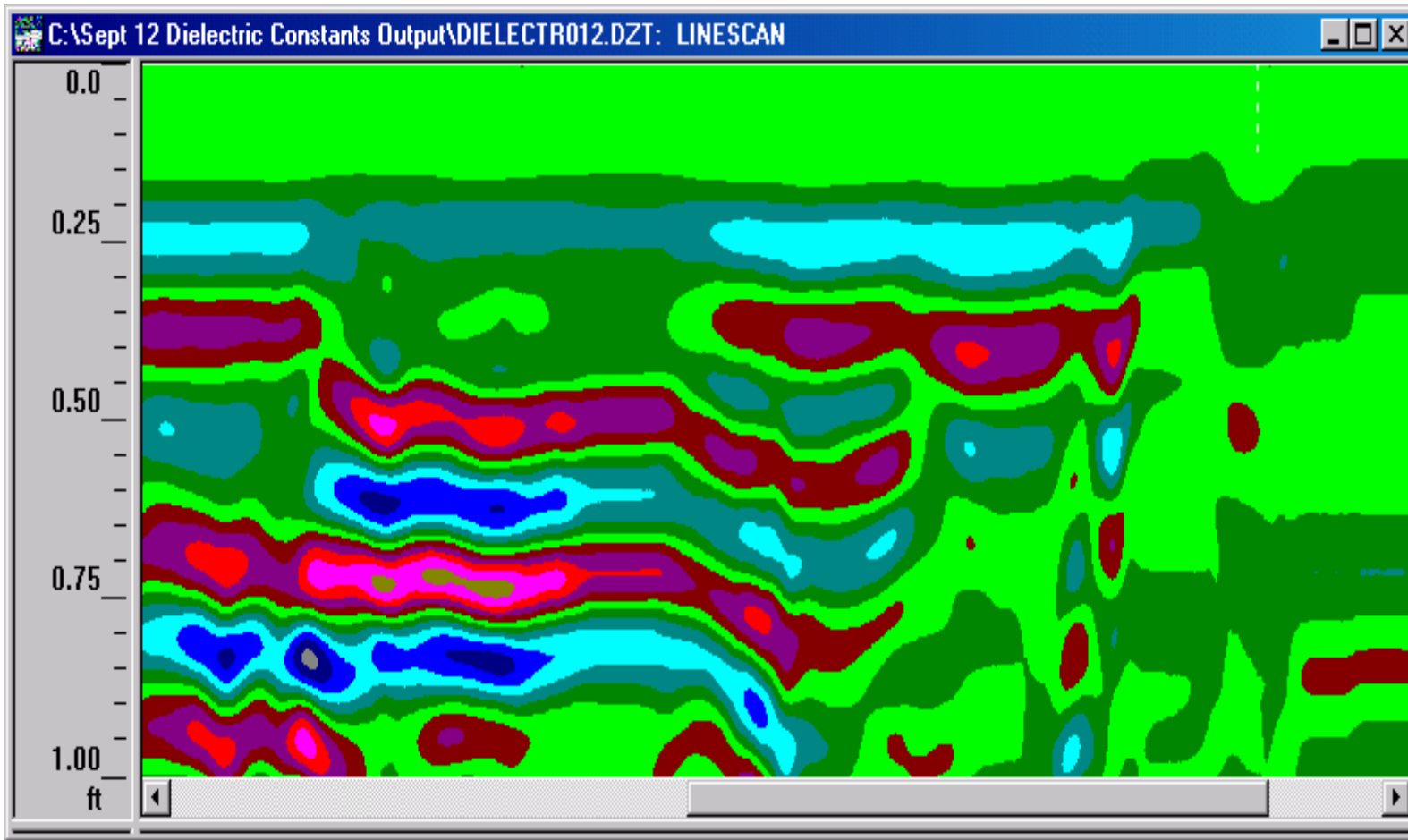
(b)

Figure 28. GPR Profile of Test Pit using 900 MHz antenna with Dielectric Constant of 6 with slow walking speed

69
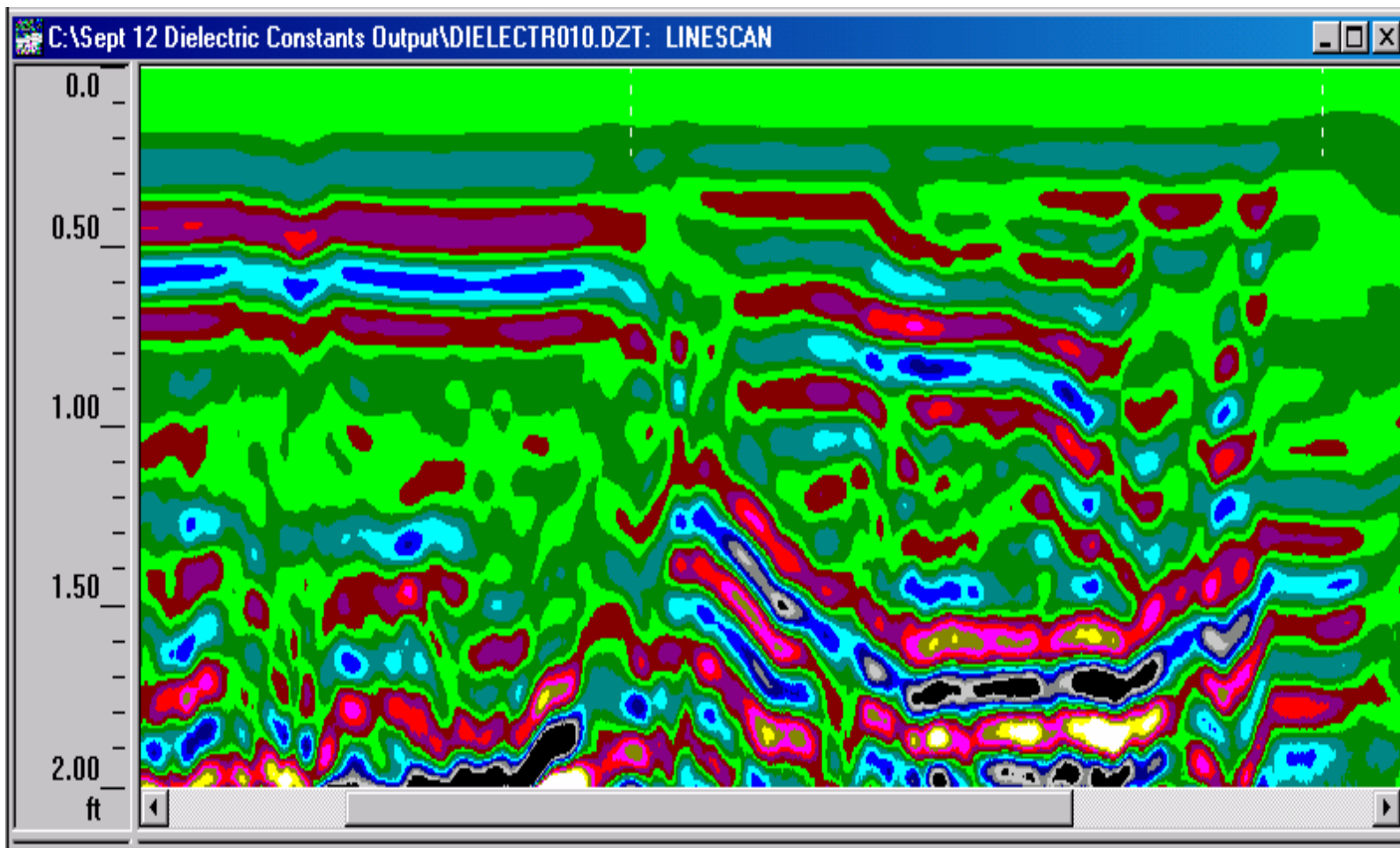
Figure 29. GPR Profile of Test Pit using 900 MHz antenna with Dielectric Constant of 6 with 15 ns or 2 feet depth

Survey Results of Downtown Orlando

The GPR profiles encoded in this report were conducted at a control time gain setting of 5 ns twt (tow-way travel time) for all traverses for best penetration depth for the targets. This ensured a clear and distinguishable view of the shallow anomalies and strata. Based on an average dielectric constant of asphalt and concrete, a dielectric constant of 6 was used. The penetration capabilities of GPR are depended upon the electrical properties of the investigated earth material and the antenna frequency:

$$D = \frac{twt}{2\sqrt{\varepsilon_r}}$$

(8)

where the two-way of the wave travel time (twt) is controlled by the processor units range adjustments and the dielectric constant (ε_r) can be found in the literature. Thus, based on the dielectric constant of 6, the penetration depth at 5 ns twt time span is approximately 1.02 feet. The depth scale for time span is labeled on GPR profile, although, not all profiles have the same distribution of scale. The results of the findings and suspected brick base and other conditions observed are shown and discussed within.

Results of GPR Survey on Summerlin Avenue

On South Summerlin Avenue, bricks were successfully detected beneath the new asphalt at the intersection of South Summerlin Avenue and Cherokee Drive to the new asphalt at the intersection of South Summerlin Avenue and Woodlawn Boulevard. However, bricks were not located near the North side curb approximately 3 feet from the curb (intersection of Summerlin

71

Avenue and Cherokee Drive). This area was measured to be 188 square feet (17ft x 4ft) after the existing asphalt was removed from Summerlin Avenue. The operation of asphalt removal is shown in Figures 30 (a) and (b), and GPR profile reflected to this area is shown in Figure 31. None of brick signals were observed from the GPR profile for this area. In spite of this section, bricks were detected on the entire section surveyed on Summerlin Avenue including a few inches over the new asphalt. A typical GPR profile for Summerlin Avenue with brick base is presented in Figure 32.

(a)   (b)

Figure 30. Removal of Asphalt at the Curb
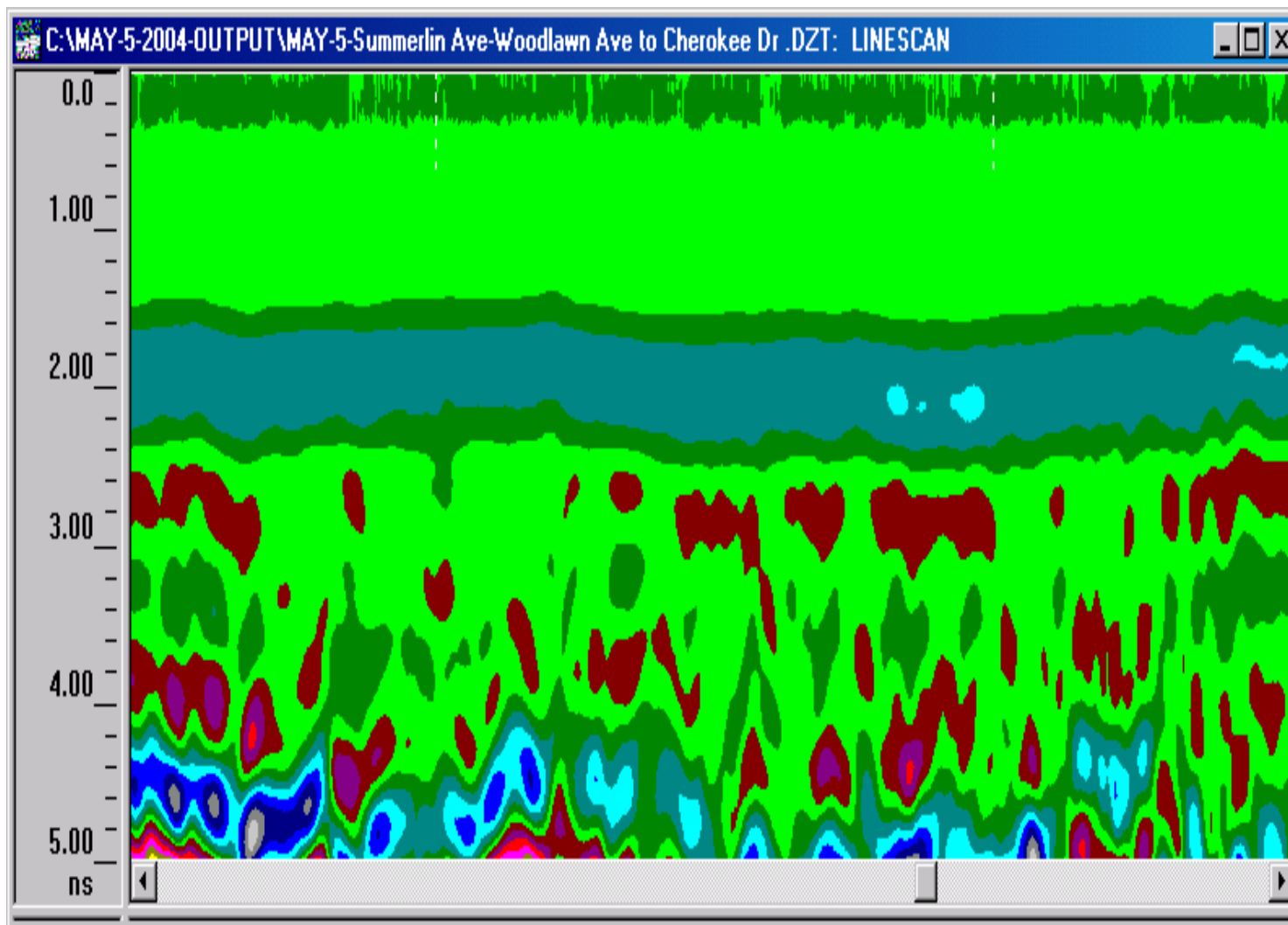
Figure 31. GPR Profile without brick base at the intersection of Summerlin Avenue and Cherokee Drive (North Curb)
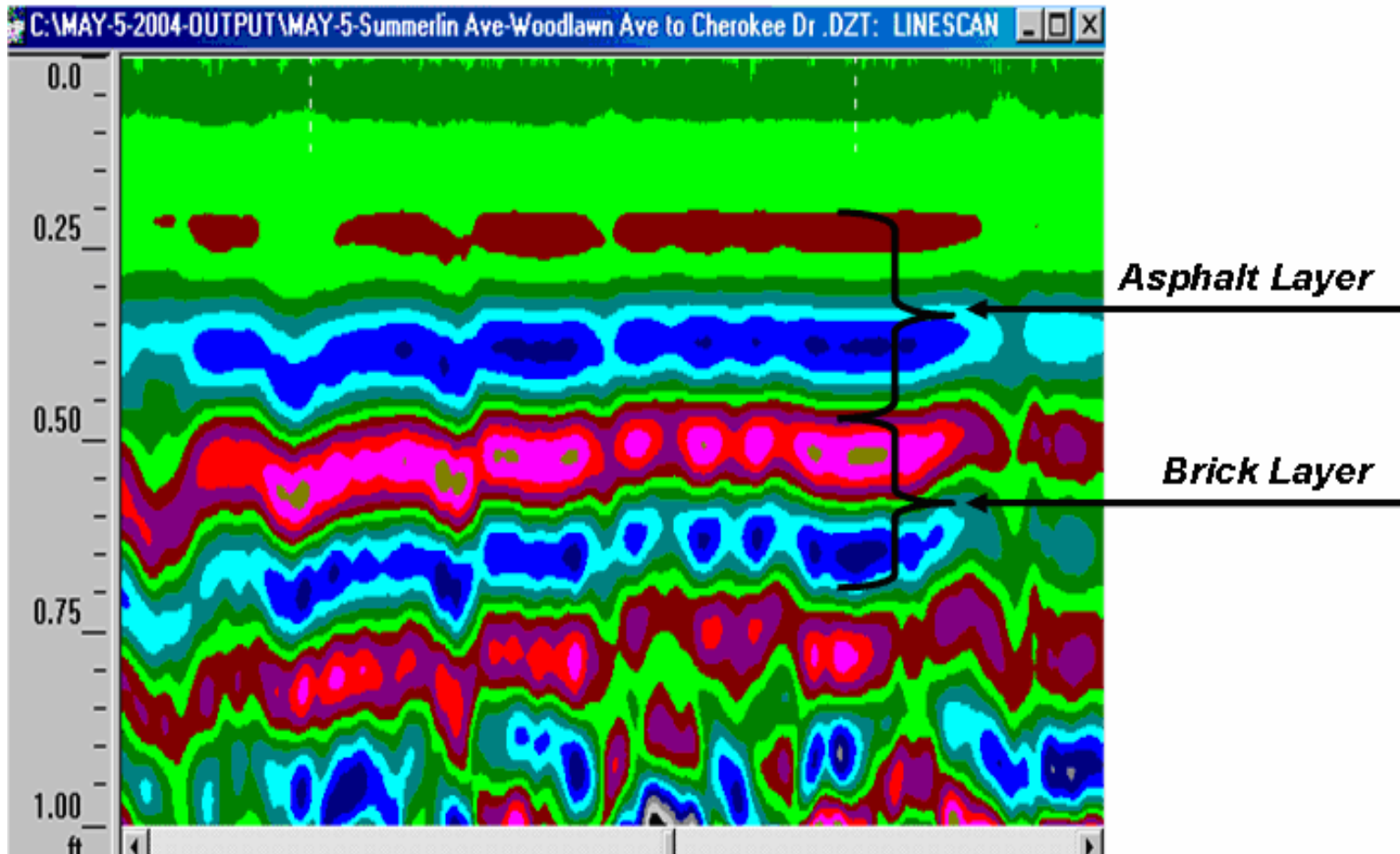
Figure 32. GPR Pavement Profile for Summerlin Avenue with Brick Base

Results of GPR Survey on Cherokee Drive

Cherokee Drive (from the intersection of South Summerlin Avenue to Delaney Avenue) was the longest line of GPR survey. The total length of GPR survey for Cherokee Drive was measured approximately 1900 feet. From the GPR profiles (Figures 34-40) it was observed that on several areas of the street did not have brick base, especially three feet from the edge of pavement eastbound and westbound. Figure 33 is a schematic map that shows approximate locations of no brick areas while Figures 34 and 35 are GPR profile correspond two of the no-brick areas. Furthermore, in several instances, it was seen that the signals of the radar was lost. For example, the GPR profile shown in Figure 36 it suggests the disappearance of GPR signal. Figure 36 shows a typical GPR profile on the street where signal was lost and Figures 37 and 38 shows a typical brick base profile. Bricks were

The loss of radar signals in this project may be attributed to reasons of motor vehicles driving by, power lines situated overheard, or utility cables that are buried within a few inches of the surface. Furthermore, utility lines, depressions, change in subgrades, or loose soils may also have caused interruptions in the antenna's signal. Depression was spotted at approximately 625 feet and 813 feet from Summerlin Avenue to Delaney Avenue on Cherokee Drive, which is clearly seen in Figure 39. Bricks were spotted over the entire roadway system; however, it was observed that several areas with distorted subbase (Figures 34, 39, and 40) were in between 1380 feet – 1400 feet and 1650 feet to 1670 feet from starting point at the intersection of Cherokee Drive and Summerlin Avenue. This could have taken place due to high moisture or high contamination that dramatically increased the conductivity of the subgrade material or simply due to an increase of seepage flow.
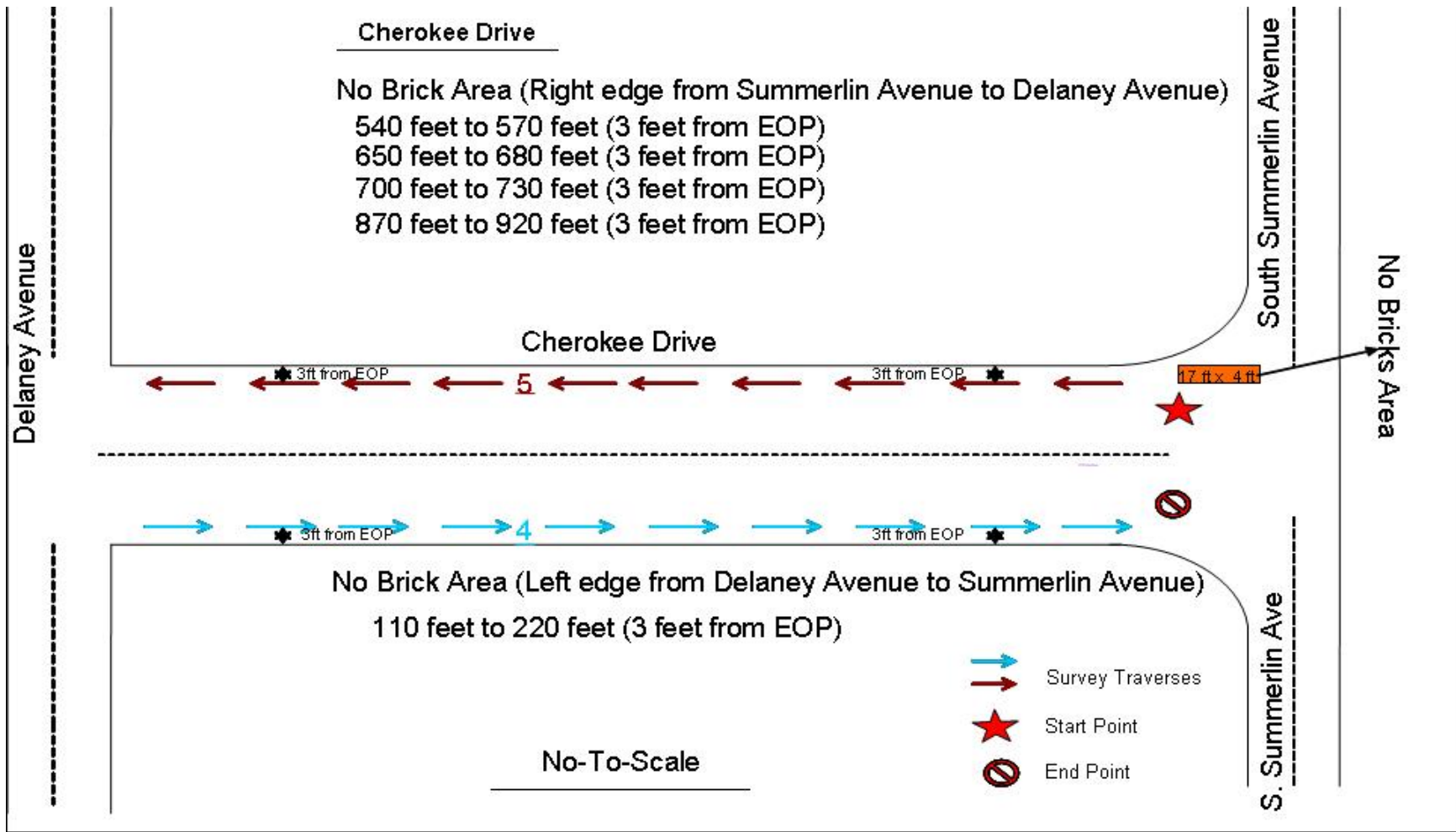
Figure 33. Approximate locations of Areas No Brick Base Detected
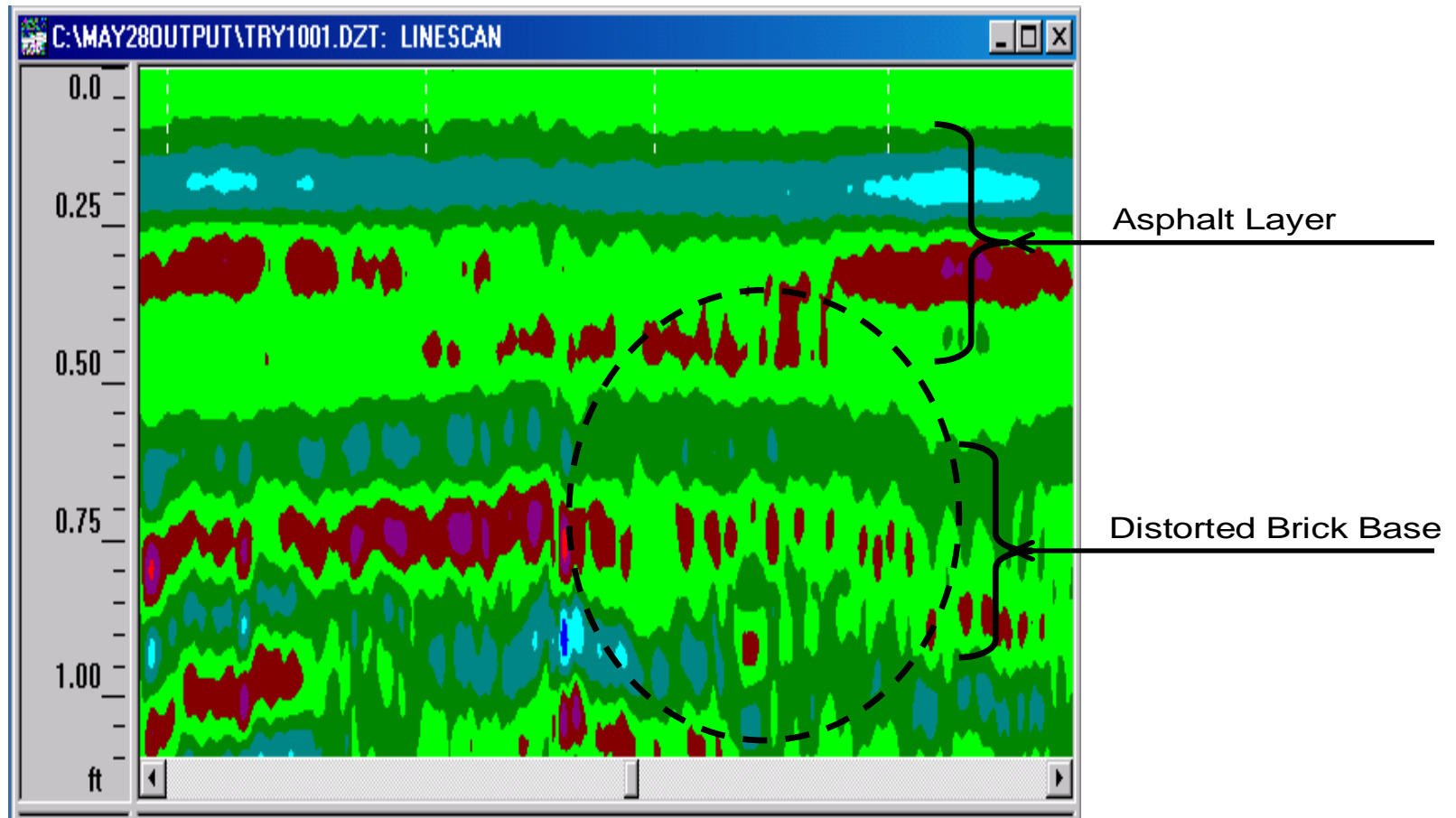
Figure 34. GPR Profile on Cherokee Drive with no Bricks
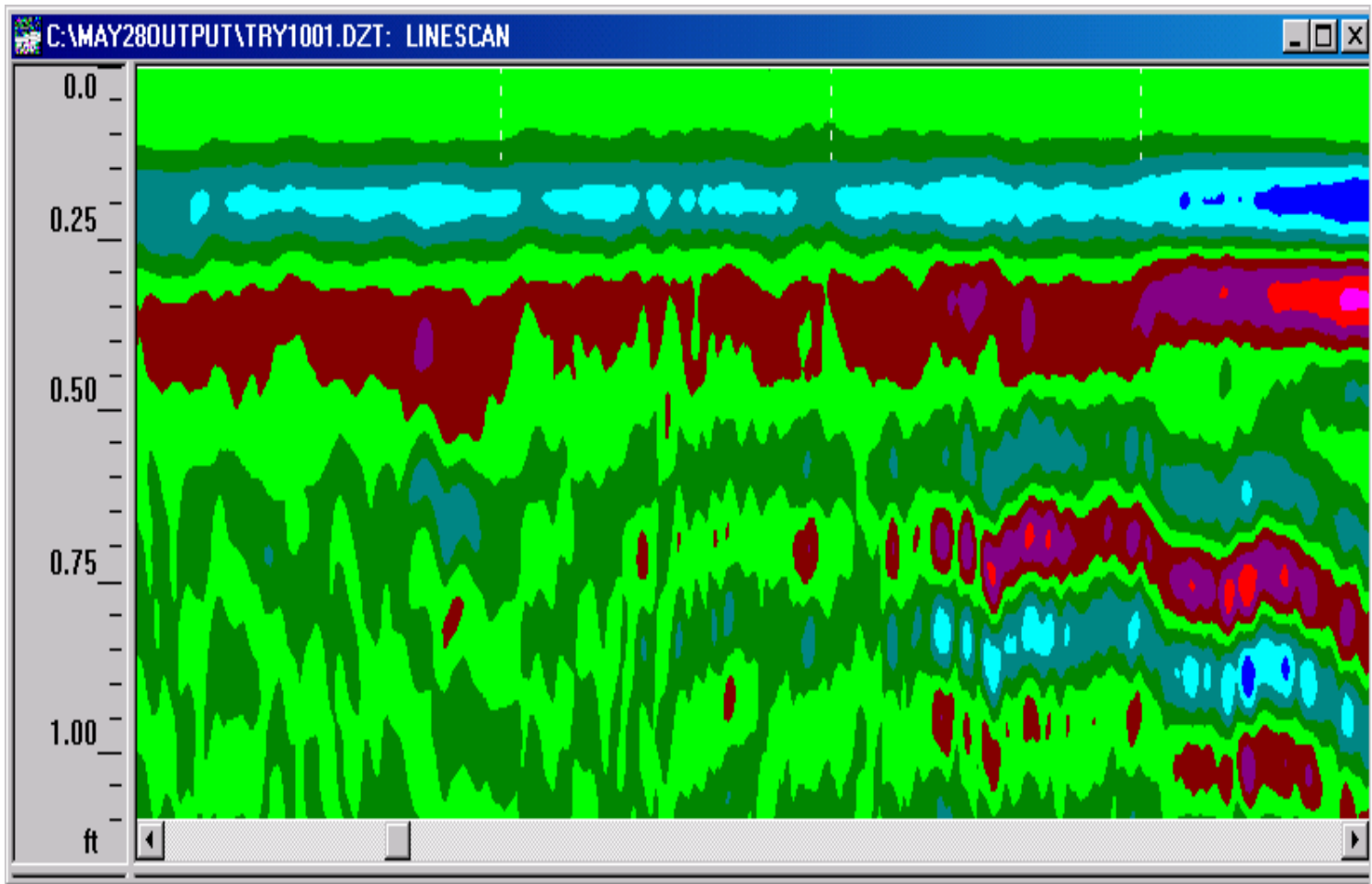
Figure 35. Typical GPR Profile on Cherokee Drive with No brick base
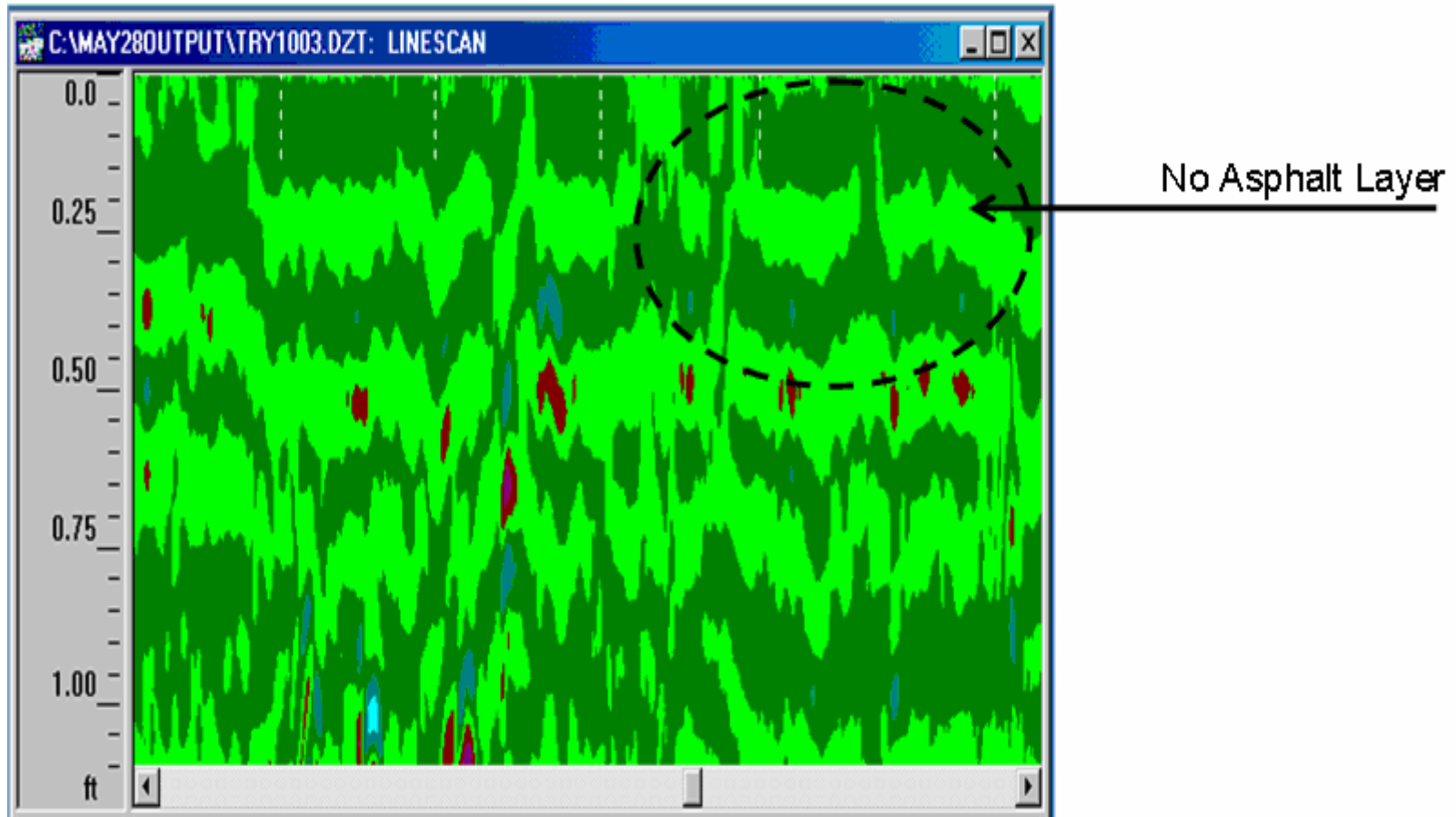
Figure 36. GPR Profile on Center of Cherokee Drive with Signal Break
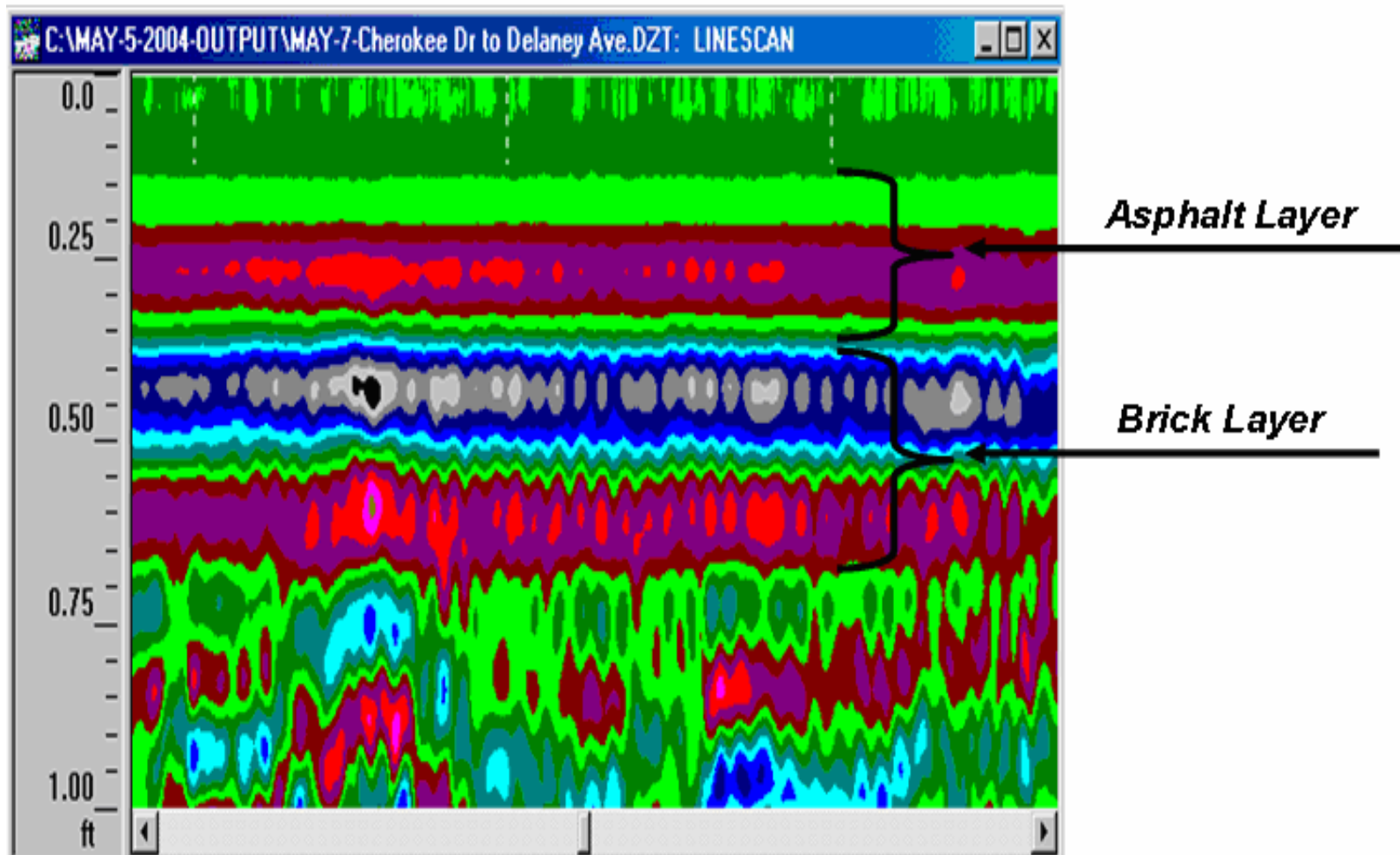
Figure 37. GPR Profile on Cherokee Drive with Brick Base

80
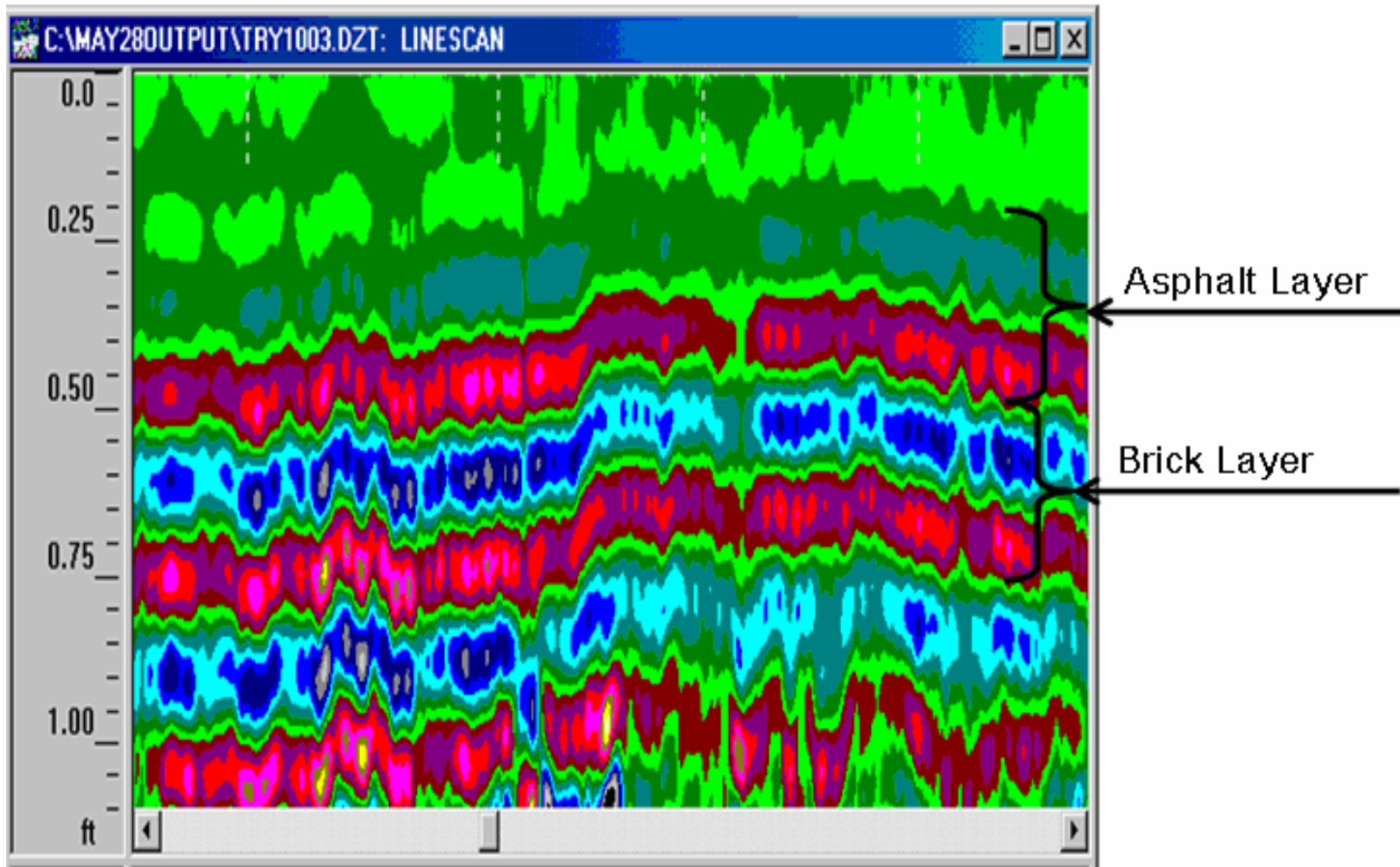
Figure 38. GPR Profile on Center of Cherokee Drive with Brick Base

81
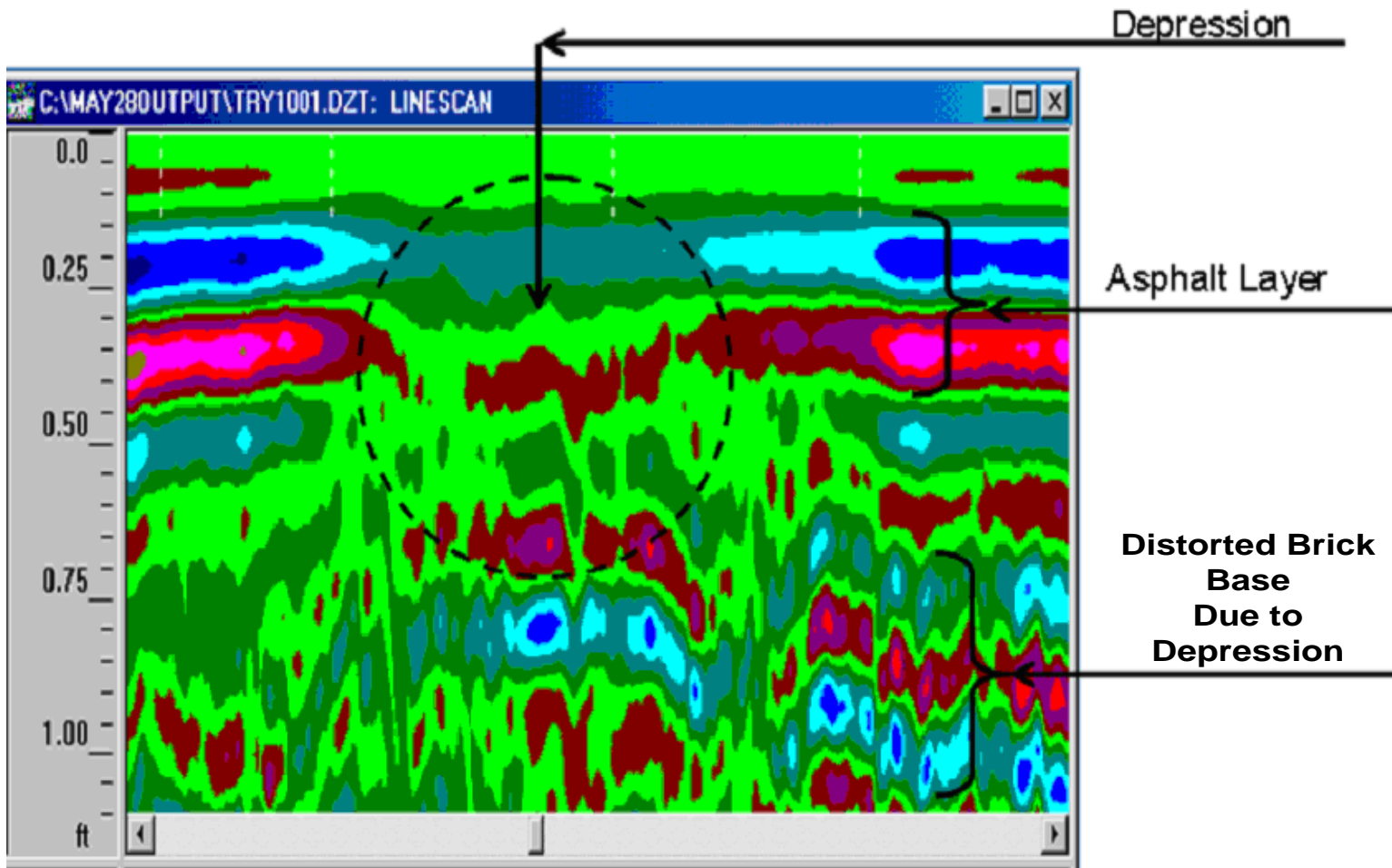
Figure 39. GPR Profile on Right Edge of Cherokee Drive with Depression
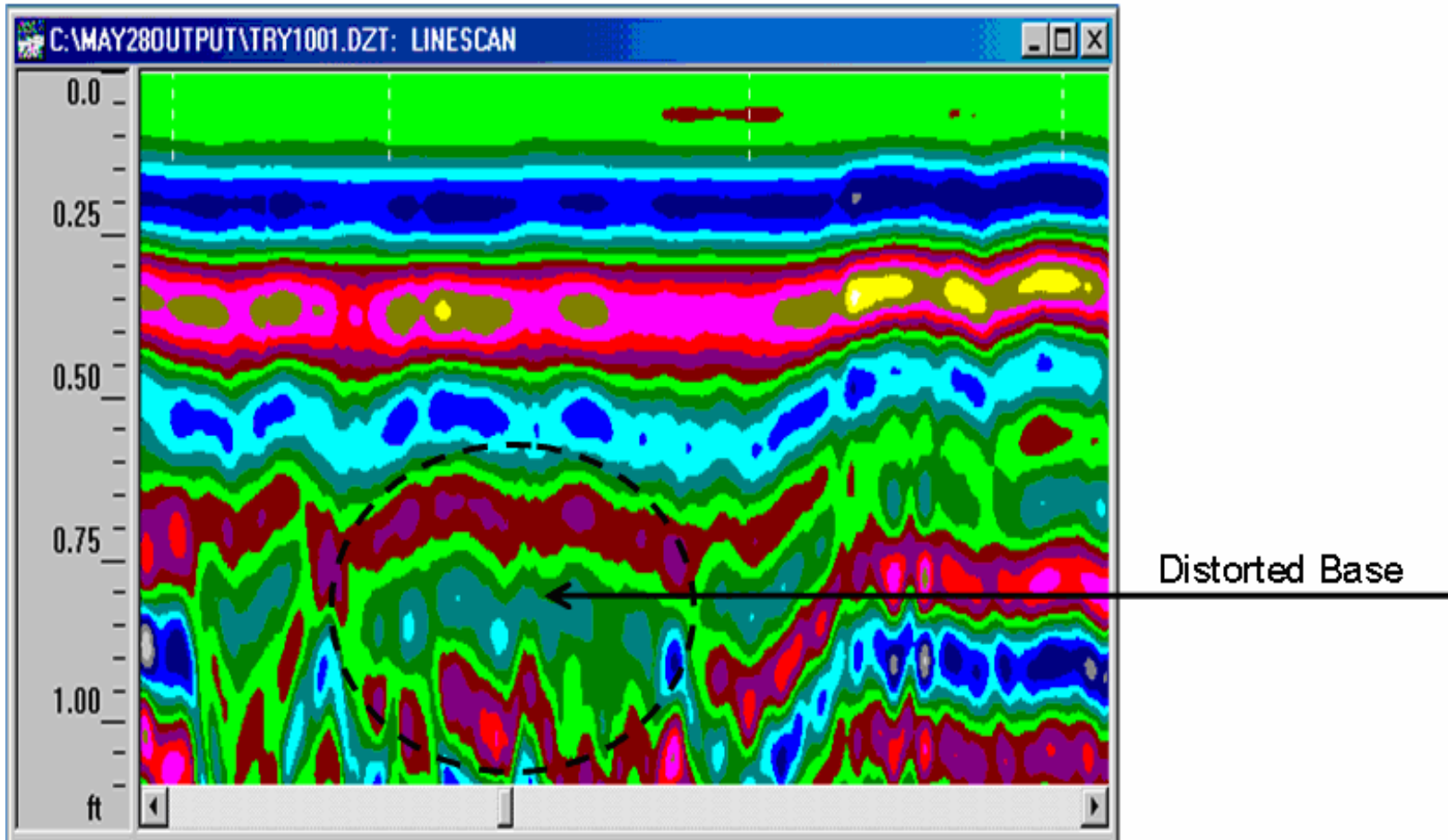
Figure 40. GPR Profile on Right Edge Cherokee Drive with Depression

83

(a)

(b)

(c)
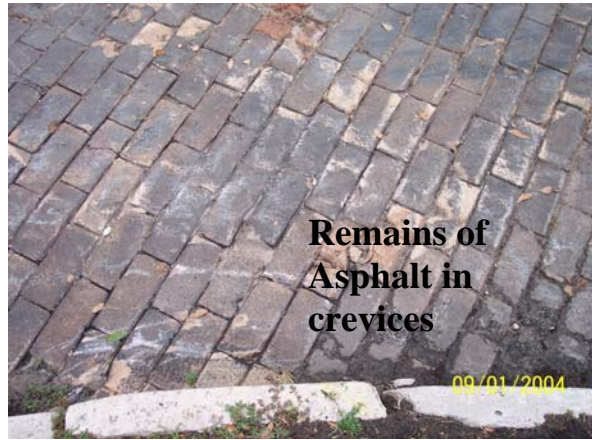
(d)

Figure 41. Areas of Cherokee Drive after Asphalt Removal and Replacement of Areas without Bricks

Figures 41 (a) − (d) shows the photographs taken on September 1, 2004, right after the removal of asphalt on Cherokee Drive. Some remaining asphalt in the crevices still existed as seen in Figure 41 (d). The areas where no brick zones were replaced with excess old and new bricks as in Figures 41 (a) − (c). In addition, in Figure 41 (a) it can be seen that smaller width of

bricks, located in the center of the figure, separates the new bricks (right) from the old (left). Areas surrounding the manholes were no brick base areas detected during the GPR survey. These areas were then replaced by the recycled bricks.

Results of GPR Survey on Church Street

The study determined that Church Street (from South Terry Avenue to South Westmoreland Drive) consists of brick base on the entire roadway surveyed except for the areas surrounding manholes. According to the GPR profile, no existence of brick base for the lane going Eastbound on Church Street for approximately 3 feet from the edge of pavement was determined. This complements the understanding of the extension of the street for a few feet on each side with suspected no of brick base. This area was located approximately 3 feet from the edge of the pavement (Figures 42 and 43). Typical GPR profiles for Church Street with and without brick base are shown above in Figures 44 through 47. Moreover, Figure 47 suggested base erosion due to the observed soil subsidence in the GPR profile.

Although, there were suspected no brick bases, there are several reasons due to which the brick base may no be detected by GPR. One of the major reasons is the lost of signal in the antenna due to a moving vehicle. Due to this reason, some investigators have tried shielding the antenna for safe detection. Other factors such as atmosphere, high moisture content, contamination of subbase material, chemical intrusion, increase of mineralization, looseness of soil are some of the reasons in missing base anomalies. The results of this study are summarized in Tables 7 and 8.
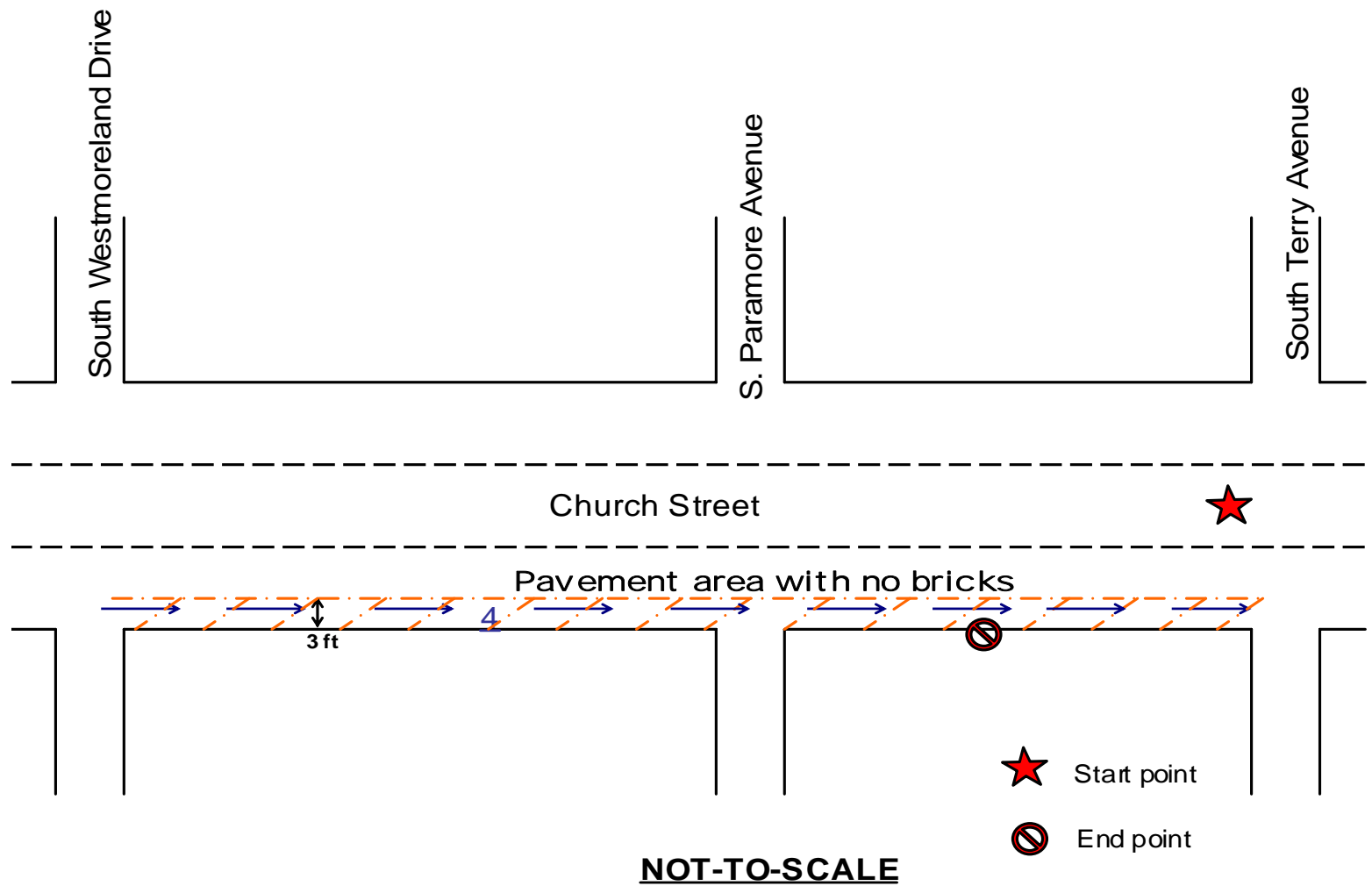
Figure 42. Line of Survey along Church Street—South Terry Avenue to South Westmoreland Drive
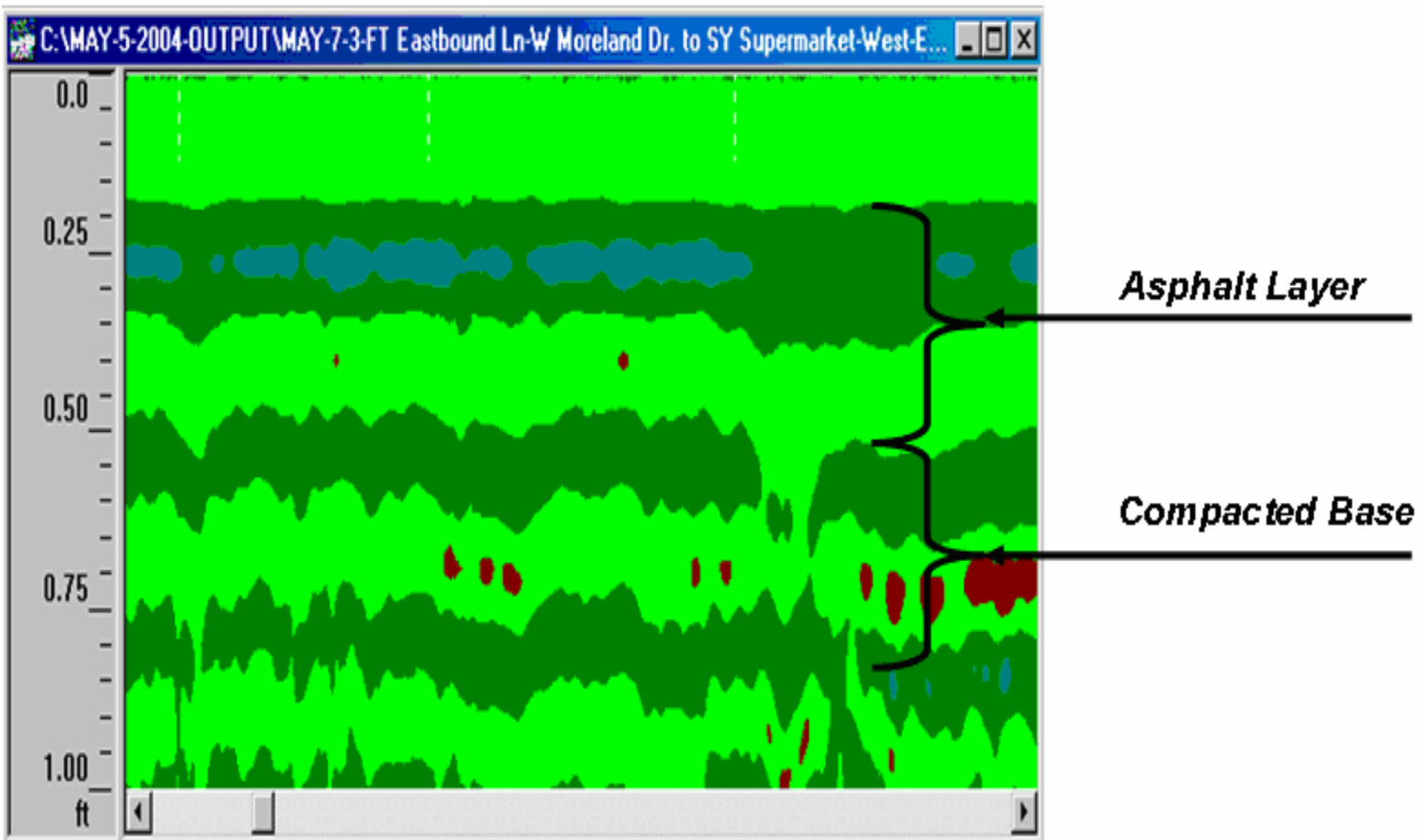
Figure 43. GPR Profile on Church Street without Brick Base 3 Feet from the Edge of Pavement
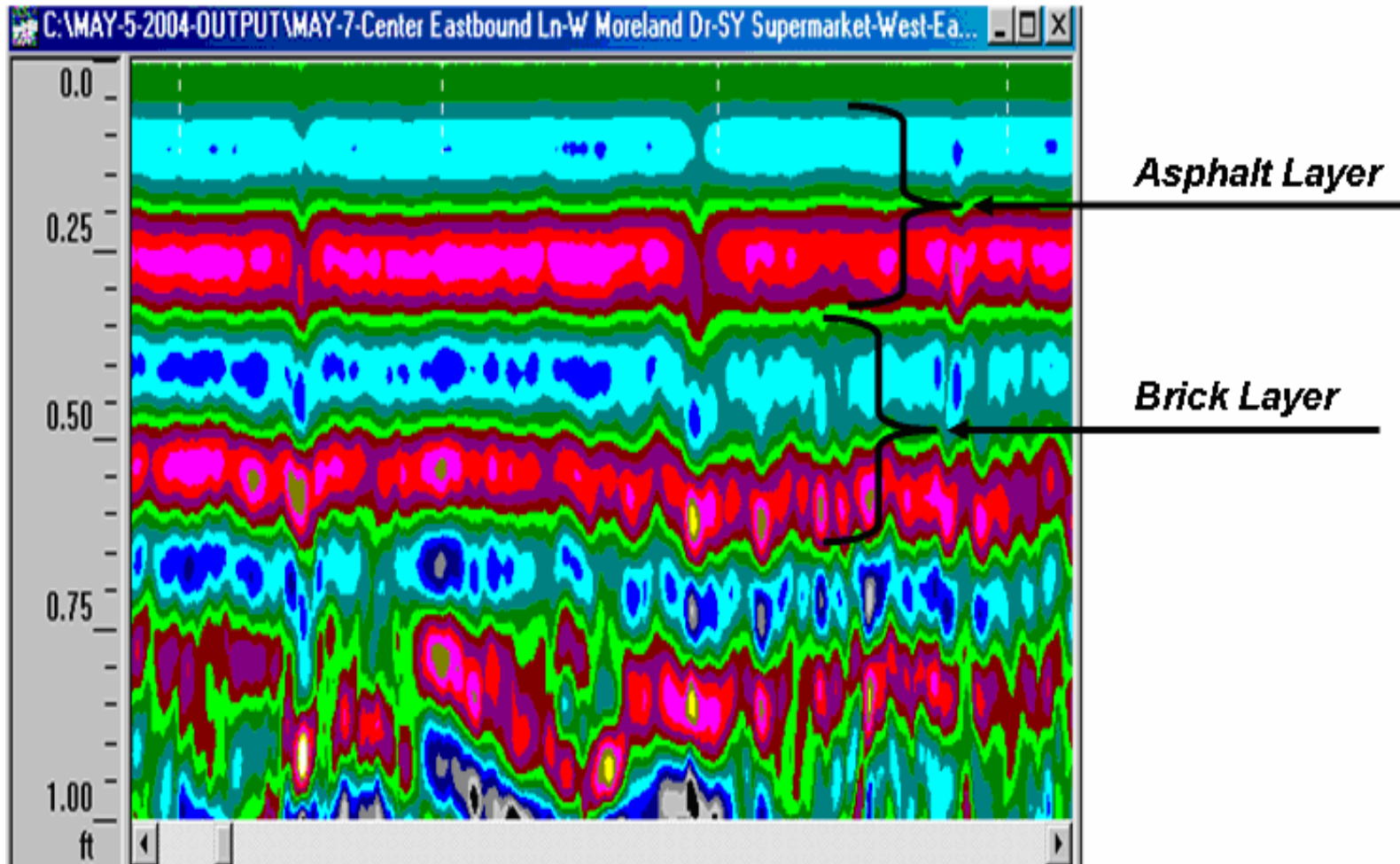
Figure 44. Typical GPR Profile on Church Street with Brick Base
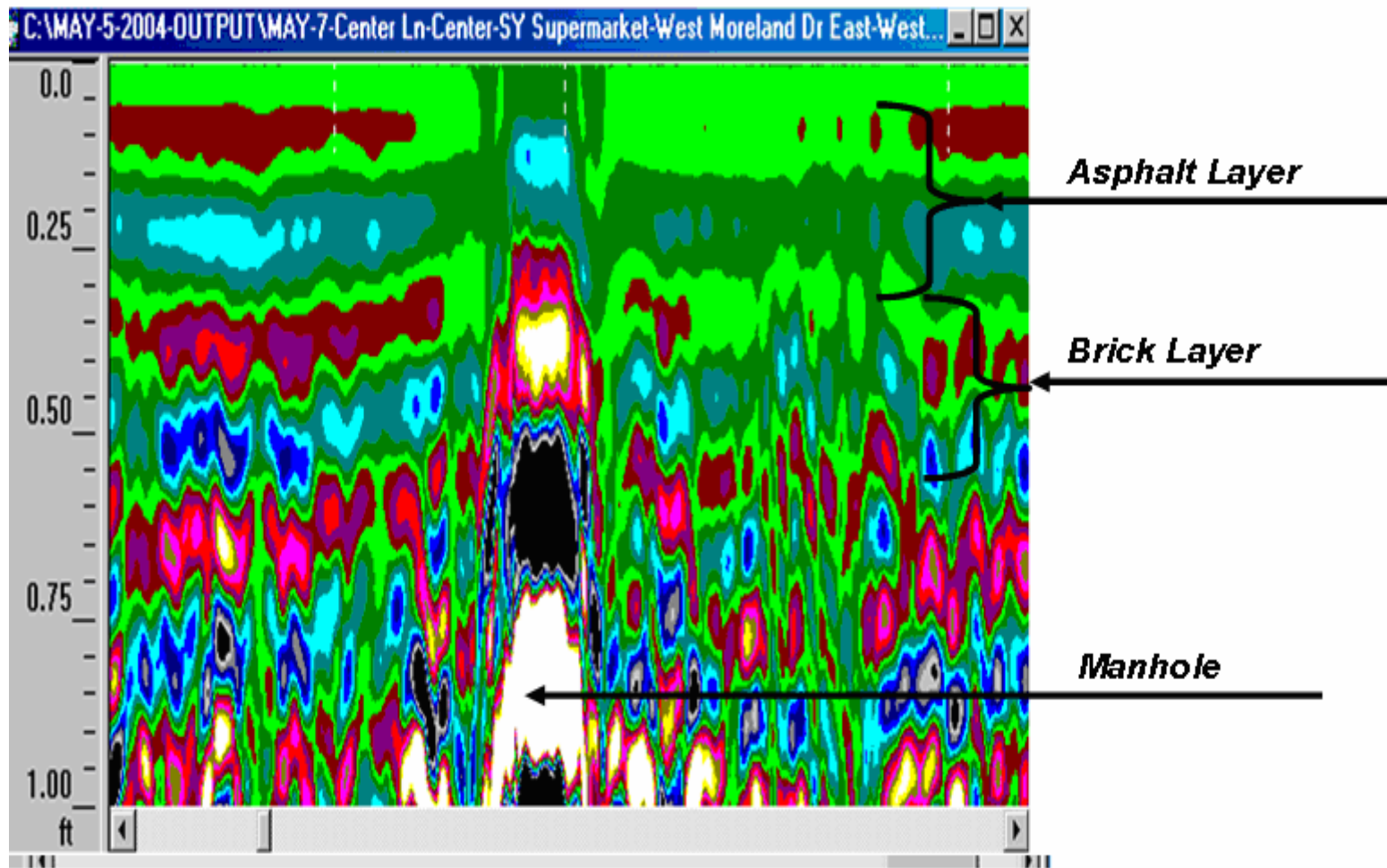
Figure 45. GPR Profile on Church Street with Brick Base and Manhole
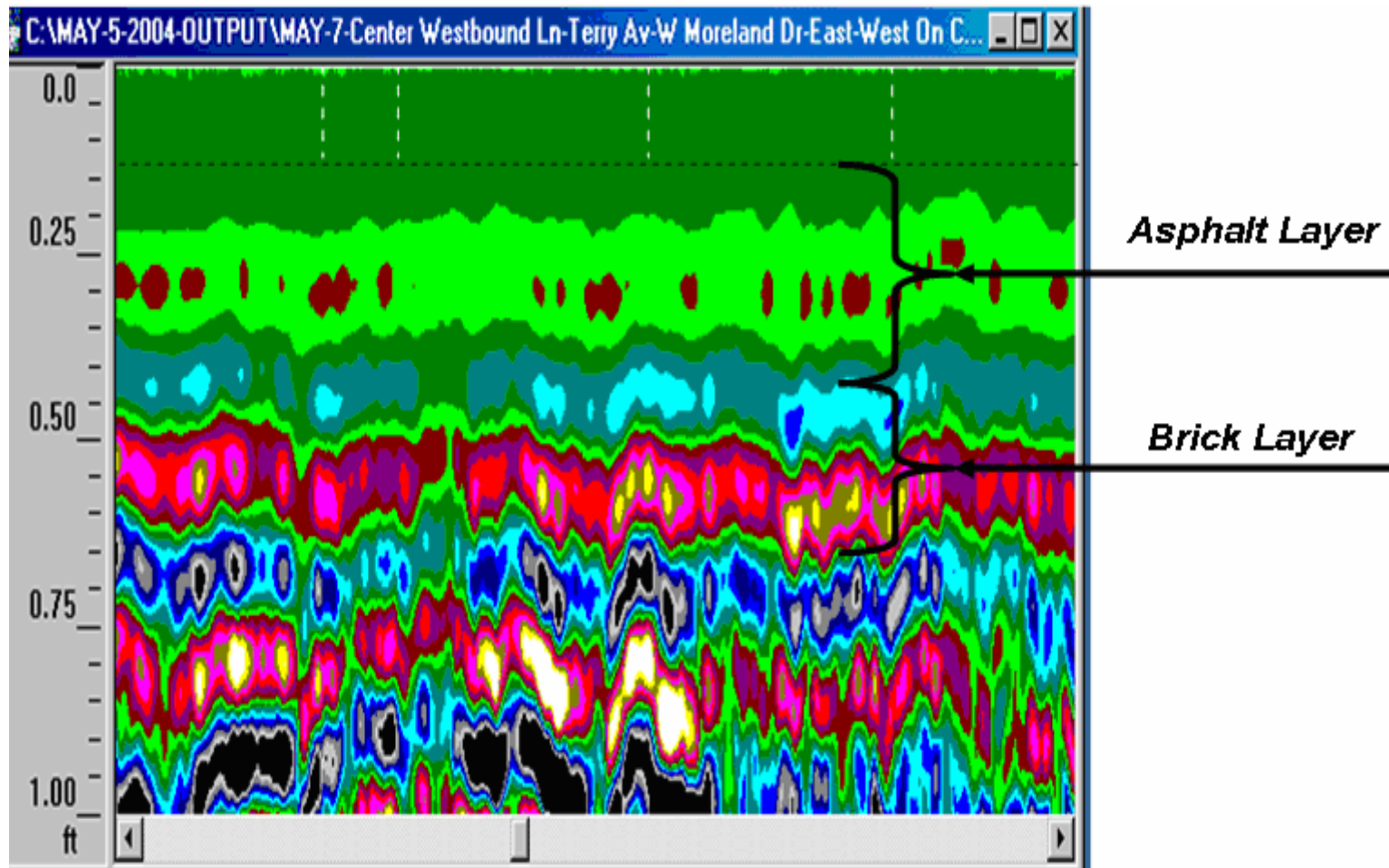
Figure 46. GPR Profile on Church Street with Brick Base with along the Center lane
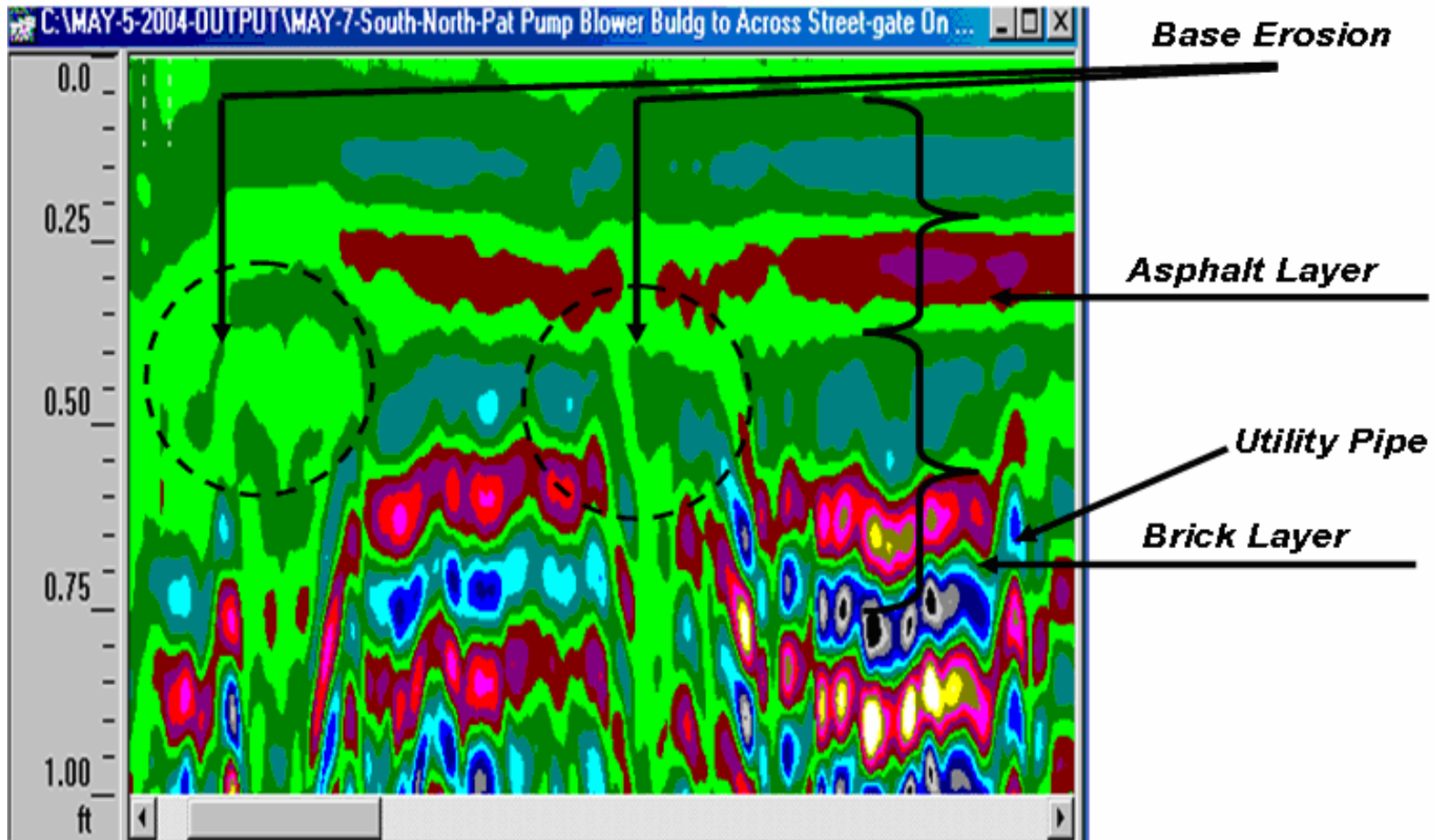
Figure 47. Cross-section GPR Profile on Church Street

Table 7

Approximate Locations of No-Brick Base Area

STREET NAME	SUSPECTED NO-BRICK LOCATIONS
Church Street	Starting at the Intersection of South Terry Avenue and Church Street on Church Street (Reference Station: SY's Supermarket) No bricks detected at 3 ft from the edge of pavement for the lane going Eastbound.
Summerlin Avenue	Starting at the Intersection of Summerlin Avenue and Cherokee Drive (Reference Station : 10 ft behind New Asphalt) No bricks detected at the North side of the curb, a strip of 17 feet by 4 feet.
Cherokee Drive	Starting at the Intersection of Summerlin Avenue and Cherokee Drive on Cherokee Drive (Reference Station : Electric Pole)
3-feet from EOP Eastbound	110 feet to 220 feet
3-feet from EOP Westbound	540 feet to 570 feet 650 feet to 680 feet 700 feet to 730 feet 870 feet to 920 feet

Table 8

Validation of GPR Data

STREET NAME	FIELD RESULTS VALIDATION GPR SURVEY
	Church Street
GPR Survey	No bricks detected at 3 ft from the edge of pavement for the lane going Eastbound.
After Removal of Asphalt	Not Applicable.
	Summerlin Avenue
GPR Survey	No bricks detected at the North side of the curb, a strip of 17 feet by 4 feet.
After Removal of Asphalt	GPR survey results were validated by 100%.
	Cherokee Drive
GPR Survey	• 110 feet to 220 feet, (3ft from EOP Eastbound) • 540 feet to 570 feet, (3ft from EOP Westbound) • 650 feet to 680 feet, (3ft from EOP Westbound) • 700 feet to 730 feet, (3ft from EOP Westbound) • 870 feet to 920 feet, (3ft from EOP Westbound)
After Removal of Asphalt	GPR survey results were validated by 75%.

Evaluation of Existing Pavement using KENLAYER Computer Program

The purpose of performing the existing pavement evaluation was to determining the structural integrity of the pavement with brick base. The only information that can be obtained from the GPR profiles for the existing pavements in this study is the thickness of the asphalt layer and the thickness of the bricks. Therefore, for the pavement evaluation, practical assumptions were to be made for several material parameters and traffic data. The traffic data was obtained from the 2003 Annual Average Daily Report from the Florida Department of Transportation's statistics office. Although specific traffic count was not reported for the downtown streets, several surrounding streets were searched for traffic data. Moreover, Church Street, located in the heart of downtown Orlando, experienced higher traffic compared to Summerlin Avenue and Cherokee Drive. It was also assumed that garbage trucks with 3 axles were the heaviest trucks traveling through the Downtown streets. Trucks with semi-trailers may travel on Church Street; however, the percentage is not as significant as of waste trucks or dump trucks. Furthermore, each axle carried a load of 8,000 lbs and contact pressure of 80 pounds per squared inches with dual spacing of 13.5 inches and tandem spacing of 48 inches. The contact radius was then calculated to be 5.64 inches.

The average daily traffic used to calculate the 18 kip equivalent single axle load (ESAL) used was obtained to be 11,358 with an assumption of 5 % trucks, growth rate of 5% and a design life of 20 years. The truck factor was obtained from Haung (1993) to be 21 percent; the percent of total truck traffic in design lane for 4 lanes gave a 45 percent of trucks in design lanes. The lane distribution factor for 2 lanes in each direction was an

average of 80 and 100 percent of 18-kip ESAL in design lane. The 18-kip ESAL was then calculated to be 582,830 repetitions for each load group.

After the survey of the Orlando streets, it was discovered that the surface course or the asphalt layer ranged from 2-inces to 6-inches in thickness, and the bricks were approximately 3 inches thick. The subbase layer of readily available sand in the sate of Florida was in general to be 10-12 inches. The material properties of the surface course, base, subbase and subgrade are presented in Table 9 from three sources. Lastly, it was also assumed that elastic stiffness of the bricks were a part of linear system. Therefore, modulus of elasticity of concrete was employed for the brick base.

Table 9

Layer Properties

Layer	Thickness (inch)	Young's Modulus (psi)	Poisson's Ratio
Asphalt Concrete	6	500,000	0.4
Brick Base	3	3,250,000	0.15
Subbase	10	10,000	0.45
Subgrade	∞	3,000	0.5

Source: Das (2004)
Efunda (2004)
Haung (1993)

All parameters were entered into KENLAYER program for damage analysis of brick based four-layered pavement system under dual-tandem tires. The damage analysis was based on horizontal tensile strain at the bottom of the asphalt layer for fatigue failure because this strain causes cracks to initiate at the bottom of the asphalt layer, and the vertical compressive strain on the top of the subgrade layer cause rutting failure. Once the data was processed, the remaining life of the existing pavements with brick base in downtown Orlando was reported to be 3.38 years, equivalent of just over 40.6 months. The resultant age is true for the assumed input parameters stated above. There have been no official records that identify rehabilitation of the existing pavement.

The compressive strain on the top of the subgrade layer was obtained to be 4.111×10^{-4} for allowable load repetition of 1.970×10^6, and the tensile strain obtained at the bottom of the asphalt layer was obtained to be a zero with allowable load repetitions to be 1.000×10^{30}. This simply means that with the reasonable assumptions of input data, in the next presumable 3.4 years as calculated. The pavement with brick base may develop permanent deformation of 0.29 inches in the pavement system before fatigue cracking.   Permanent deformation is an important factor in pavement design as the increase in traffic loads and tire pressures have a direct impact on the upper layers the roadway system.

Table 10

Damage Analysis Results

Summary of Damage Analysis	
Sum of damage ratio bottom of asphalt layer	0.000×10^{0}
Sum of damage ratio top of subgrade layer	2.959×10^{-1}
Maximum permanent deformation in inches	2.959×10^{-1}
Fatigue Life in years	3.38

The summary of damage analysis is presented in Table 10, and Figure 48 represents graphically the truck tires impacting the pavement system. The detailed printouts and program windows are available in Appendix B. In Figure 48, the first 6 inches represent the surface course of asphalt concrete. The subsequent three inches represent the brick base with an approximate thickness of 3 inches as stated in Table 9. The third layer represents the subbase layer of 10 inches thickness and the final layer is the subgrade layer of infinite depth.
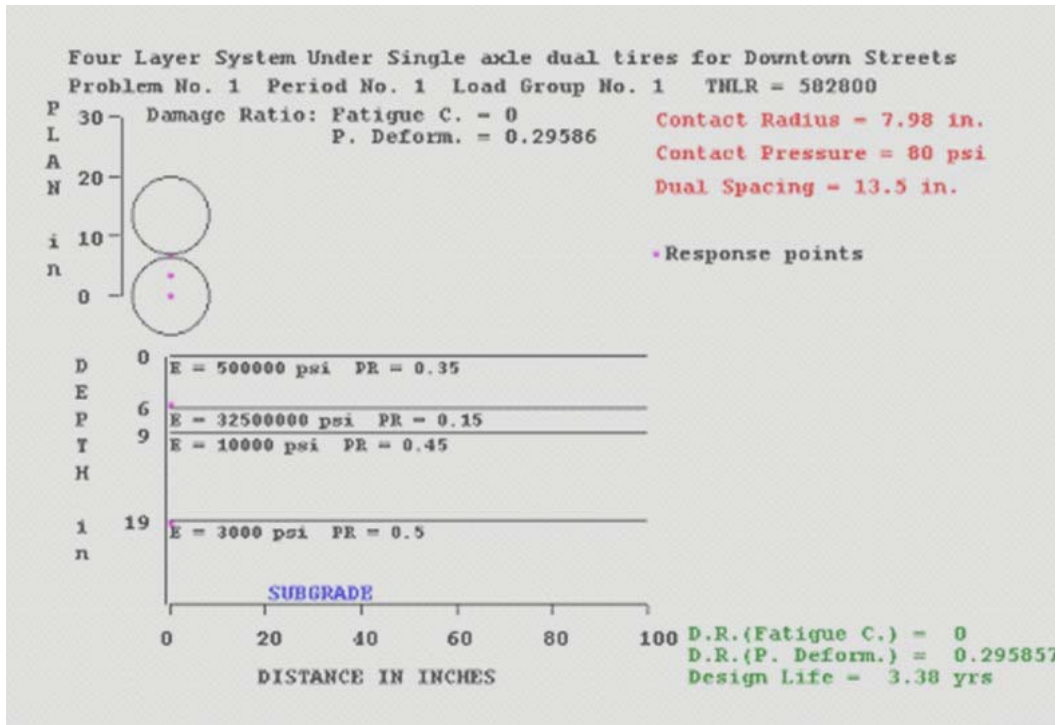
Figure 48. Graphical Representation of Four-Layer system under Single-Axle-Dual Tires

CHAPTER 6

SUMMARY AND CONCLUSIONS

As the world set its foot into the new millennium, the city of Orlando had its own plans in improving neighborhoods by involving the residents. Among many modifications and transformations requested by the downtown Orlando residents, bring back of brick roads were voted in favor of to reduce speeding and possible traffic accidents, but mainly to restore the historical integrity of the city.

With the assistance of the City of Orlando, the research team from UCF was able to successfully detect bricks that lay underneath the asphalt surface by using nondestructive testing method of the Ground Penetrating Radar (GPR). For better calibration and interpretation of the GPR profiles, a test pit was built with several types of bricks overlaid with asphalt. Several profiles were recorded at 5 ns travel time with 1-foot of penetration depth. Three city streets (Summerlin Avenue, Cherokee Drive, and Church Street) were contracted for GPR survey of brick base. Bricks that lay beneath the asphalt layer were successfully detected in most areas of the selected streets using GPR survey. Several localized areas on these streets with missing bricks were also detected. The City of Orlando was satisfied with the results of this study. Lastly, the existing pavement was analyzed for performance of fatigue cracking and permanent deformation. The traffic volume was based on the 2003 Annual Report by the Florida Department of Transportation for the nearby downtown streets. Practical assumptions for material characterization of pavement system were made for the input parameters in the Kenlayer computer program.

The following recommendations are suggested for future study for this capacity of detection and evaluation of subsurface anomalies with the use of ground penetrating radar:

1. Using GPR in detection of subsurface anomalies and conditions is a promising method. An experimental control area is highly recommended and should be build for a better calibration and understanding of the radar profiles.

2. The profiles provided by GPR are continuous and gigantic computer files of subsurface condition, which should be confirmed by ground truthing so that accurate results may be provided to the proper authorities. This is mainly because of the two dimensional profile in terms of depth or travel time.

3. Antenna choice is extremely critical for subsurface detection. This study proves that 900 MHz antenna is the optimum choice in obtaining promising quality results in detection of bricks overlaid by asphalt layer.

4. The electrical properties of the soil, rock, and ground water vary greatly from site to site. So in detection of pavements, a dielectric constant of 6 is recommended for best results for study of subsurface condition under an asphalt concrete surface.

5. Determination of the maximum penetration depth at a site is difficult before the actual radar survey is conducted due to the many variables that influence radar signals. The depth to the interface is determined by the radar wave propagation velocity and the dielectric constant of the material. For this study, the two-way travel time (twt) for the brick base is recommended of 5 nanoseconds, while the penetration depth of 1 foot can be accomplished.

6. Color scheme of 10 and 16 should be employed because it easily distinguishes and individualizes bricks by giving a non-solid profile with discontinuities.

7. If available, a 3-dimentional survey wheel should be used as it enhances GPR data to its full potential. The use of survey wheel and 3-D software overcomes the limitations of the common form 2D cross-section. 3D display has the advantage of looking at the entire survey area at once. Acquiring a 3-D display software and hardware, if necessary, for future projects is highly suggested.

8. It is highly recommended that shielding is provided to the antenna in order to minimize noise cluttering or reverberation, or interference from cell phones, or passing vehicles, and cable and electric wires.

9. The excavated asphalt should be recycled and reused. Similarly, the bricks should also be salvaged.

10. Downtown streets with brick base being existed for a long period of time have not shown significant deterioration. The use of bricks for base course for a pavement system causes difficulty in underground utility repairs where the removal and replacement of bricks does not remain cost effective items.

The use of ground penetrating radar techniques is a modern day technology that is a high-tech, non-destructive method providing promising approach for subsurface exploration. GPR has been used around the world for various applications including space; however, research on detection of brick base has not yet been reported, which makes this study exceptionally unique. GPR is expensive equipment that is scarcely available for academic research, such as this. University of Central Florida's Civil and Environmental Department is one of few colleges in the

nation that possesses and practices the application of GPR technology for the subsurface exploration.

Lastly, under actual field conditions, the earth materials being probed are often not homogenous and the signal strength may quickly be reduced due to the reflections of the signal from various stratagraphic interfaces. In the case of a specific target being detected, the size and shape will also affect the detection ability of the radar system. As a result, the interpretations and analysis submitted herein are based upon the data obtained from the GPR profiles enclosed in this report. The data reported in this thesis had been prepared for the exclusive use of the City of Orlando for specific application to the subjected sites. The report was prepared in accordance with generally accepted geophysical engineering practice. No other warranty was expressed or implied upon the study. Should other anomalous conditions be suspected, a more comprehensive investigation would be required.

APPENDIX A

MAPS AND LOCATIONS
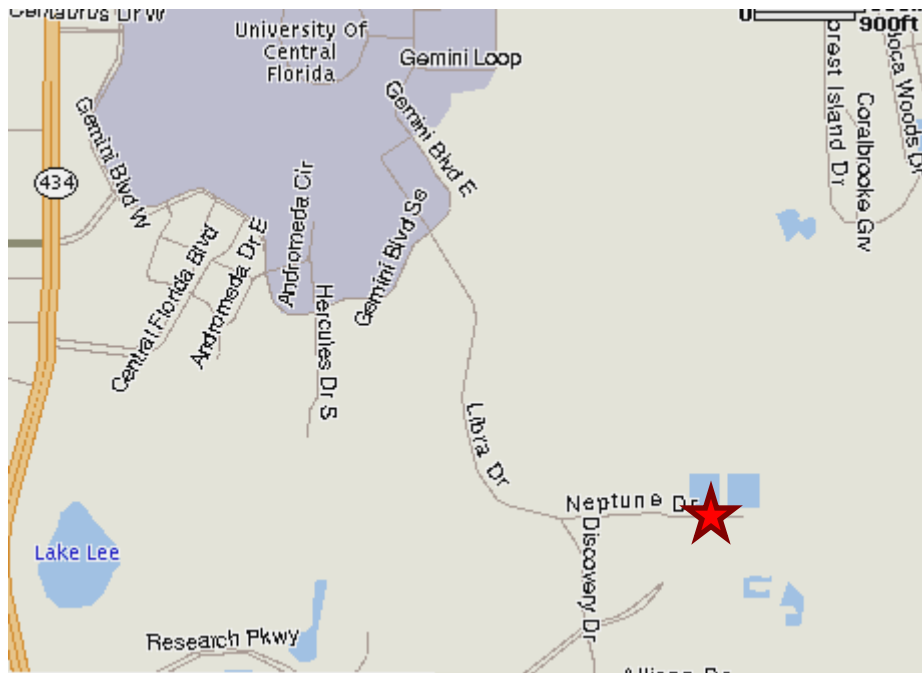
Figure A-1. Location of Test pit
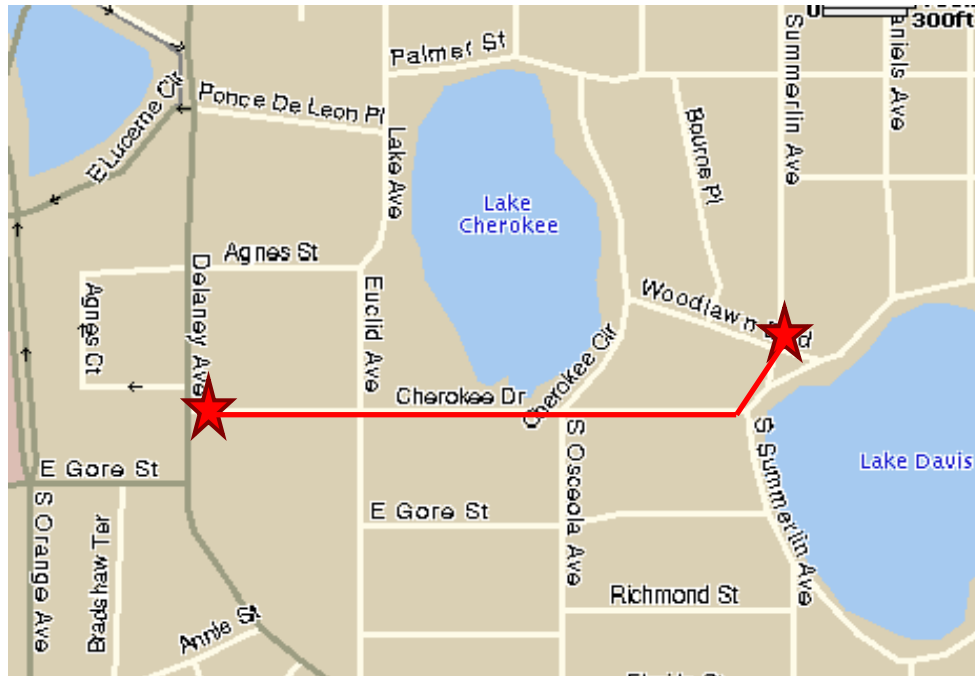
Figure A-2. South Summerlin Avenue from Cherokee Drive to Woodlawn Boulevard and Cherokee Drive from South Summerlin Avenue to Delaney Avenue (Mapquest.com)
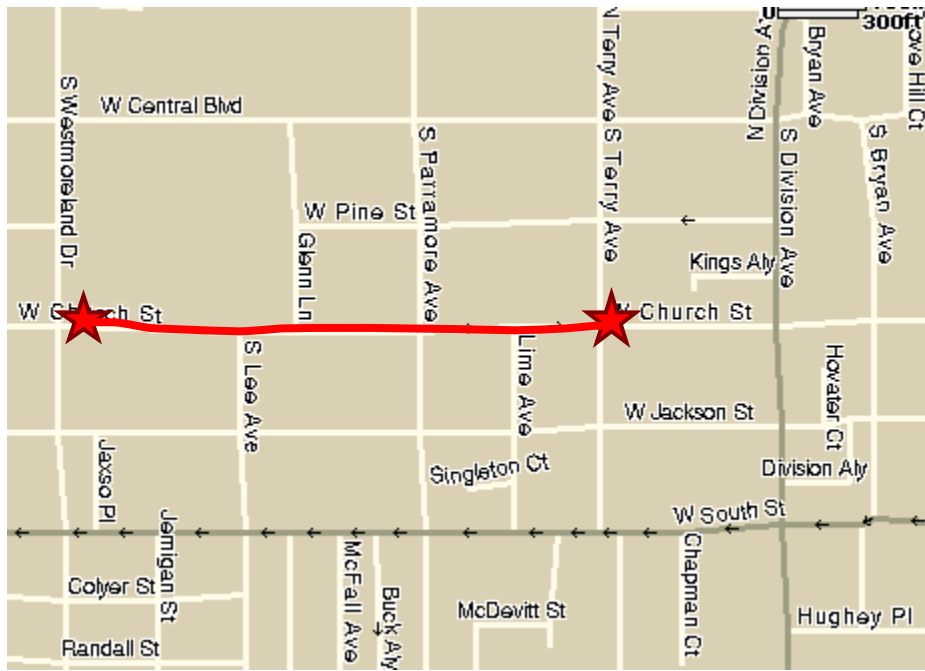
Figure A-3. West Church Street from South Terry Avenue to South Westmoreland Drive
(Mapquest.com)

CITY OF ORLANDO

FAX COVER SHEET

DATE _2/19/04_ TIME _____ FAX# _407- 823- 3315_

SENT TO _Dr. Kuo_

COMPANY NAME _UCF_

BEING SENT BY _Dennis Tipton_   Work # _407- 246- 2267_   Cell # _407- 376- 4958_

NUMBER OF PAGES INCLUDING COVER SHEET _____ 3 _____

COMMENTS _3 areas that Rick Howard wants you to look at_
are: _1. Summerlin Ave. (Woodlawn auto to Cherokee Dr)_
2. Cherokee Dr. (Summerlin Ave to Delaney Ave)
3. Church St. (Terry Ave to Westmoreland Dr)
If you need additional information, call me @ 407-246-2267.

IF YOU DO NOT RECEIVE ALL OF THE PAGES OR NEED ADDITIONAL INFORMATION, PLEASE CONTACT US AS SOON AS POSSIBLE AT 407-246-2266.

THANK YOU!

Dennis

(a)

106
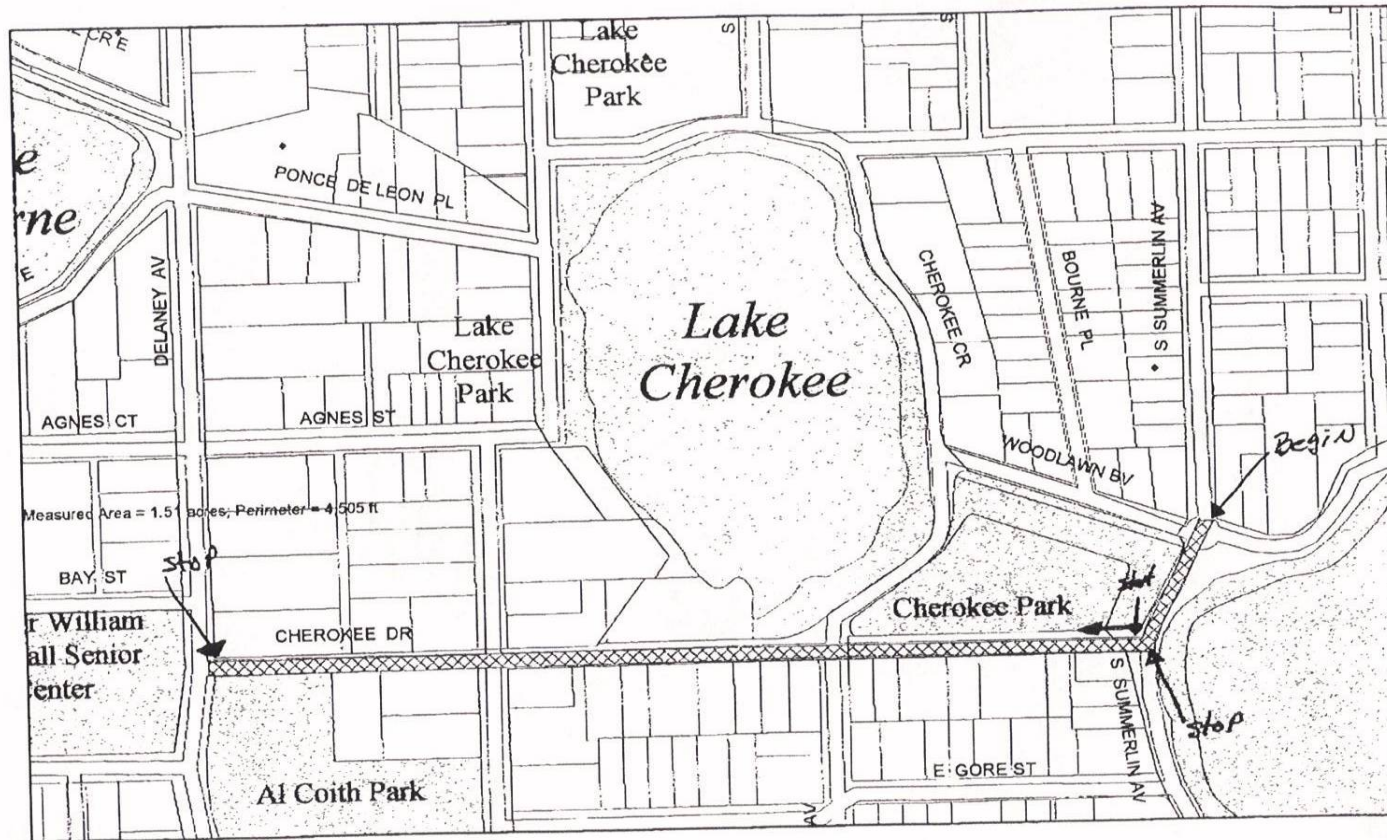
Figure A-4. Documentation received from the City of Orlando locating GPR Survey Sites

108

APPENDIX B

KENLAYER INPUTS AND OUTPUTS

General Information of LAYERINP for Set No. 1

TITLE	Four Layer System Under Single axle dual tires for Downtown Streets

Type of material (1=linear, 2=nonlinear, 3=viscoelastic, 4=combined)	(MATL)	1
Damage analysis (0=no, 1=yes with summary only, 2=yes with detailed printout)	(NDAMA)	2
Number of periods per year	(NPY)	1
Number of load groups	(NLG)	1
Tolerance for numerical integration	(DEL)	0.001
Number of layers	(NL)	4
Number of Z coordinates for analysis	(NZ)	0
Maximum cycles of numerical integration	(ICL)	80
Type of responses (1=displacements only, 5=plus stresses, 9=plus strains)	(NSTD)	9
All layer interfaces bonded (1=yes, 0=if some are frictionless)	(NBOND)	1
Number of layers for bottom tension	(NLBT)	1
Number of layers for top compression	(NLTC)	1
System of units (0=English, 1=SI)	(NUNIT)	0

OK

(1) This form appears when the 'General' on the Main Menu of LAYERINP is clicked. You can override any of the default values by typing in a new value. You can use the Tab key to move the cursor from one textbox to the next or just click on the textbox before typing. The use of click has the advantage that you don't have to delete the default before typing in the data you want. If you want to read the remaining text, you can use the scrollbar. You can also use the PgDn key after clicking this textbox to make it active.
(2) TITLE (title of run): Any title or comment can be typed on one line. The title should not be longer than 68 characters including spaces. If you make a mistake in typing, use the Del key to erase any typographical errors. When the total length reaches 68, no additional characters can be added. No comma should be used in TITLE. Use colon or semicolon instead.
(3) MATL (types of material): 1 when all layers are linear elastic, 2 when some layers are nonlinear

(a)

Layer Thickness, Poisson's Ratio and Unit Weight for Data Set No. 1

After typing the value in a cell, be sure to press the Enter key to make it effective.

Unit   in.   pcf

Layer No.	TH	PR	GAM
1	6	.35	0
2	3	.15	0
3	10	.45	0
4	XXXXXXXX	.5	0

Use <Ctrl>-<Del> to delete a line, <Ctrl>-<Ins> to insert a line, and <Del> to clear a cell.

(1) This form appears when the 'Layer' menu on the Main Menu of LAYERINP is clicked. The number of layers on this form is equal to NL, as specified in the 'General' menu. This form is different from the one used for General Information in that a dotted rectangle, instead of the cursor, is used to indicate the active cell. If the dotted rectangle is not the location for input, you can use the arrow key to move the dotted rectangle to the cell you want to input, or more conveniently by clicking the cell you want. After you type in the data, the dotted rectangle will be changed into a three dimensional box and you must press the Enter key to make it effective. You can also use the up and down arrow keys to make the entry effective. Note that the dotted rectangle is now in the upper left cell, so you can type in the data right away. If you want to read the remaining text and use the PgDn key, instead of the scrollbar, you should click this textbox to

OK

(b)

110

Layer Moduli for Period No. 1 and Data Set No. 1

Unit   psi

Layer No.	E
1	500000
2	3250000
3	10000
4	3000

(1) This form appears when the period button on the Layer Modulus of Each Period is clicked. The number of layers on this form is equal to NL, as specified in the 'General' menu.

(2) E (elastic modulus of each layer): Use as the assumed modulus for the first iteration when the layer is nonlinear. Assign 0 or any value for viscoelastic layer.

(3) After typing the data in the first cell, move to the next cell by pressing the Enter or arrow down key. After the last cell is filled, be sure to click the Enter key.

(4) You can delete a line, or one layer, by first clicking anywhere on the line to make it active and then press the <Ctrl>-<Del> keys. The NL in the 'general' menu will be reduced automatically by 1.

(5) You can add a new line, or one more layer, above any given line by first clicking the cell in the given line to make it active and then press the <Ctrl>-<Ins>. A blank line will appear for you to enter the necessary data. The NL in the 'General' menu will increase automatically by 1. If you want to add a line after the last line, you can change NL in the 'General' menu by adding 1 and a blank line will appear as the last line. Remember that always use the <Ctrl>-<Ins> keys to add a line unless the line to be added is the last line. By so doing, you don't have to retype any of the existing lines.

(6) Upon completion, click the OK button to return to the

Use <Ctrl>-<Del> to delete a line, <Ctrl>-<Ins> to insert a line, and <Del> to clear a cell.

OK

(c)

Load Information for Data Set No. 1

Double click anywhere on a line to get auxiliary form for NR or NPT.

Unit   in.   psi   in.   in.

Load Group No	LOAD	CR	CP	YW	XW	NR or NPT
1	1	7.98	80	13.5	0	3

Use <Ctrl>-<Del> to delete a line, <Ctrl>-<Ins> to insert a line, and <Del> to clear a cell.

(1) This form appears when the 'Load' menu on the Main Menu of LAYERINP is clicked. The number of lines, or load groups, is equal to NLG, as specified in the 'General' menu. Please refer to Figure 3.8 for wheel and axle arrangements.

(2) LOAD (type of loading): Assign 0 for single axle with single tire, 1 for single axle with dual tires, 2 for tandem axles, and 3 for tridem axles.

(3) CR (contact radius of circular loaded ares).

(4) CP (contact pressure on circular loaded ares).

(5) YW (center to center spacing between two dual wheels along the y axis): Assign 0 if there is only one wheel or LOAD = 0.

(6) XW (center to center spacing between two axles along the x axis): Assign 0 if only one axle exists, i.e. LOAD = 0 or 1.

(7) NR (number of radial coordinates to be analyzed under a single wheel, maximum 25): A single wheel

OK

(d)

111

X and Y Coordinates of Response Points for Load Group No. 1 and Data Set No. 1

Unit   in.   in.

Point No.	XPT	YPT
1	0	0
2	0	3.375
3	0	6.75

(1) This auxiliary form appears automatically when NPT of a given load is typed on the main form. If NPT was specified previously, you can also enter this auxiliary form by double clicking the main form anywhere on the given load group, instead of retyping NPT to enter this auxiliary form.
(2) XPT (x coordinates of points to be analyzed).
(3) YPT (y coordinates of points to be analyzed).
(4) After typing the data in a cell, be sure to press the Enter key to make it effective.
(5) You can delete a line, or one of the points, by first clicking anywhere on the line to make it active and then press the <Ctrl>-<Del> keys. The NPT in the main form will be reduced automatically by 1.
(6) You can add a new line, or one more point, above any given line by first clicking the cell in the given line to make it active and then press the <Ctrl>-<Ins>. A blank line will appear for you to enter the necessary data. The NPT in the main form will increase automatically by 1. If you want to add a line after the last line, you can change NPT in the main form by adding 1 and a blank line will appear as the last line. Remember that always use the <Ctrl>-<Ins> keys to add a line unless the line to be added is the last line. By so doing, you don't have to retype any of the existing lines.
(7) After completing this form, click OK to return to the main

Use <Ctrl>-<Del> to delete a line, <Ctrl>-<Ins> to insert a line, and <Del> to clear a cell.

OK

(e)

Load Repetition for Period No. 1 and Data Set No. 1

Load Group I	TNLR
1	582830

(1) This form appears when the period button on the Load Repetitions of each period is clicked. The number of load groups on this form is equal to NLG, as specified in the 'General' menu.
(2) TNLR (total number of load repetitions for each load group).
(3) After typing in the data in the first cell, move to the next cell by pressing the Enter or arrow down key.
(4) You can delete a line, or one load group, by first clicking anywhere on the line to make it active and then press the <Ctrl>-<Del> keys. The NLG in the 'general' menu will be reduced automatically by 1.
(5) You can add a new line, or one load group, above any given line by first clicking the cell in the given line to make it active and then press the <Ctrl>-<Ins>. A blank line will appear for you to enter the necessary data. The NLG in the 'General' menu will increase automatically by 1. If you want to add a line after the last line, you can change NLG in the 'General' menu by adding 1 and a blank line will appear as the last line. Remember that always use the <Ctrl>-<Ins> keys to add a line unless the line to be added is the last line. By so doing, you don't have to retype any of the existing lines.
(6) Upon completion, click the OK button to return to the Load Repetitions of Each Period.

Use <Ctrl>-<Del> to delete a line, <Ctrl>-<Ins> to insert a line, and <Del> to clear a cell.

OK

(f)

112

Layer Number and Fatigue Coefficients for Data Set No. 1

After typing the value in a cell, be sure to press the Enter key to make it effective.

Sequence	LNBT	FT1	FT2	FT3
1	1	.0796	3.291	.854

Use <Ctrl>-<Del> to delete a line, <Ctrl>-<Ins> to insert a line, and <Del> to clear a cell.

(1) This form appears when the 'Bottom Tension' menu on the Damage Analysis is clicked. The number of sequences or layers for damage analysis on this form is equal to NLBT, as specified in the 'General' menu. Note that the cursor is now in the upper left cell, as indicated by the dotted rectangle, so you can type in the layer number right away. If you want to read the remaining text and use the PgDn key, instead of the scrollbar, you should click this textbox to make it active. After finishing reading, you should click the cell before typing in the data.
(2) LNBT (layer number for damage analysis of bottom tension).
(3) FT1, FT2, FT3 (fatigue coefficients, as indicated by f1, f2 and f3 in Eq. 3.6): Values suggested by the Asphalt Institute are 0.0796, 3.291, and 0.854.

OK

(h)

Layer Number and Permanent Deformation Coefficients for Data Set No. 1

After typing the value in a cell, be sure to press the Enter key to make it effective.

Sequence	LNTC	FT4	FT5
1	4	1.365E-09	4.477

Use <Ctrl>-<Del> to delete a line, <Ctrl>-<Ins> to insert a line, and <Del> to clear a cell.

(1) This form appears when the 'Top Compression' menu on the Damage Analysis is clicked. The number of sequences or layers for damage analysis on this form is equal to NLTC, as specified in the 'General' menu. Note that the cursor is now in the upper left cell, as indicated by the dotted rectangle, so you can type in the layer number right away. If you want to read the remaining text and use the PgDn key, instead of the scrollbar, you should click this textbox to make it active. After finishing reading, you should click the cell before typing in the data.
(2) LNTC (layer number for damage analysis of top compression).
(3) FT4, FT5 (permanent deformation coefficients, as indicated by f4 and f5 in Eq. 3.7): Values suggested by the Asphalt Institute are 1.365×10^{-9} and 4.477.

OK

(i)

113

```
KENLAYER - D:\Downtown Streets Pavement Analysis                    _ □ ×

FLEXIBLE PAVEMENT ANALYSIS AND DESIGN BY MULTILAYERED SYSTEM USING KENLAYER

FILENAME: D:\Downtown Streets Pavement Analysis.DAT

TITLE: Four Layer System Under Single axle dual tires for Downtown Streets
COMPLETE INPUT OF DATA

DAMAGE ANALYSIS OF PERIOD NO.  1  LOAD GROUP NO.  1
COMPLETE LAYERS SUBROUTINE WITH INTEGRATION CYCLES IC= 20
COMPLETE LAYERS SUBROUTINE WITH INTEGRATION CYCLES IC= 14
COMPLETE LAYERS SUBROUTINE WITH INTEGRATION CYCLES IC= 13

AT BOTTOM OF LAYER  1     SUM OF DAMAGE RATIO = 0.000E+00

AT TOP OF LAYER  4       SUM OF DAMAGE RATIO = 2.959E-01

MAXIMUM DAMAGE RATO =    2.959E-01   DESIGN LIFE IN YEARS = 3.38

Your text output is stored in a file called D:\Downtown Streets Pavement
Analysis.TXT

              kenlayer                    ×

              Please click the OK button to exit.

                        OK
```

(j)

(k)

Figure A-5. Documentation received from the City of Orlando locating GPR Survey Sites

114

INPUT FILE NAME -D:\Downtown Streets Pavement Analysis.DAT

NUMBER OF PROBLEMS TO BE SOLVED = 1

TITLE -Four Layer System Under Single axle dual tires for Downtown Streets

MATL = 1 FOR LINEAR ELASTIC LAYERED SYSTEM

NDAMA=2, SO DAMAGE ANALYSIS WITH DETAILED PRINTOUT WILL BE PERFORMED

NUMBER OF PERIODS PER YEAR (NPY) = 1

NUMBER OF LOAD GROUPS (NLG) = 1

TOLERANCE FOR INTEGRATION (DEL) -- = 0.001

NUMBER OF LAYERS (NL)------------- = 4

NUMBER OF Z COORDINATES (NZ)------ = 0

LIMIT OF INTEGRATION CYCLES (ICL)- = 80

COMPUTING CODE (NSTD)------------- = 9

SYSTEM OF UNITS (NUNIT)------------= 0

Length and displacement in in., stress and modulus in psi

unit weight in pcf, and temperature in F

THICKNESSES OF LAYERS (TH) ARE : 6 3 10

POISSON'S RATIOS OF LAYERS (PR) ARE : 0.35 0.15 0.45 0.5

ALL INTERFACES ARE FULLY BONDED

FOR PERIOD NO. 1 LAYER NO. AND MODULUS ARE :   1 5.000E+05   2 3.250E+07

  3 1.000E+04   4 3.000E+03

LOAD GROUP NO. 1 HAS 2 CONTACT AREAS

CONTACT RADIUS (CR)--------------- = 7.98

CONTACT PRESSURE (CP)------------- = 80

NO. OF POINTS AT WHICH RESULTS ARE DESIRED (NPT)-- = 3

WHEEL SPACING ALONG X-AXIS (XW)------------------- = 0

WHEEL SPACING ALONG Y-AXIS (YW)------------------- = 13.5

RESPONSE PT. NO. AND (XPT, YPT) ARE: 1 0.000 0.000 2 0.000 3.375

  3 0.000 6.750

NUMBER OF LAYERS FOR BOTTOM TENSION (NLBT)---- = 1

NUMBER OF LAYERS FOR TOP COMPRESSION (NLTC)--- = 1

LAYER NO. FOR BOTTOM TENSION (LNBT) ARE: 1

LAYER NO. FOR TOP COMPRESSION (LNTC) ARE: 4

LOAD REPETITIONS (TNLR) IN PERIOD 1 FOR EACH LOAD GROUP ARE : 582800

DAMAGE COEF.'S (FT) FOR BOTTOM TENSION OF LAYER 1 ARE: 0.0796 3.291 0.854

DAMAGE COEFICIENTS (FT) FOR TOP COMPRESSION OF LAYER 4 ARE: 1.365E-09 4.477

DAMAGE ANALYSIS OF PERIOD NO. 1 LOAD GROUP NO. 1

POINT	VERTICAL COORDINATE	VERTICAL DISP.	VERTICAL STRESS (STRAIN)	MAJOR PRINCIPAL STRESS (STRAIN)	MINOR PRINCIAL STRESS (STRAIN)	INTERMEDIATE P. STRESS (HORIZONTAL P. STRAIN)
1	6.00000	0.07016	60.778	78.622	44.841	66.114
	(STRAIN)		3.140E-05	7.958E-05	-1.163E-05	3.655E-05
1	19.00010	0.06739	2.553	2.568	1.353	1.379
	(STRAIN)		3.930E-04	4.009E-04	-2.070E-04	-2.070E-04
2	6.00000	0.07066	65.664	77.121	55.799	70.307
	(STRAIN)		3.504E-05	6.597E-05	8.398E-06	3.933E-05
2	19.00010	0.06780	2.603	2.607	1.368	1.395
	(STRAIN)		4.065E-04	4.085E-04	-2.110E-04	-2.110E-04
3	6.00000	0.07087	72.746	74.622	71.655	72.760
	(STRAIN)		4.309E-05	4.815E-05	4.014E-05	4.016E-05
3	19.00010	0.06797	2.622	2.622	1.375	1.402
	(STRAIN)		4.111E-04	4.111E-04	-2.123E-04	-2.123E-04

AT BOTTOM OF LAYER 1 TENSILE STRAIN = 0.000E+00

ALLOWABLE LOAD REPETITIONS = 1.000E+30 DAMAGE RATIO = 0.000E+00

AT TOP OF LAYER 4 COMPRESSIVE STRAIN = 4.111E-04

ALLOWABLE LOAD REPETITIONS = 1.970E+06 DAMAGE RATIO = 2.959E-01

****

* SUMMARY OF DAMAGE ANALYSIS *

****

AT BOTTOM OF LAYER 1   SUM OF DAMAGE RATIO = 0.000E+00

AT TOP OF LAYER 4   SUM OF DAMAGE RATIO = 2.959E-01

MAXIMUM DAMAGE RATO =   2.959E-01   DESIGN LIFE IN YEARS = 3.38

LIST OF REFERENCES

1. Cardimona, Steve (2002). Subsurface Investigation Using Ground Penetrating Radar: Proceedings of the Second International Conference on the Application of Geophysical and NDT Methodologies to Transportation Facilities and Infrastructures. Los Angeles, California, USA.

2. Chen Chi-Chih, Kishor Rama Rao, and Robert Lee. "A Tapered-Permittivity Rod Antenna for Ground Penetrating Radar Applications," Journal of Applied Geophysics. Vol. 47, Issue 3-4, July 2001: 309-316.

3. Das, Braja M (2004). Principles of Foundation Engineering (5th Ed.) Pacific Grove, CA: Brocks/Cole—Thomson Learning Inc.

4. Daniels, D. J. Surface-Penetrating Radar (1996). London, U.K.: The Institution of Electrical Engineers.

5. Engineering Fundamental (efunda) (2004). Properties of Common Solid Materials, [Online].
http://www.efunda.com/materials/common_matl/Common_Matl.cfm?MatlPhase=Solid&MatlProp=Mechanical

6. Pavement Distress (2003). Hawaii Asphalt Pavement Guide. [Online].
http://www.hawaiiasphalt.com/HAPI/index.htm

7. Huang, Yang H. (1993). Pavement Analysis and Design. Upper Saddle River, NJ: Prentice Hall.

8. Hunaidi, Osama and Peter Giamou (1998). Ground-Penetrating Radar for Detection of Leaks in Buried Plastic Water Distribution Pipes: Proceedings of the Seventh International Conference on Ground-Penetrating Radar. Lawrence, Kansas, USA.

9. Geophysical Surveys Systems, Inc (2002). User's Manual Subsurface Interface Radar SIRveryorSIR-20 System, North Salem, NH.

10. Geophysical Surveys Systems, Inc (2003). User's Manual Radan for Windows Subsurface Interface Radar SIRveyor SIR-20 System, North Salem, NH.

11. Kestler, Maureen A. (2000). Extending Pavement Life and Other Benefits of Reduced Tire Pressure: A Multi-Partner Cooperative Program. United States Army Corps of

Engineers: Fact Sheet. [Online].
http://www.crrel.usace.army.mil/techpub/factsheets/pdfs/110.pdf

12. Lacko, Peter R., William W. Clark, Kelly Sherbondy, James M. Ralston, and Elvis Dieguez (2003). Studies of Ground Penetrating Radar Antennas: Proceedings of the Second International Workshop on Advanced GPR. Delft, Netherlands.

13. Lake Eola Heights: Neightborhood Horizon's Program (2002). City or Orlando Publication [Online].
http://www.cityoforlando.net/planning/cityplanning/Neighborhood_Horizons/Lake%20Eola%20Final%20For%20Web.pdf

14. Leuschen C. J., S. P. Gogineni, S. M. Clifford, and R. K. Raney (2001). Simulation and Design of Ground-Penetrating Radar for Mars Exploration: Proceedings of the International Geosciences and Remote Sensing Symposium (IGARSS). Sydney, Australia.

15. Mikhail, Magdy Y. and Michael S. Mamlouk (1997). "Effect of Vehical-Pavement Interaction on Pavement Response." Transportation Research Record. No. 1570: 78-88.

16. Olhoeft, Gary R. (1996). Application of Ground Penetrating Radar: Proceedings of the Sixth International Conference on Ground Penetrating Radar. Sendai, Japan.

17. Olhoeft, Gary R. (2000).   Automatic Processing and Modeling of GPR Data for Pavement Thickness and Properties: Proceedings of the 8th International Conference on Ground Penetrating Radar. Gold Coast, Australia.

18. Olhoeft, Gary R. (2003). Electromagnetic Field and Material Properties in Ground Penetrating Radar: Proceedings of the Second International Workshop on Advanced GPR. Delft, Netherlands.

19. Powell, Kathryn (2004). Detecting buried human remains using near-surface geophysical instruments: Proceedings of the Sixteenth Australian Society of Exploration Geophysicist Geophysical Conference and Exhibition. Adelaide, South Australia.

20. STATS Geophysical (2003).   The Ground Penetrating Radar Technique. [Online].
http://www.stats.co.uk/Geophysics/GPR.pdf

21. Sweeney, Marianne. (1986).   Ground Penetrating Radar in the Detection of Subsurface Cavities Related to Sinkhole Activity in Florida, M.S. Thesis, University of Central Florida, Orlando, FL.

22. Tannous, Bishar S. (1987). Investigation of Electrical Properties of Earth Materials by Ground Penetrating Radar, M.S. Thesis, University of Central Florida, Orlando, FL.

23. Ullidtz, Per (1999a). Deterioration Models for Managing Flexible Pavements. Transportation Research Record. No. 1655: 31-34.

24. Ullidtz, Per, Wei Zhang, and Susanne Baltzer (1999b). Validation of Pavement Response and Performance Models: Proceedings of the first International Conference on Accelerated Pavement Testing. Reno, Nevada.

25. Uzan, Jacob (1997). Evaluation of Fatigue Cracking. Transportation Research Record. No. 1570: 89-95.

26. Weissman, Samuel L. (1999). Influence of Tire-Pavement Contact Stress Distribution on Development of Distress Mechanisms in Pavements. Transportation Research Record. No. 1655: 161-167.

27. Zeng, Xiaoxian and George A. McMechan (1997). "GPR characterization of buried tanks and pipes," Journal of Geophysics. Volume 62, Number 3, May-June 1997: 797-806.